Dynamics and Control of a Quadrotor with Active Geometric Morphing

Dustin A. Wallace

A thesis
submitted in partial fulfillment of the
requirements for the degree of

Master of Science in Aeronautics & Astronautics

University of Washington

2016

Reading Committee:

Kristi Morgansen, Chair

Christopher Lum

Program Authorized to Offer Degree:
Aeronautics & Astronautics

University of Washington

Abstract

Dynamics and Control of a Quadrotor with Active Geometric Morphing

Dustin A. Wallace

Chair of the Supervisory Committee:
Professor Kristi Morgansen
Aeronautics & Astronautics

Quadrotors are manufactured in a wide variety of shapes, sizes, and performance levels to fulfill a multitude of roles. Robodub Inc. has patented a morphing quadrotor which will allow active reconfiguration between various shapes for performance optimization across a wider spectrum of roles. The dynamics of the system are studied and modeled using Newtonian Mechanics. Controls are developed and simulated using both Linear Quadratic and Numerical Nonlinear Optimal control for a symmetric simplificiation of the system dynamics. Various unique vehicle capabilities are investigated, including novel single-throttle flight control using symmetric geometric morphing, as well as recovery from motor loss by reconfiguring into a trirotor configuration. The system dynamics were found to be complex and highly nonlinear. All attempted control strategies resulted in controllability, suggesting further research into each may lead to multiple viable control strategies for a physical prototype.

TABLE OF CONTENTS

LIST OF FIGURES

ACKNOWLEDGMENTS

I would first like to thank my advisor, Professor Kristi Morgansen. Her insight and guidance set me on a path to learn an abundant number of new mathematical techniques and approaches for analyzing complex dynamic and control problems such as this one. I would also like to thank Nathan, Jake, and Natalie for their technical assistance and for talking through and validating my approaches to problems I came across throughout the process, as well as my mother, father, and sisters for their emotional support. Lastly, I would like to thank Robodub Inc. for providing the subject of this research. I hope to see further development on their part which results in a flying prototype in the near future.

DEDICATION

To Lillian, for without your love and support, this work would not have been possible.

Chapter 1

INTRODUCTION

1.1 Background

Unmanned aerial vehicles (UAVs) have become an industry unto themselves in recent years. While remotely controlled aircraft have existed in some form or another since the late nineteenth century when small-scale blimps were primitively controlled using radio waves created by a sparking mechanism [1], they tended to have somewhat of a niche appeal throughout much of the twentieth century. A surge in production and implementation of unmanned aerial vehicles has been seen in recent years however, as the increasing power and decreasing cost of electronic computational resources have allowed for the flying and stabilization of the aircraft to be handled electronically while the operators focus on achieving flight objectives. These objectives cover a wide spectrum of activities from military surveillance and interdiction, to aerial photography and entertainment.

The U.S. Department of Defense (DOD) has been utilizing drones for multiple decades as aerial targets, modifying outdated fighter jets with rudimentary control systems to create extremely realistic test scenarios for new anti-aircraft weapons. During the Cold War, the DOD recognized the potential benefits of purpose-built unmanned aircraft, including operator protection, force multiplication, and the removal of pilot-restricted mission limitations on duration and maneuver intensity. Purpose-built surveillance drones began flying in the early 1990s, eventually evolving into the modern RQ-1 Predator, which first flew in 1994. By the late 1990s, armed versions of the Predator, which would eventually lead to the development of the more heavily armed MQ-9 Reaper, were flying and providing strike capabilities for the U.S. military [2]. In recent years, smaller, man-portable fixed-wing drones like the RQ-11 Raven have entered service, providing over-the-wall type tactical military information

to soldiers on the battlefield [3].

While the use of fixed-wing unmanned vehicles has grown, the advent of vertical take off and landing (VTOL) drones has truly ignited the industry in recent years. Suddenly, drones could be flown by almost anyone, anywhere. The Los Angeles Times reports as many as 10% of feature films and television shows now use aerial photography shot by drones [4]. Corporations including Amazon [5], DHL [6], Google [7], and more are all developing the means to deliver packages using VTOL drones. Hobbyists have even created leagues centered around racing drones through courses of obstacles while using virtual-reality goggles to view the flight from the vehicle's perspective [8].

The most common design used in VTOL drones is the quadrotor, which uses four fixed-pitch propellers on brushless motors rigidly mounted to a frame to provide full controllability in 3D space. The basic design requires two motors to spin clockwise and two to spin counterclockwise, allowing all rotors to contribute to lifting the vehicle, while still balancing the yaw-inducing drag torques on the propellers. Quadrotors are typically flown in two configurations: "plus" or "X", depending on the yaw reference frame of the vehicle, and control authority is derived by modulating relative propeller thrusts to affect attitude and direct the combined lift vector in the direction of desired movement. Examples of this relative modulation are shown in Figure 1.1.

Due to their relative simplicity and ability to be used in small spaces such as a laboratory setting, quadrotors have been the subject of a great deal of control development and research. A multitude of control techniques have been applied, both linear and nonlinear, and from across the fields of both classical and modern control. In fairly early quadrotor testing dating to 2004, researchers implemented both classical and modern techniques for quadrotor control in simulation, on test stands, and finally in flight. Proportional-Integral-Derivative (PID) control was found to be robust to moderate perturbations without a particularly accurate dynamic model, however the utility of Linear Quadratic (LQ) models were found to be limited by the fidelity of the dynamic model being used, as simulated flights went well, yet results were mixed on the test stand and flight tests [9].

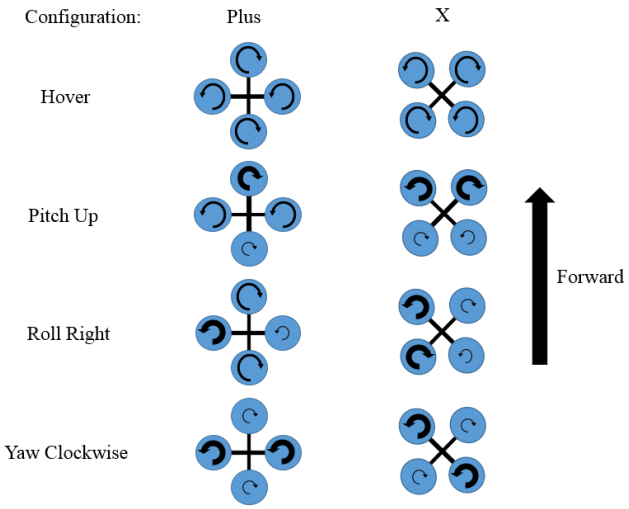

Figure 1.1: Relative motor throttling to perform basic quadrotor maneuvers. Arrows indicate direction of propeller rotation.

In [10], a particularly prolific team developed a nested controller, using PD gains to control the vehicle attitude in response to a PID controlled outer loop for translational navigation. System observability was achieved using a VICON motion capture system, which uses a fixed array of cameras to track markers on vehicles, providing high-fidelity position and velocity information. The team found very favorable results in the study, showing agile, controllable flight for both individual vehicles and small formations of multiple vehicles. The team continued their work in [11], demonstrating the same core controller in flight through tightly constricted spaces, as well as fast, aggressive maneuvers for perching on vertical and inverted surfaces. The team additionally achieved robustness to failed perching and quick return to stable flight for repeated attempts. Other work from this team includes [12], in which a nonlinear optimal controller calculates quadrotor trajectories in real time minimizing the second time derivative of acceleration, referred to as snap. The team found precision in trajectory following was a trade off with vehicle speed, however in certain trials, acceptable precision was maintained up to a speed of 10 body lengths per second.

Traditional quadrotor drones are simple and useful, however control strategies designed

for the basic configuration are only truly valid for quadrotors with fixed payloads at the center of the body. Studies of moving payloads improve the utility of quadrotors greatly. An often-studied field of quadrotor research concerns the handling of swing loads representative of any potential unactuated payload suspended beneath the vehicle. In [13], an eight degree of freedom (DOF) model is considered in which the position of the unactuated swing load is described by two angles. A dynamic model was constructed using Newtonian mechanics and validated using a Lagrangian formulation, and then Model Based Control (MBC) was implemented. The controller was found to compensate for the swing load and hold to its prescribed trajectory, however the load did exhibit large oscillations throughout the initial simulations. This was alleviated through the addition of a feed-forward controller which compensated for swinging through higher-order control of the vehicle throttles, and the swinging was dramatically reduced. In [14], learning algorithms were applied to a similar 8 DOF model, resulting in an actual flying prototype which was able to successfully navigate a cluttered environment while carrying an unactuated swing load.

A further extension of the idea of underslung mass is the implementation of an actuated robotic arm mounted on the belly of a quadrotor. In [15], a quadrotor is fitted with a three link actuated arm intended for completing construction tasks. In this study, the system was modeled, and separate controller loops were built for the quadrotor and arm. The arm control was physically implemented using PID, but was merely considered an outside disturbance in this study of its effects on the helicopter dynamics. The quadrotor was initially controlled using a traditional quadrotor PID, however this was found to be insufficient in its response to arm-movment perturbations. The response was found to improve dramatically when the quadrotor was converted to a Variable Parameter Integral Backstepper (VPIB) controller. This controller allowed for rapid response to the arm states, passed along as parameters. The vehicle was found to be capable of holding very stable despite perturbations caused by arm movements.

In [16], researchers modeled the dynamics of a quadrotor carrying an underslung gimballing camera with the goal of keeping the camera pointed at a target position as the quadro-

tor flies a given trajectory. The study developed the dynamics of the combined quadrotor-camera system using the Lagrangian mechanics, and then implemented both backstepping and sliding-mode nonlinear control. The backstepper controller was found to yield moderate results, while the sliding mode controller was found to be insufficient, and in both cases, further work was intended.

A logical step beyond compensating for a moving load is to actively consider the moving load as a flight control input. This type of behavior is observed not only in novel man made aerial vehicles, but in nature as well. Research in [17] proposed the rapid articulation of a hawk moth's abdomen during agile flight maneuvers may be actuating flight via inertial, rather than aerodynamic effects. They constucted a dynamic model based upon the hawk moth and simulated the use of dynamic inertia as a control input, then compared responses in the actual animal when responding to visual stimuli in a lab setting. Comparing the transfer functions, it was concluded the hawk moth was indeed utilizing inertial actuation.

The hawk moth research inspired work by a previous student in the Nonlinear Dynamics and Control Laboratory, who sought to further swing load quadrotor dynamics through actuation of the load as dynamic inertia. An 8 DOF model similar to the previously discussed studies was constructed and modeled using Lagrangian Mechanics, however the motor throttles were combined from four independent inputs to only a total throttle and a yaw input. All pitch and roll control authority was generated by applying torques to the underslung load. This actuated mass was found to provide sufficient control authority for a variety of trajectories when controlled using LQR, as well as strong robustness to modeling errors [18].

Direct torque and inertia effects from actuating inert masses are only one way of utilizing additional degrees of freedom of a quadrotor to alter or improve performance for a target mission. Another notable approach is to modify how and where aerodynamic forces are imparted on the vehicle. One example of this is through implementation of a tilt-rotor mechanism. In [19], a tilting mechanism is modeled on a quadrotor with the goal of allowing the vehicle to fly without requiring the complete vehicle to lean in the direction of desired motion, thus improving the utility of body-fixed directional payloads such as non-gimbaled

cameras. PID control is used to fly desired trajectories, and favorable results were found, leading the author to suggest further experimentation with a physical prototype. An additional step from here is a complete conversion into a fixed wing aircraft by mounting the four motors into tilting airfoil wings. This approach was studied in [20]. LQR control was implemented for the quadrotor in its VTOL configuration, and dynamics were modeled for the vehicle both as a quadrotor and as a fixed wing aircraft for horizontal flight, using coupled rotation of the rear arms as elevators for pitch actuation, and independent rotation of the front arms as ailerons for roll actuation. The authors did not address control during the transitional period, but found favorable results in both the horizontal and vertical flight regimes, with future work intended concerning the conversion.

Each variation of the basic design is useful in addressing a drawback of standard quadrotors. The tilting motors allow a body-fixed payload to be pointed independently of the direction of travel. The tilting wings allow improved speed and efficiency in horizontal travel. A novel variable-geometry quadrotor design can address other areas of improvement, such as the ability to better balance loads by actively repositioning the center of lift, navigating tight spaces, and the ability to recover from the typically catastrophic event of a motor loss by reconfiguring into a trirotor.

The research presented here represents an initial study into the dynamics and control of such a morphing quadrotor through a combination of inertial actuation and aerodynamic load shifting. The vehicle is capable of actively varying its shape by controlling the rotation of the arms with respect to the vehicle body about their yaw axes, as well as sliding the motors and propellers along the arms as commanded, a similar but mathematically simpler analogue for telescoping arms. This design is patent pending by Robodub Inc. [21], whose early prototypes are shown in Figures 1.2 and 1.3.

Energy storage constraints imposed by battery volumes and masses subject small-scale drones to fairly limited mission durations. In order to maximize the efficiency of flight operations, and therefore longevity, Linear Quadratic optimal control is selected as the preferred controller design for this study. Further work for early flying prototypes may benefit from

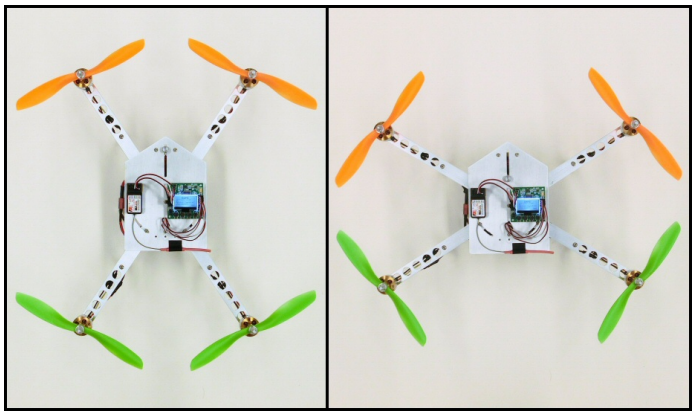

Figure 1.2: Early Robodub prototype exhibiting a degree of arm angle variation. Photograph provided by Robodub Inc. and used with permission.

Figure 1.3: Early Robodub prototype quadrotor with variable length arms. Photograph provided by Robodub Inc. and used with permission.

additional exploration of PID control design, or potentially a combination using PID tuned by LQR as proposed and simulated for quadrotor control in [22].

It is worth noting this present study accounts for drag only in the propeller torques and not on the body due to translation or rotation, as all maneuvers are assumed to be performed at a substantially low velocity to where they can be neglected. Lift and drag on the propellers are assumed to be only a point thrust and a rotational couple centered on the motors and do not account for p-factor torques and other effects which act on propellers rotating at high speeds. Lastly gyroscopic effects are ignored. All of these factors are areas for further consideration beyond the scope of this research.

1.2 Outline of the Thesis

This paper will investigate various aspects of the dynamics and control of the variable-geometry quadrotor. Chapter 2 describes the dynamic model, develops dynamic equations governing its movement, and simplifies the dynamics to the most capable yet tractable form presently feasible. Chapter 3 investigates the implementation of LQR control on the full model, and then to the vehicle in a trirotor state to which it would transition in the event of a motor loss. Chapter 4 considers Set Point LQR Gain Scheduling control in which controlling the vehicle is investigated during shape transitions by modeling the vehicle as a series of unconventionally-shaped fixed-geometry quadrotors. Chapter 5 investigates nonlinear numeric optimal control of the quadrotor using a single throttle input with all attitude control achieved through geometric morphing. Finally, Chapter 6 concludes the paper by briefly reviewing findings and making suggestions for further research.

1.3 Contributions of the Thesis

The unique contributions of this research are diverse, as no existing publications have been found concerning the dynamics and control a quadrotor which transforms in the manner of the vehicle in this study. First, dynamic equations governing the vehicle are methodologically determined. Second, LQR controls are applied to the vehicle and found to be stabilizing, and

therefore a good candidate for development into controls for an eventual prototype. Third, controllability was confirmed for the linearized trirotor configuration to which the vehicle can transform to recover from a motor loss, indicating further work should make the recovery executable for a physical prototype. Fourth, Set Point Gain Scheduling was investigated and found to be stabilizing for the vehicle during shape transitions, and an early study into the optimal number of set points for a transformation was conducted, determining simple transitions can be completed with only three set point gain combinations. Fifth, and lastly, the ability to fly the vehicle using a single throttle channel and actuating roll and pitch through geometric morphing was verified in simulation with numerical nonlinear control. Each of these initial examinations of various topics form a basic foundation for further investigation into the control of a variable-geometry quadrotor.

Chapter 2

DYNAMIC MODEL

This chapter will define the dynamic model of the conceptual morphing quadrotor in terms of state and parametric values. An explanation is then provided for the process by which the complete quadrotor dynamics are derived. The model is then simplified to a symmetric form which is more mathematically tractable while continuing to enable the desired novel system capabilities. The chapter concludes by declaring specific numerical values for the system parameters used for control rule calculations in the following chapters.

2.1 Model Description

The full variable geometry quadrotor is modeled as a nine-mass system consisting of a central body, four variable-angle arms rotating about pivot points on the body, and four motors, each sliding along one of the arms. This sliding motor model is mathematically similar to the concept of telescoping arms, and it can be easily adapted to whichever method of motor positioning is selected for a final physical prototype. Body-fixed coordinate axes are defined with the origin at the center of the body, and with the body-fixed x-axis pointed forward, the body-fixed y-axis pointed to the right, and the body-fixed z axis pointed downward as shown in Figure 2.1. This selection allows for a right-handed coordinate convention in which the pitch angle, θ, rotating about the y-axis is positive in a nose-up attitude. The other two rotations used to relate the body orientation to the inertial reference frame are the roll angle, ϕ, positive clockwise when viewed from behind, and the yaw angle, ψ, positive clockwise when viewed from above.

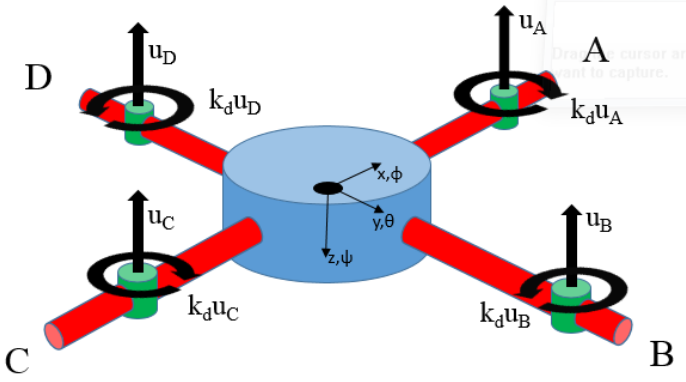

Figure 2.1: Basic initial model for the quadrotor, showing the orientation of the body-frame axes and the external forces imparted by the motors and propellers.

The orientation of the body-fixed and inertial axes are related through the use of the Roll-Pitch-Yaw Euler angle rotation matrix. This particular rotation sequence was selected due to its containment of singularities far from the expected maneuvering regime of the vehicle, a reason why it is commonly used in aerospace modeling. This rotation matrix is given below using the space-saving trigonometric notation used throughout this paper and exemplified by $s_\phi = sin(\phi)$:

$$\bar{R} = \begin{bmatrix} c_\theta c_\psi & -c_\theta s_\psi & s_\theta \\ c_\psi s_\theta s_\phi + c_\phi s_\psi & c_\phi c_\psi - s_\theta s_\phi s_\psi & -c_\theta s_\phi \\ -c_\phi c_\psi s_\theta + s_\phi s_\psi & c_\psi s_\phi + c_\phi s_\theta s_\psi & c_\theta c_\phi \end{bmatrix}.$$

The vehicle was chosen to be modeled in the "plus" configuration common in quadrotor development due to mathematical simplicity. This configuration places the arm base locations directly along the fore-aft and lateral axes. The four arm-motor pairs are designated A, B, C, and D, beginning with the forward arm and continuing clockwise when viewed from above. The arm orientations are defined by angles α_A, α_B, α_C, and α_D, each quantified as the clockwise rotation from the forward-pointing, body-fixed x-axis. The position of each motor on its corresponding arm is described by its distance outboard from the pivot point on

the body, designated d_A, d_B, d_C, and d_D. Examples of these quantities are shown in Figure 2.2.

The physical properties of the quadrotor are defined by parameters of fixed distances and masses. The body of the quadrotor is modeled as a homogeneous cylinder of mass m_{body}, radius ρ_{body}, and height h_{body}. Each pivot is allowed is own distance from the center of the body along the corresponding body-fixed axis to allow for maximum versatility in adapting the model to the eventual prototype. These distances are designated b_A, b_B, b_C, and b_D. The arms extend outward from these pivots, modeled as homogeneous thin rods of masses m_{armA}, m_{armB}, m_{armC}, and m_{armD}, and lengths l_A, l_B, l_C, and l_D. The motors are modeled as point masses of masses m_{motA}, m_{motB}, m_{motC}, and m_{motD}.

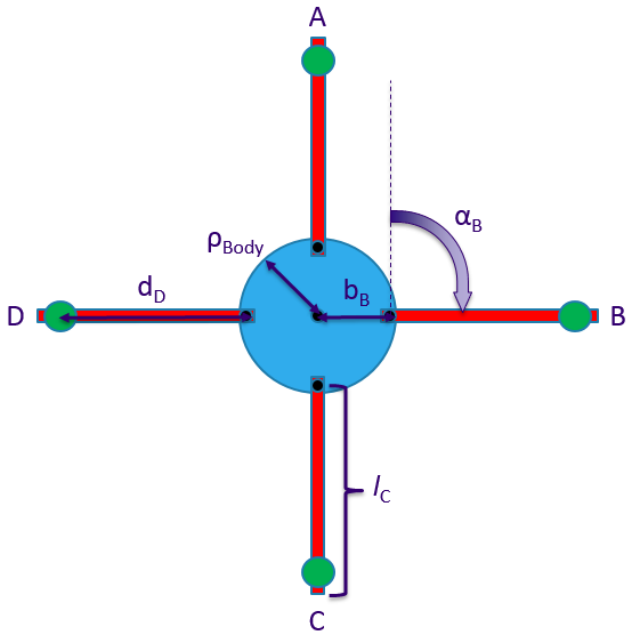

Figure 2.2: Examples of one of each dimension, duplicated in the model on each of the four arms.

2.2 Generalized Coordinates

A full state description of the system could require three translational and three rotational states be assigned and modeled for each of the nine masses, giving a total of 54 states.

Considering joint constraints reduces the state quantity greatly by locking together certain degrees of freedom of the components mounted to the body and thus reducing the model to a minimum number of generalized coordinates. In this model, the arms are fixed translationally to the body at the pivot points. The pivot joint constraints fix the roll and pitch of the arms to match that of the body, only allowing differences in yaw, which are directly quantified by the α angles. The complete position and orientation of each arm can therefore be described relative to the body by a single generalized coordinate each, the arm angle, α. The motors are fixed to the arms on sliding joints. Such a joint locks all orientation angles, as well as two of the three translational dimensions. The one remaining translational dimension for each motor is quantified by the distance, d. A full six degree of freedom state description is thus only necessary for a single component, from which other parts can be related through a single generalized coordinate each. The model places the body-fixed axes at the center of the body, and thus the same states relating the body to the inertial frame can serve as the six body states of the system. The remaining eight shape states bring the minimum full dimensionality of the complete quadrotor system up to fourteen, given by the state vector,

$$q = [x, y, z, \phi, \theta, \psi, \alpha_A, \alpha_B, \alpha_C, \alpha_D, d_A, d_B, d_C, d_D]^T .$$

2.3 System Mechanics

The dynamics of the full quadrotor are highly shape-dependent. As the shape changes, the center of gravity (CG) will shift through the vehicle. Calculating the location of the CG in the body frame requires first describing the position of each component as a function of the shape variables and fixed geometric parameters. The model is assumed to be planar, with all components at the same body-frame $z = 0$, and thus coordinates are written in x and y only. The position vectors are thus given by:

$$\vec{r}_{body} = [0, 0]$$

$$\vec{r}_{armA} = \left[b_A + \frac{l_A}{2} c_{\alpha_A}, \frac{l_A}{2} s_{\alpha_A} \right]$$

$$\vec{r}_{armB} = \left[\frac{l_B}{2}c_{\alpha_B}, b_B + \frac{l_B}{2}s_{\alpha_B}\right]$$

$$\vec{r}_{armC} = \left[-b_C + \frac{l_C}{2}c_{\alpha_C}, \frac{l_C}{2}s_{\alpha_C}\right]$$

$$\vec{r}_{armD} = \left[\frac{l_D}{2}c_{\alpha_D}, -b_D + \frac{l_D}{2}s_{\alpha_D}\right]$$

$$\vec{r}_{motA} = [b_A + d_A c_{\alpha_A}, d_A s_{\alpha_A}]$$

$$\vec{r}_{motB} = [d_B c_{\alpha_B}, b_B + d_B s_{\alpha_B}]$$

$$\vec{r}_{motC} = [-b_C + d_C c_{\alpha_C}, d_C s_{\alpha_C}]$$

$$\vec{r}_{motD} = [d_D c_{\alpha_D}, -b_D + d_D s_{\alpha_D}]\,.$$

Having expressions for the body-frame position of the center of mass of each component, the shape-dependent CG location in the body frame can now be found from the position vectors and component masses. First, for simplicity in writing, the total mass is calculated as the sum of the constituent masses,

$$m_{total} = \sum_{i=1}^{9} m_i.$$

Now, the system's combined CG can be expressed as,

$$\vec{CG} = \frac{\sum_{i=1}^{9} m_i \vec{r}_i}{m_{total}}.$$

The moments of inertia for each component are found, including parallel axis effects from the shape-dependent CG. The body inertias are found using the moment of inertia equations for a homogeneous cylinder:

$$I_{body\phi} = m_{body}\left(\frac{3\rho_{body}^2 + h_{body}^2}{12} + CG_y^2\right)$$

$$I_{body\theta} = m_{body}\left(\frac{3\rho_{body}^2 + h_{body}^2}{12} + CG_x^2\right)$$

$$I_{body\psi} = m_{body}\left(\frac{\rho_{body}^2}{2} + CG_x^2 + CG_y^2\right).$$

The inertias of the arms are found using the thin rod inertia equations, considering the length projected onto the x and y axes for roll and pitch:

$$I_{armi\phi} = m_{armi}\left(\frac{(l_i s_{\alpha_i})^2}{12} + (r_{armiy} - CG_y)^2\right)$$

$$I_{armi\theta} = m_{armi}\left(\frac{(l_i c_{\alpha_i})^2}{12} + (r_{armix} - CG_x)^2\right)$$

$$I_{armi\psi} = m_{armi}\left(\frac{l_i^2}{12} + (r_{armix} - CG_x)^2 + (r_{armiy} - CG_y)^2\right).$$

The motors are modeled as point masses, and therefore have only parallel axis effects contributing to their inertias:

$$I_{moti\phi} = m_{moti}\left(r_{motiy} - CG_y\right)^2$$

$$I_{moti\theta} = m_{moti}\left(r_{motix} - CG_x\right)^2$$

$$I_{moti\psi} = m_{moti}\left((r_{motiy} - CG_y)^2 + (r_{motix} - CG_x)^2\right).$$

Each contributing inertia is next summed to find the total state-dependent moments of inertia of the system:

$$I_\phi = I_{body\phi} + \sum_{i=1}^{4}\left(I_{armi\phi} + I_{moti\phi}\right)$$

$$I_\theta = I_{body\theta} + \sum_{i=1}^{4}\left(I_{armi\theta} + I_{moti\theta}\right)$$

$$I_\psi = I_{body\psi} + \sum_{i=1}^{4}\left(I_{armi\psi} + I_{moti\psi}\right).$$

The primary flight controls for the full quadrotor are the four throttles, modeled as thrust inputs u_A, u_B, u_C, and u_D. These forces act in the body-frame negative z direction at the corresponding motor positions. Rotating these forces through the system's rotation matrix, $\bar{R}$, for the vehicle's current orientation state gives the thrust in each translational coordinate direction as trigonometric functions of the orientation:

$$u_{total} = u_A + u_B + u_C + u_D$$

$$F_x = -u_{total} s_\theta$$

$$F_y = u_{total} s_\phi c_\theta$$

$$F_z = -u_{total} c_\phi c_\theta.$$

One method of calculating pitching and rolling moments due to applied thrusts is to find the lever arm between the combined Center of Lift (CL) of the four motors and the CG of the quadrotor in each axis direction. The CL is calculated using a similar equation to the CG, however considering motors only for positions and corresponding applied thrust forces in place of masses,

$$\vec{CL} = \frac{\sum_{i=1}^{4} \vec{r}_{moti} u_i}{u_{total}}$$

$$\tau_\phi = u_{total}(CG_y - CL_y)$$

$$\tau_\theta = u_{total}(CL_x - CG_x).$$

Motors A and C are assumed to rotate their propellers counterclockwise, and B and D rotate clockwise. The motors therefore exert opposite torques, assumed to be linearly proportional to the thrust inputs by the propeller drag coefficient k_d. These torques represent the external forcing on the quadrotor in the ψ dimension,

$$\tau_\psi = k_d(u_A - u_B + u_C - u_D).$$

With forces, torques, masses, and inertias known, the system dynamics are calculated using Newton's Second Law. The original momentum form of the equation must be used due to the time-variance of the state-dependent moments of inertia:

$$F = \frac{d}{dt} mv = ma$$

$$\tau = \frac{d}{dt} I\omega = \dot{I}\omega + I\dot{\omega}.$$

Internal forces used to actuate the motor positions on the arms will have no effect on the inertial-frame behavior of the quadrotor's CG, and they therefore are fully accounted for in the shifting CG terms of the dynamic derivation. Considering the translational dynamics of

the CG rather than the body frame axes allows the translational dynamics to be easily and compactly expressed:

$$\ddot{x}_{CG} = \frac{F_x}{m_{total}}$$
$$\ddot{y}_{CG} = \frac{F_y}{m_{total}}$$
$$\ddot{z}_{CG} = g + \frac{F_z}{m_{total}}.$$

CG dynamics suffice for mathematical modeling and early simulations, however sensor equipment used to detect state information for stabilizing feedback control of an eventual prototype will be rigidly mounted to the body, and thus body-frame dynamics will be necessary. These dynamics can be found using the second derivative of the CG shift rotated through the rotation matrix, which will give much more complicated translational dynamic equations in terms of the positions, velocities, and accelerations of the eight shape states. These equations are given in expression form,

$$\ddot{x} = \ddot{x}_{CG} - [[C\ddot{G}_x, C\ddot{G}_y, 0]\bar{R}]_x$$

$$\ddot{y} = \ddot{y}_{CG} - [[C\ddot{G}_x, C\ddot{G}_y, 0]\bar{R}]_y$$

$$\ddot{z} = \ddot{z}_{CG} - [[C\ddot{G}_x, C\ddot{G}_y, 0]\bar{R}]_z.$$

Internal torques used to actuate the arms act entirely in the yaw direction, and the forces which slide the motors act in the plane of body-frame $z = 0$, and therefore no additional acceleration appears in the roll and pitch dynamics due to shape changes, allowing for simple expressions of the roll and pitch dynamics:

$$\ddot{\phi} = \frac{\tau_\phi - \dot{I}_\phi \dot{\phi}}{I_\phi}$$

$$\ddot{\theta} = \frac{\tau_\theta - \dot{I}_\theta \dot{\theta}}{I_\theta}.$$

The torques used to actuate the arm angles will act equal and opposite on the body and corresponding arm of the vehicle, producing accelerations in the angles of each which sum

to the angle change in each body-relative arm angle α. Direct control of the shape-state accelerations is assumed to avoid necessitating consideration of constraint forces and torques in this initial study, instead allowing the focus to be only on the desired shape changes. Translational effects on the system CG are again accounted for in the shifting CG terms, however the proportion of angular acceleration imparted upon the body, and therefore on the body yaw angle ψ requires not only knowledge of the instantaneous relative inertias, but also due to the continuous shape changes, the time derivative of not only the relative inertias, but also the angular velocities of each portion. While not impossible to solve for, these terms are very difficult to determine in closed form, and the current schedule for this research will not allow for it. A similar situation arises when considering the yaw torques imparted by the sliding motor forces when the arms are not perpendicular to the body. The resulting unknown internal torques are expressed together in the term $\tau_{\psi internal}$ in the complete dynamic expression for the yaw,

$$\ddot{\psi} = \frac{\tau_{\psi} - \dot{I}_{\psi}\dot{\psi} + \tau_{\psi internal}}{I_{\psi}}.$$

One simple method of removing the need to consider internal torques from the requirements of the model is to constrain movement to where canceling torques will always be applied during shape transitions, thus enforcing $\tau_{\psi internal} = 0$. This cancellation can be achieved by requiring opposite arm-motor pairs be symmetric with matching geometric and mass properties, as well as mirrored arm and motor movements. This simplification does remove some degree of capability from the system, however it will nonetheless allow for modeling all suggested novel capabilities. Further work should investigate the influence of these internal torques, perhaps investigating the effects of using the forces and torques as the selected control channels as opposed to the direct shape state acceleration control currently being investigated.

2.4 Symmetric Analytic Model

Requiring mirrored arm properties and movements reduces the dimensionality of the system, and makes redefining certain states favorable. The mirroring of motor positions can be accounted for by setting $d_C = d_A$ and $d_D = d_B$, thus eliminating the shape states d_C and d_D. Arms A and C are also now positioned using a single angle. To avoid constant use of phase shift angles, a new angle is defined, α_ϕ, describing the arms' angular displacement left of the body-frame x axis. This orientation was selected such that a positive α_ϕ displacement should shift the CL in such a way it produces a positive moment in ϕ. Likewise, the angles of arms B and D are defined as the angle forward of the body-frame y axis, shifting the CL to produce a positive moment in θ. These new definitions are shown in Figure 2.3. The new ten element state vector now contains six body states and four shape states. This new state vector is written as,

$$q = [x, y, z, \phi, \theta, \psi, \alpha_\phi, \alpha_\theta, d_A, d_B]^T .$$

Balancing forces and torques produced by shape changes requires geometric and mass parameters be made symmetric. Therefore, parameters m_{armC}, m_{motC}, and l_C are set equivalent to m_{armA}, m_{motA}, and l_A. An identical equivalency is set for the D parameters and the B parameters. The eventual physical prototype will likely be constructed symmetrically, so resulting losses in model versatility are minimal. The process continues identically to before, however adjusted for the new matching properties and arm angle definitions. The new position vectors are given:

$$\vec{r}_{body} = [0, 0]$$
$$\vec{r}_{armA} = \left[b_A + \frac{l_A}{2} c_{\alpha_\phi}, -\frac{l_A}{2} s_{\alpha_\phi} \right]$$
$$\vec{r}_{armB} = \left[\frac{l_B}{2} s_{\alpha_\theta}, b_B + \frac{l_B}{2} c_{\alpha_\theta} \right]$$
$$\vec{r}_{armC} = \left[-b_A - \frac{l_A}{2} c_{\alpha_\phi}, -\frac{l_A}{2} s_{\alpha_\phi} \right]$$
$$\vec{r}_{armD} = \left[\frac{l_B}{2} s_{\alpha_\theta}, -b_B - \frac{l_B}{2} c_{\alpha_\theta} \right]$$

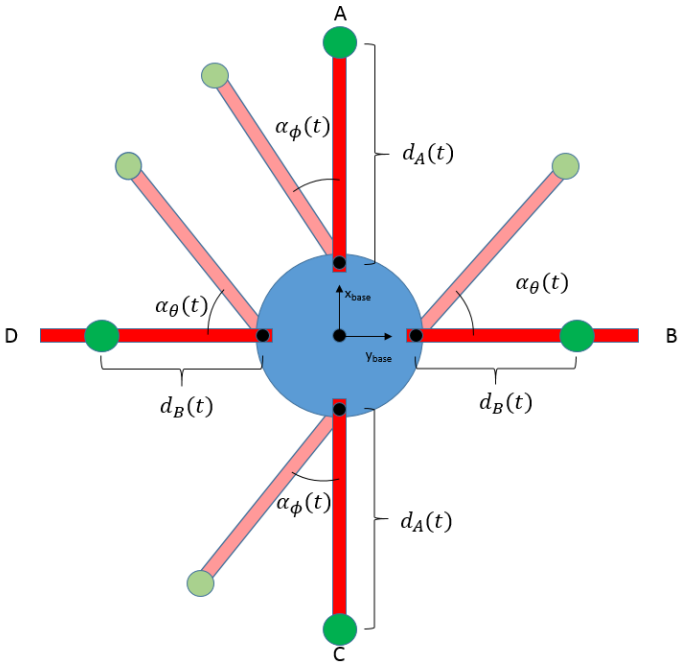

Figure 2.3: Simplified model using symmetrically constrained body shapes to cancel internal torques.

$$\vec{r}_{motA} = \left[b_A + d_A c_{\alpha_\phi}, -d_A s_{\alpha_\phi}\right]$$

$$\vec{r}_{motB} = \left[d_B s_{\alpha_\theta}, b_B + d_B c_{\alpha_\theta}\right]$$

$$\vec{r}_{motC} = \left[-b_A - d_A c_{\alpha_\phi}, -d_A s_{\alpha_\phi}\right]$$

$$\vec{r}_{motD} = \left[d_B s_{\alpha_\theta}, -b_B - d_B c_{\alpha_\theta}\right].$$

The CG calculation equation is identical to before, as are the equations for the moments of inertia of the body and motors with the exception of the new mass property equivalencies. The roll and pitch inertias of the arms change to match the new arm angle definitions:

$$I_{armA\phi} = m_{armA}\left(\frac{(l_A s_{\alpha_\phi})^2}{12} + (r_{armAy} - CG_y)^2\right)$$

$$I_{armA\theta} = m_{armA}\left(\frac{(l_A c_{\alpha_\phi})^2}{12} + (r_{armAx} - CG_x)^2\right)$$

$$I_{armB\phi} = m_{armB}\left(\frac{(l_B c_{\alpha_\theta})^2}{12} + (r_{armBy} - CG_y)^2\right)$$

$$I_{armB\theta} = m_{armB}\left(\frac{(l_B s_{\alpha_\theta})^2}{12} + (r_{armBx} - CG_x)^2\right)$$

$$I_{armC\phi} = m_{armA}\left(\frac{(l_A s_{\alpha_\phi})^2}{12} + (r_{armCy} - CG_y)^2\right)$$

$$I_{armC\theta} = m_{armA}\left(\frac{(l_A c_{\alpha_\phi})^2}{12} + (r_{armCx} - CG_x)^2\right)$$

$$I_{armD\phi} = m_{armB}\left(\frac{(l_B c_{\alpha_\theta})^2}{12} + (r_{armDy} - CG_y)^2\right)$$

$$I_{armD\theta} = m_{armB}\left(\frac{(l_B s_{\alpha_\theta})^2}{12} + (r_{armDx} - CG_x)^2\right).$$

Once the new arm inertias have been accounted for in terms of the newly defined arm angles, the equations of motion take the same form as they did previously, however with internal torques now canceling each other, the yaw dynamics simplify to a tractable form,

$$\ddot{\psi} = \frac{\tau_\psi - \dot{I}_\psi \dot{\psi}}{I_\psi}.$$

The full expressions for the dynamics are gargantuan when calculated through, and are expressed here only in terms of constituent calculations for brevity. The full dynamic equations for the symmetric quadrotor may be found in Appendix A.

2.5 Selected Numerical Values

Before applying Linear Quadratic Regulator (LQR) control to the quadrotor, numerical values are assigned to each geometric and mass property. The eventual physical implementation of the system has not yet been designed, and therefore realistic numbers were estimated for a hobby-sized vehicle. The selected values are given in Table 1.

Masses (kg)	
m_{body}	0.3
m_{armA}	0.1
m_{armB}	0.1
m_{motA}	0.1
m_{motB}	0.1
Lengths (m)	
ρ_{body}	0.1
h_{body}	0.1
b_A	0.1
b_B	0.1
l_A	0.3
l_B	0.3
Gravity (m/s^2)	
g	9.81
Prop Drag Coefficient	
k_d	0.5

Table 1: Quadrotor Physical Properties

Chapter 3
LQR CONTROL

This chapter examines the use of Linear Quadratic control on the symmetric morphing quadrotor including all eight control inputs. The system dynamics are linearized about a hover condition, and LQR control gains are calculated and applied in simulation to both the linearized and nonlinear models. An LQR controller is then examined as a possibility for controlling the vehicle in a trirotor configuration to which the system could convert for continued stable flight upon loss of a motor. The vehicle dynamics are linearized about this trirotor configuration, and the resulting LQR gains are tested again on both the linearized and nonlinear dynamic models.

3.1 Full System Control

As briefly mentioned in the proceeding chapter, direct control of shape state accelerations is assumed, with physical realization of this left to be achieved by the prototyper. Four shape states, combined with four throttle inputs, give the system a total of eight inputs:

$$\vec{u} = \left[u_A, u_B, u_C, u_D, \ddot{\alpha}_\phi, \ddot{\alpha}_\theta, \ddot{d}_A, \ddot{d}_B\right]^T.$$

The most fundamental flight regime for the quadrotor is that of a stationary hover, and therefore the hover is the first condition considered for linearization. The nonlinear model is linearized about a full zero state with the exception of placing the motors at the mid-spans of the arms to maximize available travel in each direction and throttle inputs each equal to a quarter of the vehicle weight, expressed in the form $\dot{\vec{x}} = \bar{A}\vec{x} + \bar{B}u$, where:

$$\vec{x} = \left[x, y, z, \phi, \theta, \psi, \alpha_\phi, \alpha_\theta, d_A, d_B, \dot{x}, \dot{y}, \dot{z}, \dot{\phi}, \dot{\theta}, \dot{\psi}, \dot{\alpha}_\phi, \dot{\alpha}_\theta, \dot{d}_A, \dot{d}_B\right]^T.$$

The dynamic matrices are found to be very sparse and are able to be compactly written in equation form shown below, excluding the obvious position-velocity dependencies and direct state control equations. The linearized equations are relatively simple, allowing easy verification against intuition about the system's behavior:

$$\ddot{x} = -9.81\theta$$

$$\ddot{y} = 9.81\phi$$

$$\ddot{z} = -0.9091(u_A + u_B + u_C + u_D)$$

$$\ddot{\phi} = 8.0264\alpha_\phi - 9.0909(u_B - u_D)$$

$$\ddot{\theta} = 8.0264\alpha_\theta + 9.0909(u_A - u_C)$$

$$\ddot{\psi} = 9.1743(u_A - u_B + u_C - u_D)$$

The controllability matrix produced using $\bar{A}$ and $\bar{B}$ was found to be full row rank, indicating the linearized system is controllable. To develop an optimal control rule for the linearized system using LQR methods, cost weighting matrices must be declared in the cost function:

$$\int_0^\infty \left(\vec{x}^T \bar{Q} \vec{x} + \vec{u}^T \bar{R} \vec{u}\right) dt.$$

The cost matrices $\bar{Q}$ and $\bar{R}$ correspond to the magnitude of the state deviation and control inputs from the linearization condition. The first case study will investigate recovery from perturbation and return to the origin. All states and controls are cost-weight normalized by setting $\bar{Q} = I_{20x20}$ and $\bar{R} = I_{8x8}$. Bryson's rule for constrained states is then applied to constrain the arm angles to less than $\frac{\pi}{4}$ in either direction and motor positions to stay on the arms with less than $\frac{l}{2}$ travel in either direction. The corresponding LQR gains were calculating using Mathematica's $LQRegularGains$ function. The resulting $8x20$ gain matrix is shown below, expressed in block notation to fit to the page:

$$\bar{K} = \left[\bar{K}_{1(8x7)}, \bar{K}_{2(8x7)}, \bar{K}_{3(8x6)}\right]$$

$$\bar{K}_1 = \begin{bmatrix} -0.7071 & 0 & -0.5 & 0 & 4.57 & 0.5 & 0 \\ 0 & -0.7071 & -0.5 & -4.57 & 0 & -0.5 & -0.4447 \\ 0.7071 & 0 & -0.5 & 0 & -4.57 & 0.5 & 0 \\ 0 & 0.7071 & -0.5 & 4.57 & 0 & -0.5 & 0.4447 \\ 0 & -0.0032 & 0 & -0.0424 & 0 & 0 & 1.4181 \\ 0.0032 & 0 & 0 & 0 & -0.0424 & 0 & 0 \\ 0 & 0 & 0 & 0 & 0 & 0 & 0 \\ 0 & 0 & 0 & 0 & 0 & 0 & 0 \end{bmatrix}$$

$$\bar{K}_2 = \begin{bmatrix} 0.4447 & 0 & 0 & -1.0765 & 0 & -0.7246 & 0 \\ 0 & 0 & 0 & 0 & -1.0765 & -0.7246 & -1.0014 \\ -0.4447 & 0 & 0 & 1.0765 & 0 & -0.7246 & 0 \\ 0 & 0 & 0 & 0 & 1.0765 & -0.7246 & 0 \\ 0 & 0 & 0 & 0 & -0.0065 & 0 & 0.0003 \\ 1.4181 & 0 & 0 & 0.0065 & 0 & 0 & 0 \\ 0 & 6.6667 & 0 & 0 & 0 & 0 & 0 \\ 0 & 0 & 6.6667 & 0 & 0 & 0 & 0 \end{bmatrix}$$

$$\bar{K}_3 = \begin{bmatrix} 1.0014 & 0.5265 & 0 & 0.0029 & 0 & 0 \\ 0 & -0.5265 & -0.0029 & 0 & 0 & 0 \\ -1.0014 & 0.5265 & 0 & -0.0029 & 0 & 0 \\ 0 & -0.5265 & 0.0029 & 0 & 0 & 0 \\ 0 & 0 & 1.9586 & 0 & 0 & 0 \\ 0.0003 & 0 & 0 & 1.9586 & 0 & 0 \\ 0 & 0 & 0 & 0 & 3.7859 & 0 \\ 0 & 0 & 0 & 0 & 0 & 3.7859 \end{bmatrix}.$$

These gains were applied first on the linear model to study the response and ensure convergence. The dynamics were modeled for five seconds using Mathematica's *NDSolve* function with the dynamic equation $\dot{\vec{x}} = \left(\bar{A} - \bar{B}\bar{K}\right)\vec{x}$. The resultant state trajectories are

shown in Figure 3.1.

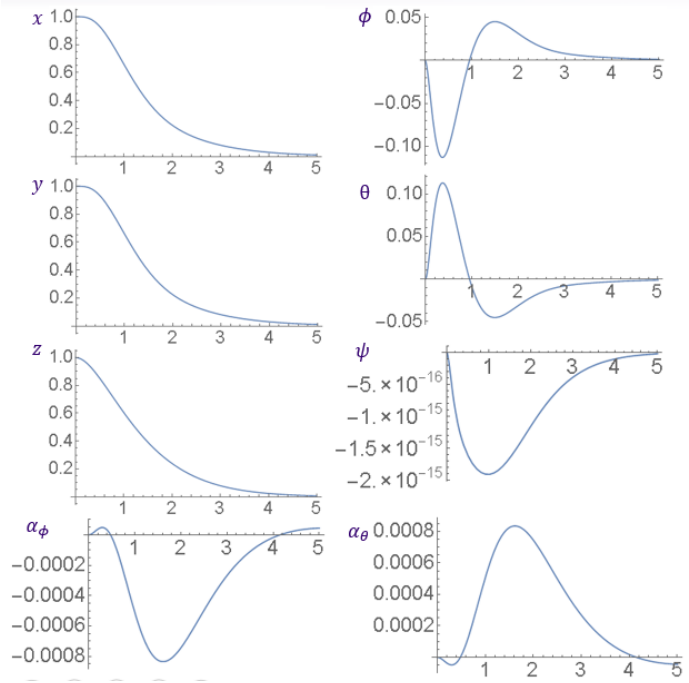

Figure 3.1: State trajectory of linearized quadrotor initialized at $[x, y, z] = [1, 1, 1]$.

The linearized system response was found to be stable and controllable back to the origin as expected. The return to the origin was achieved using a combination of differential throttling and arm movements to actuate the vehicle in the pitch and roll directions. No response was found on the motor positions, as their movement in the perpendicular-arm configuration would effect only the rotational inertia of the system, and with the model linearized about a zero angular velocity state, no other state dynamics are effected by d_A or d_B. Having verified the control on the linear model, the hover controls are next applied to the nonlinear model using the same initialization and the control substitution $\vec{u} = -\bar{K}\vec{x}$. The resulting state trajectories are shown in Figure 3.2.

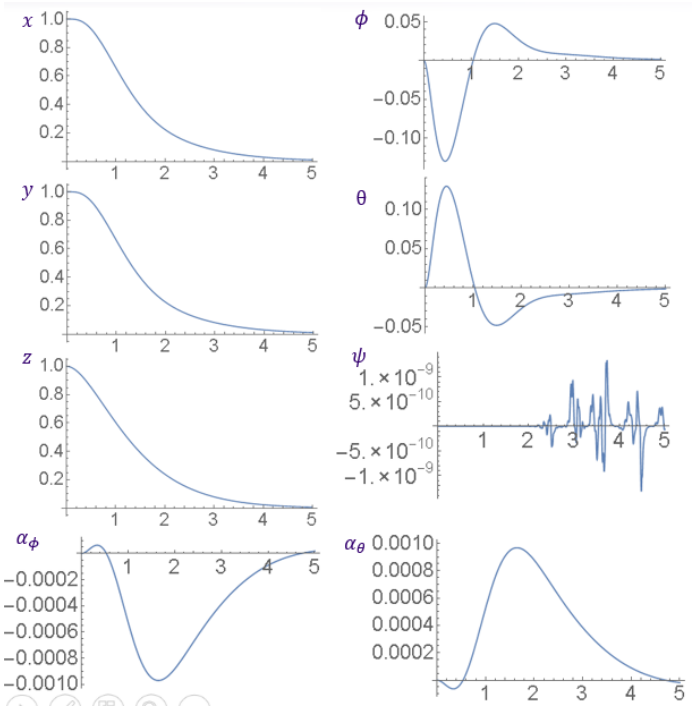

Figure 3.2: State trajectory of nonlinear quadrotor initialized at $[x, y, z] = [1, 1, 1]$.

The dynamics are again found to be stabilized, with x and y returning to the origin through actuation of the pitch and roll using a combination of differential throttling and arm angle actuation in a similar pattern to that of the linearized model, however the z displacement did not converge back to the origin. The reason for this non-convergence is currently unknown and is an area for future investigation, however the stabilizing effect of the controller is promising, suggesting further development could lead to an LQR controller capable of flying the quadrotor in real time.

3.2 LQR After Motor Loss Recovery

A quadrotor which experiences a motor loss is typically uncontrollable as motor forces and torques are impossible to balance for stable flight. Research in [23] investigates the possibility of preventing loss of a vehicle by stabilizing the angular velocity of the vehicle rather than angular position, and then controlling translation in the air by directing the axis of rotation

through use of periodic throttle controls. While this method is successful for preventing loss of the vehicle or damage to property or observers below, it will not allow for continuation of most missions as intended. One of the unique capabilities of the morphing quadrotor is the potential ability to survive a motor loss and continue with the assigned mission by transforming into a trirotor configuration.

This study investigates the controllability of the vehicle after experiencing a loss of motor C. Motors A and C are assumed to rotate counterclockwise, while motors B and D oppose and balance their torques on the system. Assuming the thrust-torque relationship to be linear through the propeller drag coefficient k_d, the hover input on motor A after losing motor C must now double to equal half of the vehicle weight. This doubling will intuitively require shortening of the moment arm for motor A by reducing d_A while simultaneously moving motors B and D to the rear to maintain pitch stability. A solver was written which sought acceptable shape combinations by positioning the CL over the CG. The resultant configuration selected for modeling is given by $d_A = 0.025$, $d_B = 0.3$, and $\alpha_\theta = -1.1597$. An approximation of this configuration is shown in Figure 3.3.

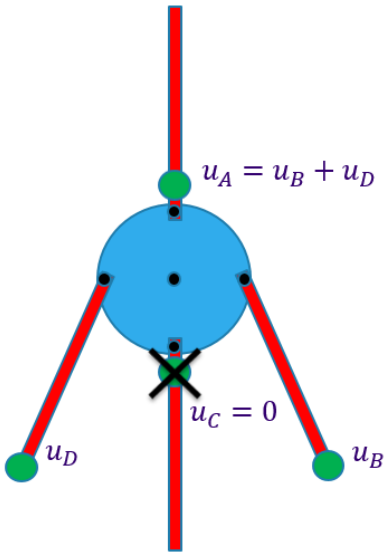

Figure 3.3: Selected Trirotor hover configuration which balances the doubling of u_A.

This configuration was used as the linearization configuration for the model, again linearizing the dynamics into the form $\dot{\vec{x}} = \bar{A}\vec{x} + \bar{B}u$, now with a reduced seven element input vector resulting from the loss of u_C. The dynamic matrices were again found to be very sparse, and are compactly expressed in linear equation form, omitting again the position-velocity dependencies and the direct shape control equations:

$$\ddot{x} = -9.81\theta$$

$$\ddot{y} = 9.81\phi$$

$$\ddot{z} = -0.9091(u_A + u_B + u_D)$$

$$\ddot{\phi} = -57.5535\alpha_\phi + 27.3432(u_B - u_D)$$

$$\ddot{\theta} = 14.8923\alpha_\theta + 120.867d_A - 73.7785d_B + 4.7553u_A - 5.4721(u_B + u_D)$$

$$\ddot{\psi} = 19.4444(u_A - u_B - u_D).$$

These equations mostly match intuition for the system, apart from the ϕ dynamics, which have signs opposite of what intuition would expect. Troubleshooting of the dynamic code has not yet resulted in the discovery of any process errors, however continued work and possible reprogramming of the code may yield improved linearized dynamics.

A standard fixed-geometry trirotor is under-actuated and thus non-controllable due to coupling between pitch, roll, and yaw. The underactuation is typically alleviated by adding a servo which controls axial rotation of one arm, thus vectoring thrust for independent yaw control [24]. An initial examination of whether or not the shape modulation used in this study is an acceptable replacement for the axial rotation can be done by examining the controllability matrix calculated from $\bar{A}$ and $\bar{B}$. The controllability matrix was found to be full row rank, indicating the linearized system is controllable, and likely would remain so even if the dynamic equations were altered slightly such as reversing the signs on the ϕ dynamics to better match intuition concerning the system. The gaining of controllability via addition of geometric modulation was further validated by calculating the controllability matrix with

the geometry fixed in the trirotor configuration, which was found not to be full-row rank, and thus match the understanding of non-controllability for fixed-geometry trirotors.

Despite the conflict with intuition, the latter portion of the code executed and results were found. First, using the same cost-weighting matrices from the quadrotor hover state except reducing the length of the $\bar{R}$ matrix by one to match the shortened control vector length, a gain matrix $\bar{K}$ was found, again expressed using block notation:

$$\bar{K} = \left[\bar{K}_{1(7x7)}, \bar{K}_{2(7x7)}, \bar{K}_{3(7x6)}\right]$$

$$\bar{K_1} = \begin{bmatrix} -0.0828 & 0 & -0.2591 & 0 & 0.6438 & 0.16 & 0 \\ 0.1273 & 0.2235 & -0.1247 & 1.4541 & -1.0513 & -0.1351 & -1.0881 \\ 0.1273 & -0.2235 & -0.1247 & -1.4541 & -1.0513 & -0.1351 & 1.0881 \\ 0 & 0.0331 & 0 & 0.2546 & 0 & 0 & 4.8090 \\ -0.0815 & 0 & -0.0138 & 0 & 0.9889 & -0.0641 & 0 \\ -0.6617 & 0 & -0.1120 & 0 & 8.0256 & -0.5198 & 0 \\ 0.4039 & 0 & 0.0683 & 0 & -4.8989 & 0.3173 & 0 \end{bmatrix}$$

$$\bar{K_2} = \begin{bmatrix} 0.2879 & 2.3363 & -1.4261 & -0.1330 & 0 & -0.5976 & 0 \\ -0.5608 & -4.5518 & 2.7785 & 0.2083 & 0.3409 & -0.2829 & 0.3212 \\ -0.5608 & -4.5518 & 2.7785 & 0.2083 & -0.3409 & -0.2829 & -0.3212 \\ 0 & 0 & 0 & 0 & 0.0554 & 0 & -0.0069 \\ 2.1964 & 9.7101 & -5.9272 & -0.1520 & 0 & -0.0325 & 0 \\ 9.7101 & 79.808 & -48.1052 & -1.2336 & 0 & -0.2636 & 0 \\ -5.9271 & -48.1052 & 30.3639 & 0.7530 & 0 & 0.1609 & 0 \end{bmatrix}$$

$$\bar{K}_3 = \begin{bmatrix} 0.1694 & 0.1781 & 0 & 0.0175 & 0.1419 & -0.0866 \\ -0.2913 & -0.1398 & -0.0188 & -0.0380 & -0.3083 & 0.1882 \\ -0.2913 & -0.1398 & 0.0188 & -0.0380 & -0.3083 & 0.1882 \\ 0 & 0 & 3.2575 & 0 & 0 & 0 \\ 0.3685 & -0.0826 & 0 & 1.8749 & 1.1596 & -0.7078 \\ 2.9904 & -0.6707 & 0 & 1.1596 & 11.1431 & -5.7446 \\ -1.8254 & 0.4094 & 0 & -0.7078 & -5.7446 & 5.2386 \end{bmatrix}.$$

These control gains were first applied to the linearized dynamics, with the same $[x, y, z] = [1, 1, 1]$ initialization used for the full quadrotor dynamics study. The resulting state trajectories are shown in Figure 3.4.

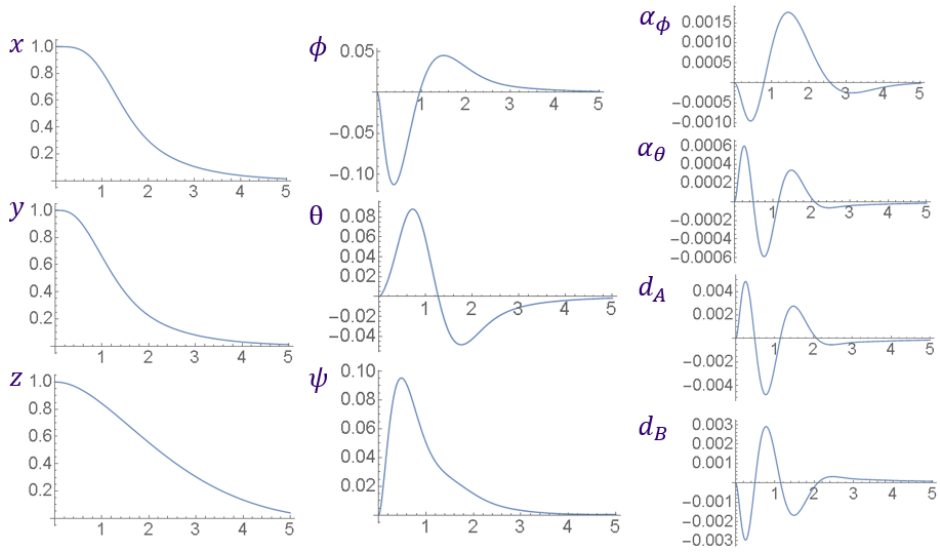

Figure 3.4: State response of the linearized trirotor with LQR control.

The system was verified to be completely stabilized and controllable in the linear model, now utilizing motor positions as controls as well due to their new effect on the θ dynamics. Having verified controllability on the linearized model, the LQR control gains were next applied to the full nonlinear trirotor dynamics. The response is shown in Figure 3.5.

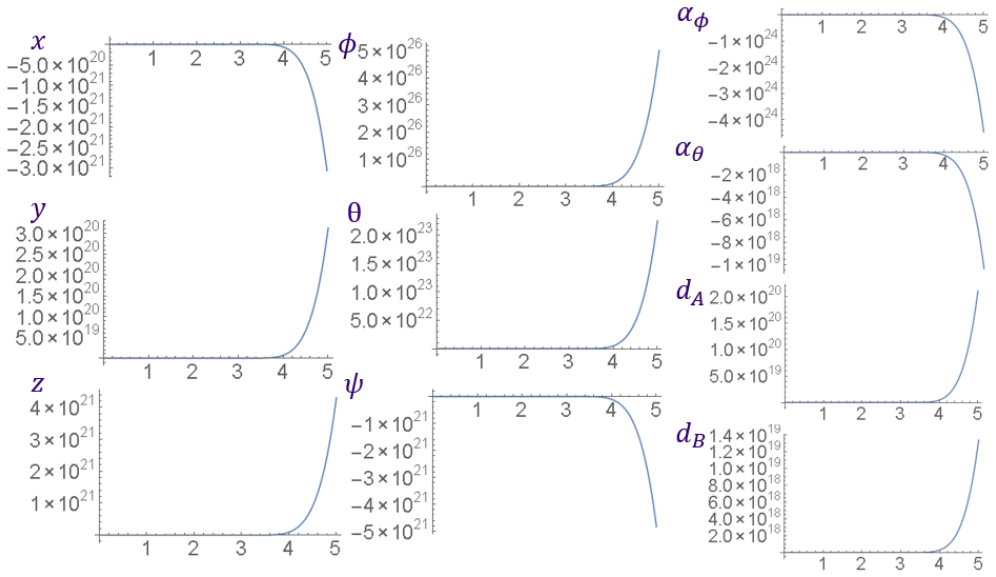

Figure 3.5: State response of the full nonlinear trirotor with LQR control.

The nonlinear dynamics of the trirotor-configured vehicle were found to be unstable in every degree of freedom when controlled with the calculated LQR gains. This instability is being attributed to the unexpected signage in the ϕ dynamics, as well as the nonlinearity of the system near the linearization condition, as upon parsing the dynamic equations, they are found to be dependent on α_θ through various trigonometric functions, including $sin(\alpha_\theta)$, $cos(\alpha_\theta)$, $sin^2(\alpha_\theta)$, and $sin(2\alpha_\theta)$.

Chapter 4

LQR GAIN SCHEDULING

This chapter proposes the strategy of utilizing traditional quadrotor LQR gains calculated for various unconventional but fixed configurations to govern an inner control loop utilizing the throttle inputs only while relegating shape control and actuation to an outer control loop which commands shape transitions based upon specific mission requirements such as navigating a constricted space. Using this controller, the quadrotor transitions through a gain schedule to utilize the gains for the fixed geometry closest to the instantaneous configuration while executing a transition. The objective of this study is to first test the validity of the control strategy, and then to investigate the optimal number of gain set points throughout the trajectory.

A basic transition is selected for the initial evaluation of the set point gain schedule strategy. The quadrotor is assumed to begin hovering at the origin in the basic configuration used for the initial hover linearization in the proceeding chapter. The quadrotor is then modeled as rotating arms B and D back while extending motor A and C to the ends of their arms. The vehicle thus transitions from an initial shape state of $\alpha_\theta = 0$ and $d_A = \frac{l_A}{2}$ to a final shape of $\alpha_\theta = -\frac{\pi}{3}$ and $d_A = l_A$. The transition is modeled assuming bang-bang control of the shape state accelerations, completing the transition in first two seconds and then one second.

A single MATLAB script was written which linearly spaces a user-specified number of set point geometries along the programmed transition. The script then iterates the linearization procedure and determines optimal gain matrices using the same LQR process and cost-weighting matrices as in the proceeding chapter for each of the linearization conditions, and then propagates the nonlinear dynamics of the controlled quadrotor using forward Euler

with a time step of 1 millisecond. In each iteration, the shape state is read and the gains for the nearest available set point geometry are applied to the throttle inputs. The first study utilized a single transition between two set points, one each for the beginning and ending configurations. The model is initialized stationary at the origin with the goal of maintaining a stable hover at the origin throughout and after the transition. The control inputs and corresponding state trajectories for the two second trial are shown in Figures 4.1 and 4.2, respectively.

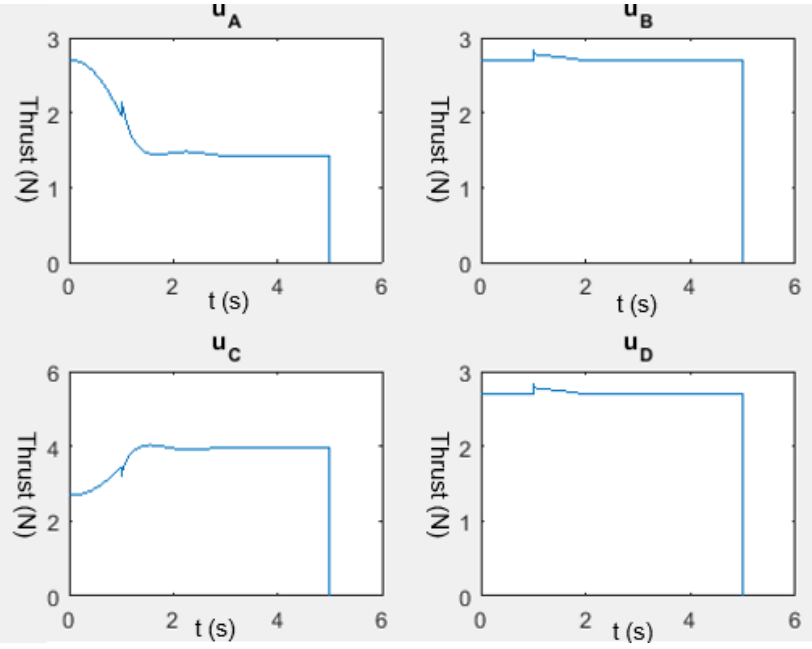

Figure 4.1: Throttle controls applied during two second transition using two set points.

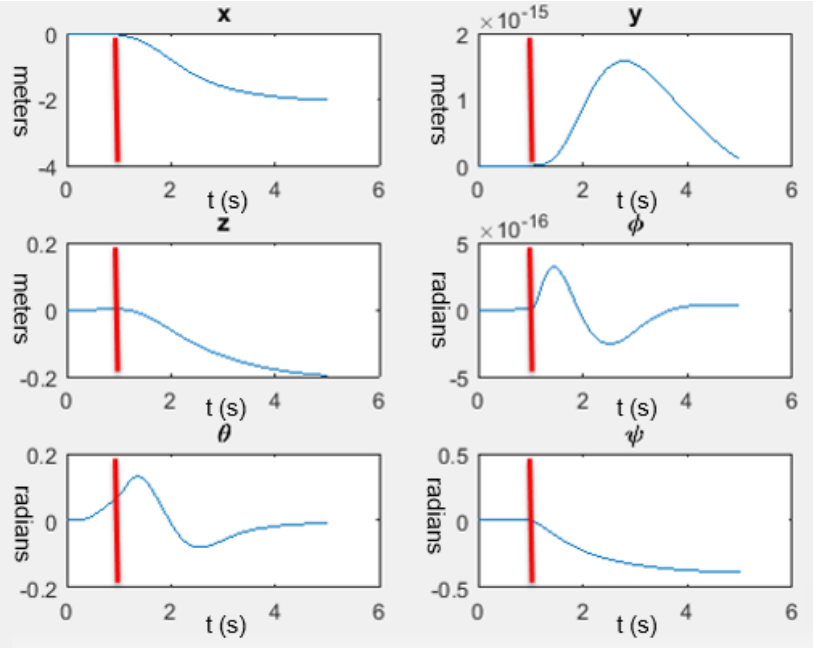

Figure 4.2: State trajectories during two second transition using two set points. The red lines indicate the gain switching time.

Small step discontinuities appear in the throttle controls at the transition point, indicating a non-fluid transition between the gains. The state trajectories are observed to be destabilized as α_θ deviates from a perpendicular arm configuration. Upon switching gains, the vehicle is stabilized and returns to stable level flight, although it does not return to the origin. This stabilization verifies the potential for set point gain scheduling control, however further work will be necessary to isolate the cause of the nonzero position.

The previous case was repeated with a one second transition duration to study the effects of the transition time on the dynamics of the system. The resulting controls and state trajectories are shown in Figures 4.3 and 4.4.

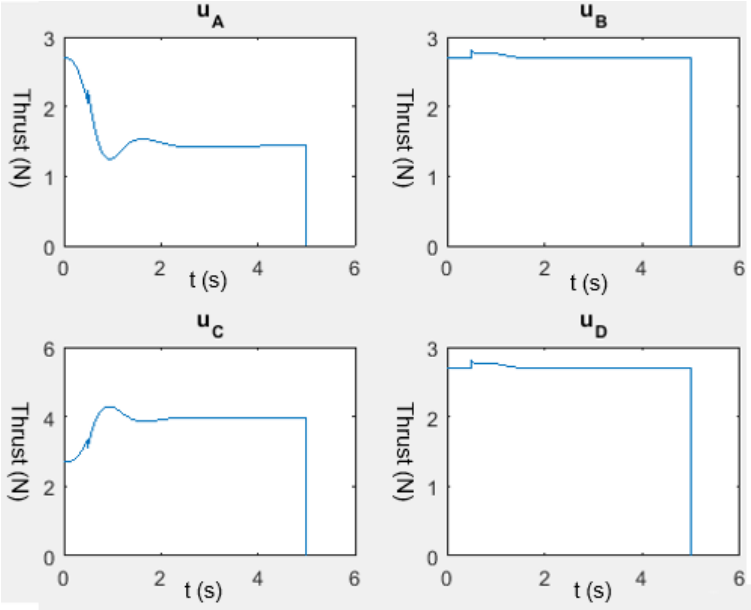

Figure 4.3: Throttle controls applied during one second transition using two set points.

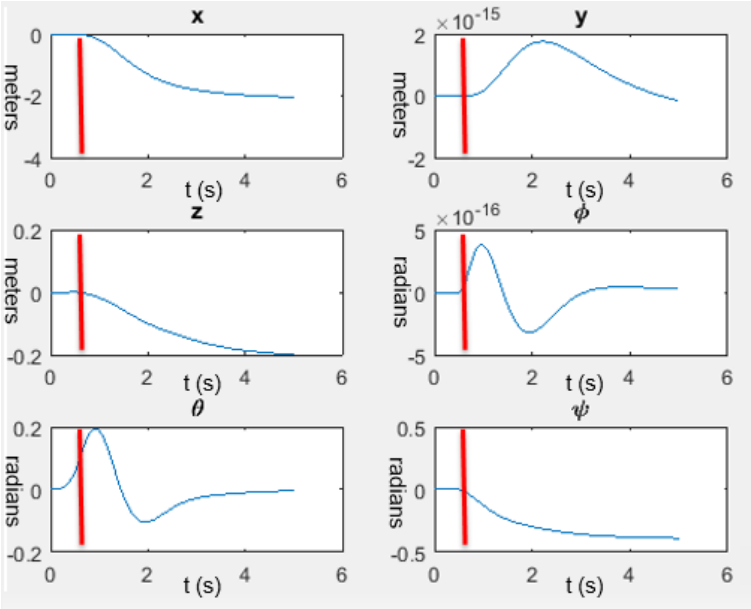

Figure 4.4: State trajectories during one second transition using two set points. The red lines indicate the gain switching time.

The trajectories are found to be similar in characteristics, however slightly greater pitch deviation is noted before the system restabilizes. To allow greater time for dynamic deviation during transformation, further trials were conducted using the two second duration, examining the effects of varying the number of set points on the system behavior during shape transitions.

The simplest additional set point to examine is that of halfway through the transition, when $\alpha_\theta = -\frac{\pi}{6}$ and $d_A = \frac{3l_A}{4}$. To adhere to the closest set point, the controller switches gains when the position is a quarter through the transition, and then switches to the final gains when a only a quarter remains. Half of the transition distance is thus controlled with the new gain matrix. The controls and state trajectories produced by the three set point controller are shown in Figures 4.5 and 4.6.

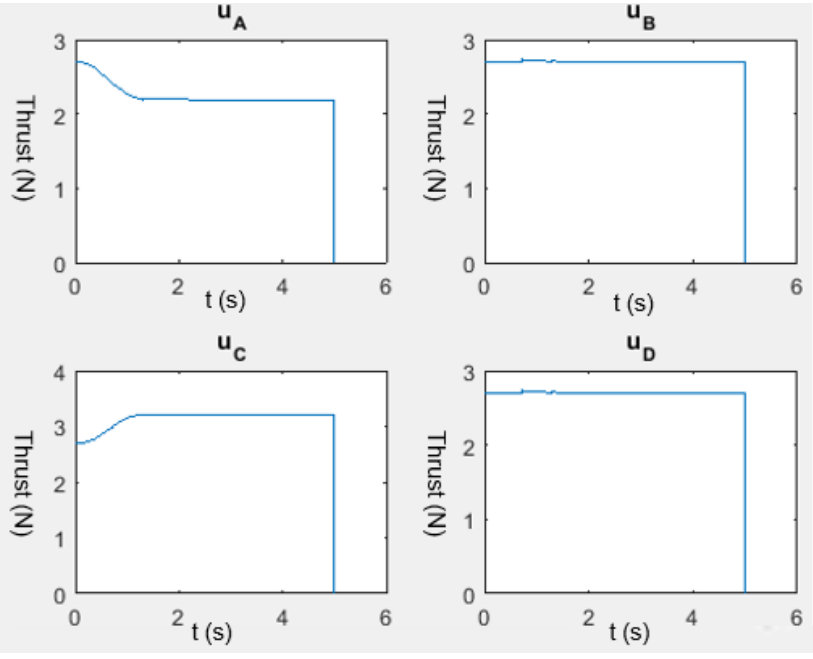

Figure 4.5: Throttle controls applied during two second transition using three set points

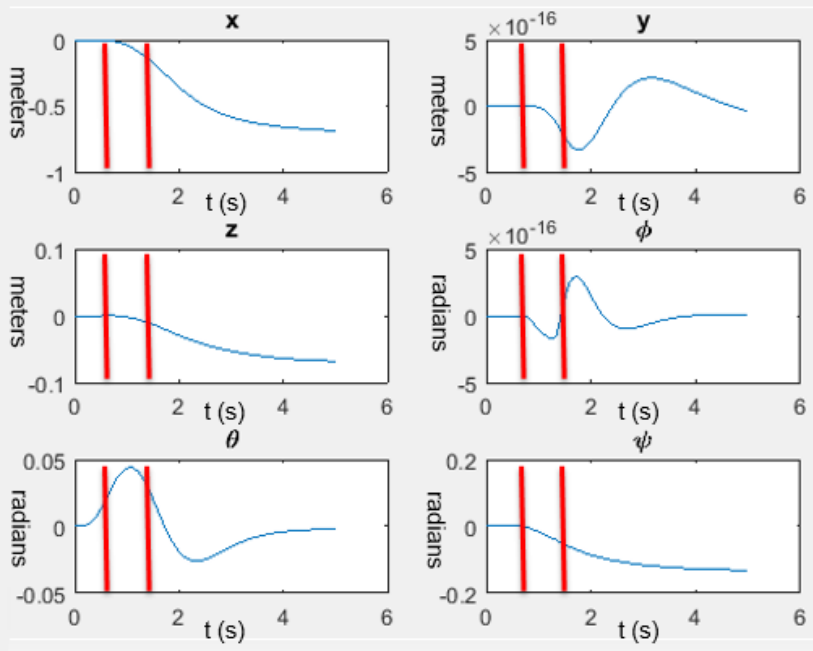

Figure 4.6: State trajectories during two second transition using three set points. The red lines indicate the gain switching times.

The magnitude of transient θ deviation is dramatically reduced, as is the final translational steady-state error. The step discontinuities in u_A and u_C appear to have vanished, and those in u_B and u_D have become exceedingly small. A further trial was conducted with 5 set points, with new set points evenly spaced between the starting, middle, and final configurations. The resulting state trajectory is shown in Figure 4.7.

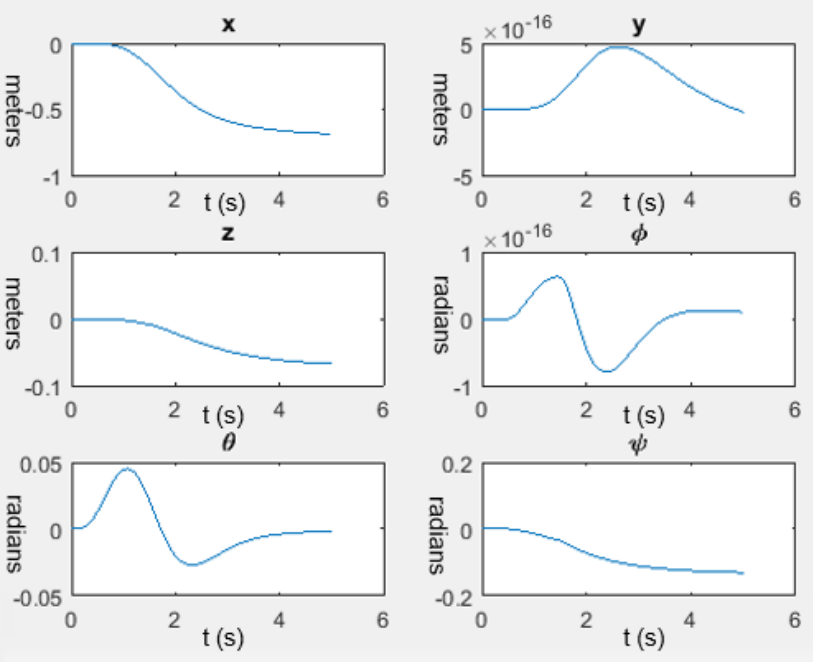

Figure 4.7: State trajectories during two second transition using five set points.

The state trajectory behavior with five set points is observed to be essentially identical to that of the three set point model. The maximum θ deviation appears identical, as do the steady-state translational errors. It was therefore concluded simple transitions can be handled using three set point controllers. This was further verified by calculating the state trajectory for a nine set point model, and again finding any improvement in state trajectories to be negligible. More complex transitions may require a greater number of set points, and that remains an area for further study.

Chapter 5
NUMERICAL OPTIMAL CONTROL

The variable geometry quadrotor presents an additional opportunity for unique development in moving beyond the common differential throttling control and instead generating control authority for the vehicle via geometric transformation. This chapter verifies the controllability of a quadrotor using geometric modulation in place of differential throttling using numerical simulation in MATLAB. Controls are developed using a nonlinear numerical optimizer, which although impossible to use in real time due to excessive run times, can be used to construct desired trajectories which real-time controllers can be mapped to approximate.

5.1 Code Structure

The code set used in this study consists of a series of MATLAB functions. The master file is first used to set parameters such as control point resolution and final time, then initializes a vector of control inputs at discrete time intervals. The master file then calls the $fmincon$ function, which on each iteration passes the control vector to the nonlinear constraint function. This function in turn calls the trajectory function, which propagates the dynamics of the system for the supplied control vector, linearly interpolating the controls between the discrete control points. The trajectory function passes the state trajectory back to the constraint function, which tests the trajectory against equality and inequality constraints used to set the final condition and to bound the shape states of the quadrotor. The constraint function passes back a pass/fail status to the optimizer. The $fmincon$ optimizer function also passes the control vector at each iteration to the cost function, which calculates the cost using the target cost function,

$$J = \int_0^{t_f} u_i^2 + (u_{throttle} - mg)^2 dt,$$

where u_i is each non-throttle input.

The optimizer builds a Hessian matrix comparing the changes in the cost with respect to variations in each element of the control vector until a local minimum is found. Once a feasible local minimum has been found which satisfies the supplied constraints, the optimizer passes the optimized control vector out to the master file. The master file then passes the optimal control vector again to the trajectory function and receives back the corresponding state trajectory. This trajectory is passed to the animation function, which draws the quadrotor in it's instantaneous state at each control point interval, passing back the still frames to the master file. The master file finally writes the frames to a video, then saves the video, plots of the control inputs and state trajectories, and all control and state trajectory data for later use. A flow chart approximating this structure is shown in Figure 5.1.

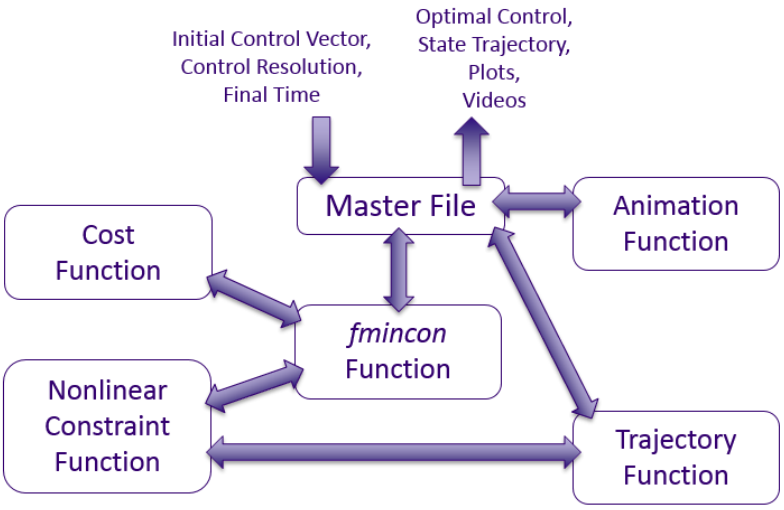

Figure 5.1: Flow diagram for the nonlinear control optimization code.

Each added control input channel increases the length of the optimization vector by the selected control resolution, thus increasing the complexity of the optimization task exponentially. As a result, the model needed to be simplified to the greatest possible extent while still demonstrating unique capabilities. Toward this end, the four throttles were assumed to

remain identical, with all attitude authority derived from the motion of the motors relative to the CG. Additionally, all motors are assumed to remain at the outer extreme of the arms, yielding all control to the arm angles.

5.2 1D Translation

This code structure was initially developed in 2D, balancing all roll and yaw forces such that rotation and translation occur only in the x, z, and θ directions. The first trial run to validate the code further simplified the model to 1D by setting the vertical component of the thrust to equal the weight of the vehicle using the reciprocal cosine function, or secant:

$$u_{total} = \frac{m_{total}g}{c_\theta} = m_{total}gsec(\theta).$$

This initial test thus used only a single input: the angular acceleration of the arms, $\ddot{\alpha}_\theta$. The quadrotor was commanded to move three meters to the right from the origin, beginning and ending at a stationary hover, and the trajectory was propagated using fixed-step 4th order Runge-Kutta numerical approximation with a dynamics stepping 100 times faster than the control. The control channel optimizer quickly converged to the input shown in Figure 5.2. The corresponding state trajectories are shown in Figure 5.3.

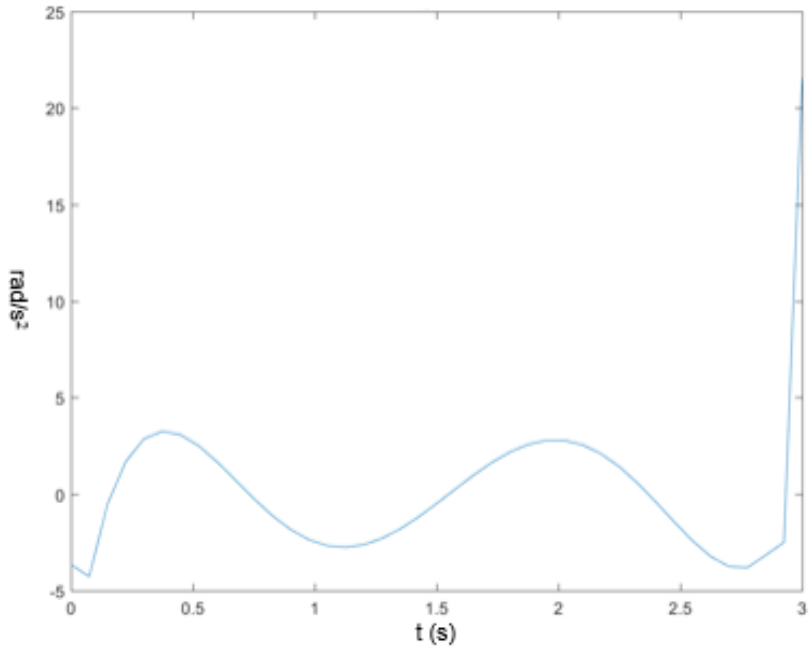

Figure 5.2: Optimal control input shown for three meter 1D translation in three seconds.

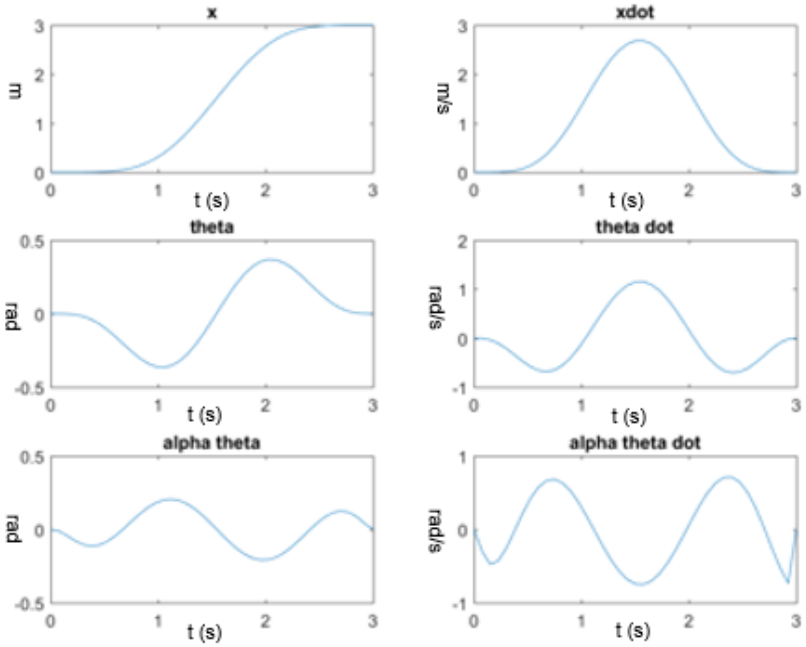

Figure 5.3: Optimal state trajectories shown for three meter 1D translation in three seconds.

As can be seen in the arm angle trajectory, the optimizer converged to a highly believable trajectory, in which the arms move back to pitch the nose down and generate horizontal thrust, then move forward to rotate the vehicle back and brake its movement. The arms then cycle through this pattern one more time to level the quadrotor as it reaches the target location. Overlaying the frames from the animated trajectory as shown in Figure 5.4, one can readily visualize this trajectory, as well as the magnitude of arm movement necessary to achieve the desired trajectory.

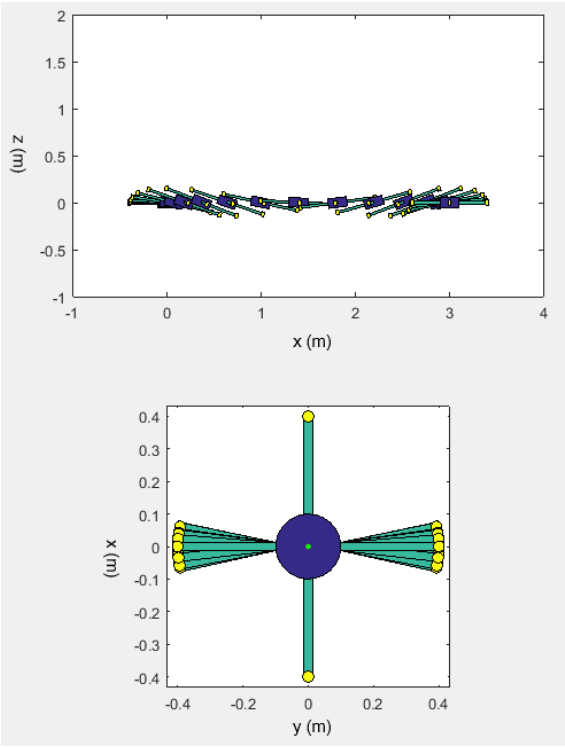

Figure 5.4: Optimal state trajectory for three meter 1D translation in three seconds, shown as overlaid animation frames.

5.3 2D Translation

The code structure has thus been verified for a very simple case. The next case to be investigated is that of the 2D model adding vertical movement. Vertical control is achieved by considering u_{total} as a second control channel. This input will provide both vertical

acceleration and pitching acceleration proportional to the lever arm between the CL and the CG.

The constraint function was modified to give a final state of a stationary, level hover at $[3, 3]$, and the code was run for final times of 2, 3, and 4 seconds. While that shape control was initialized again at zero input, the throttle was initialized near a hover to hasten and improve convergence to an optimal trajectory. Modeling the dynamics using Runge-Kutta produced convergence errors, and thus the code was converted to using Forward Euler approximation, now 300 times faster than the control steps. The optimal control input on both input channels is shown with a 4 second final time in Figure 5.5, and with a 3 second final time in Figure 5.6.

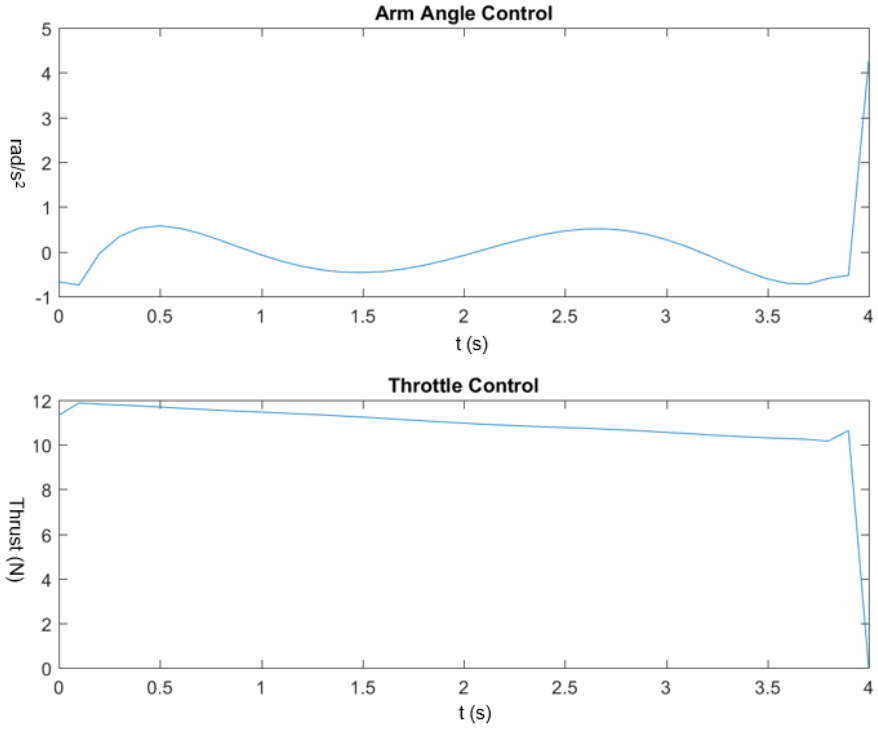

Figure 5.5: Optimal control inputs for arm angle and throttle for a four second move from the origin to $[3, 3]$.

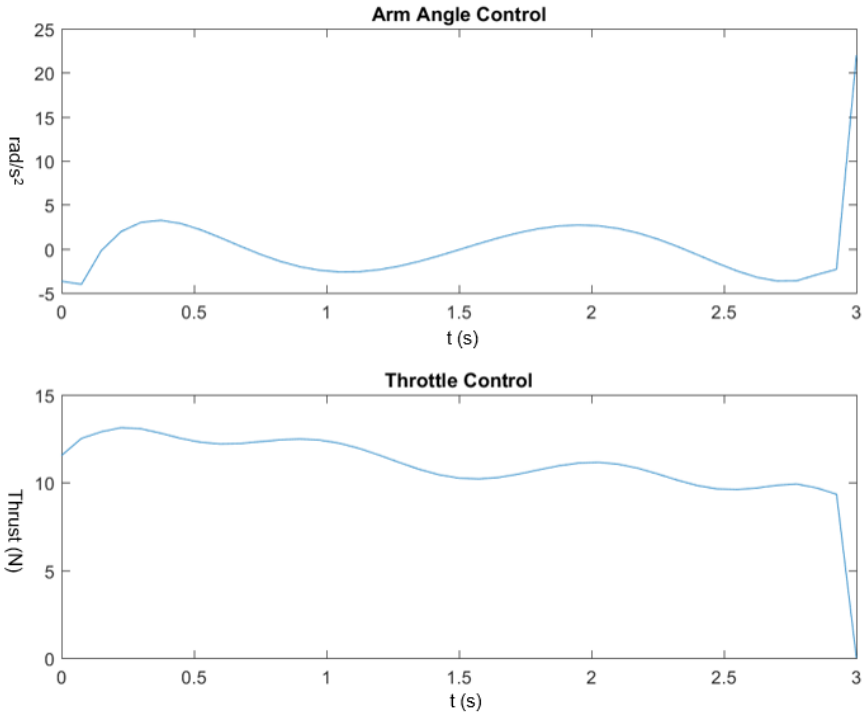

Figure 5.6: Optimal control inputs for arm angle and throttle for a three second move from the origin to $[3, 3]$.

The arm inputs again take a similar form to that observed in the 1D translational case. The throttle control exhibits interesting behavior however, as reducing the final time leads to an oscillatory optimal thrust. This is the result of synchronization with the vehicle pitch and arm angles to apply maximum thrust force when it best contributes to the required pitching and vertical actuation. This become much more noticeable when the final time is reduced to two seconds, as shown in Figure 5.7, in which the optimal throttle input even calls for shutting down the motors entirely and coasting for a brief period.

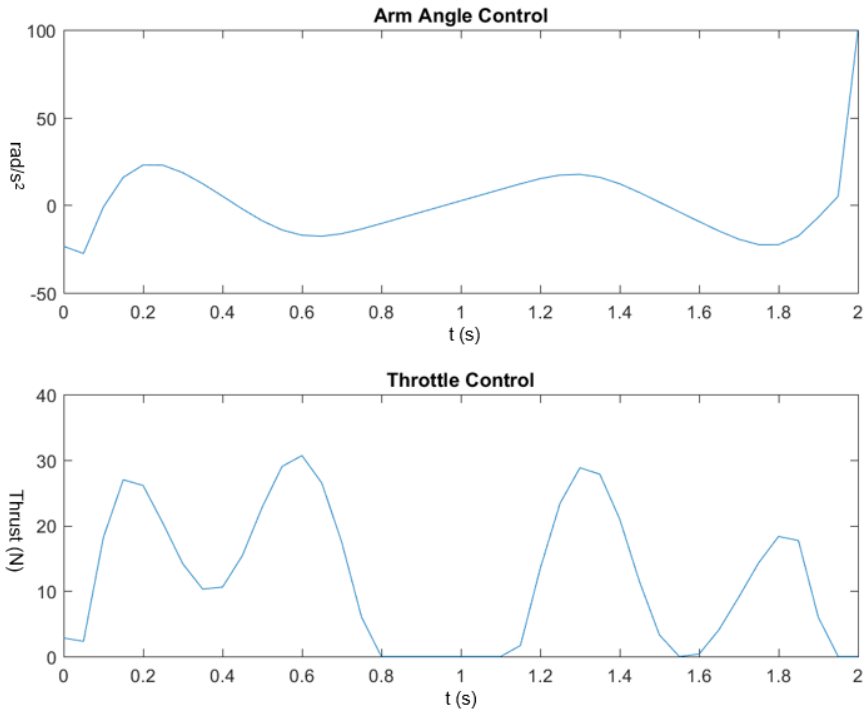

Figure 5.7: Optimal control inputs for arm angle and throttle for a two second move from the origin to $[3, 3]$. Note the total shutdown of the throttle during which the vehicle is coasting in free fall.

The state trajectories for the three cases assume very similar forms to one another, with variance observed primarily in angular and velocity magnitudes. While the four second and three second trajectories are very similar, the two second trajectory does show noteworthy plateauing and freefall due to the throttle shutdown. The trajectories for the three second and two second cases are shown in Figures 5.8 and 5.9.

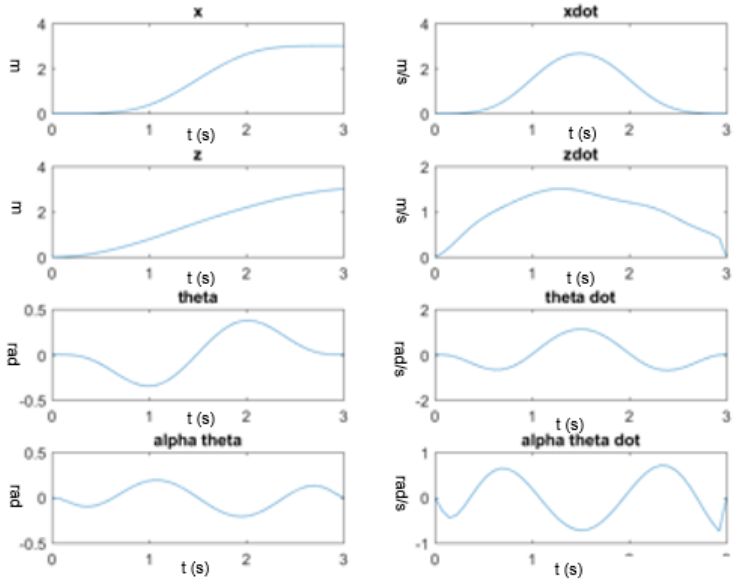

Figure 5.8: Optimal state trajectories from the origin to $[3, 3]$ with a final time of three seconds.

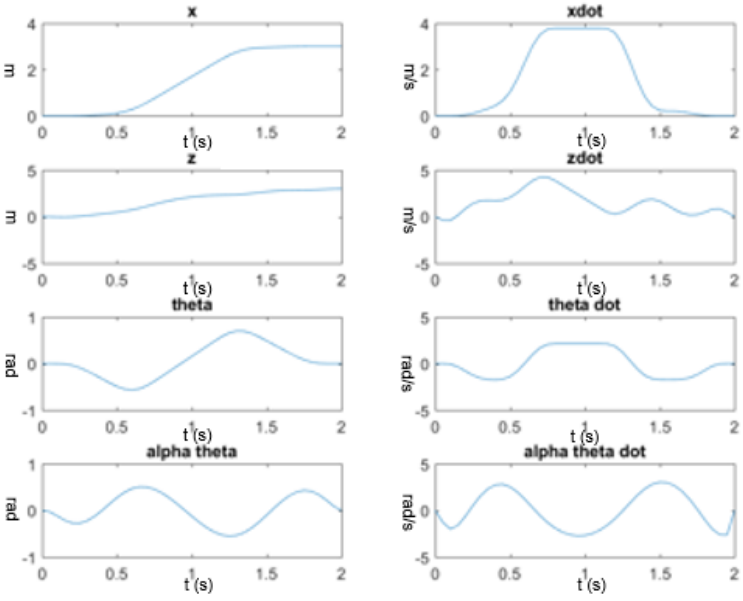

Figure 5.9: Optimal state trajectories from the origin to $[3, 3]$ with a final time of two seconds. Note the plateau in x velocity and the free-fall in z velocity.

The animation frames from these two studies show an excellent comparison of the arm angles magnitudes and spatial behavior of each trajectory. The overlaid animation frames of the three second and two second trajectories are shown in Figures 5.10 and 5.11, respectively.

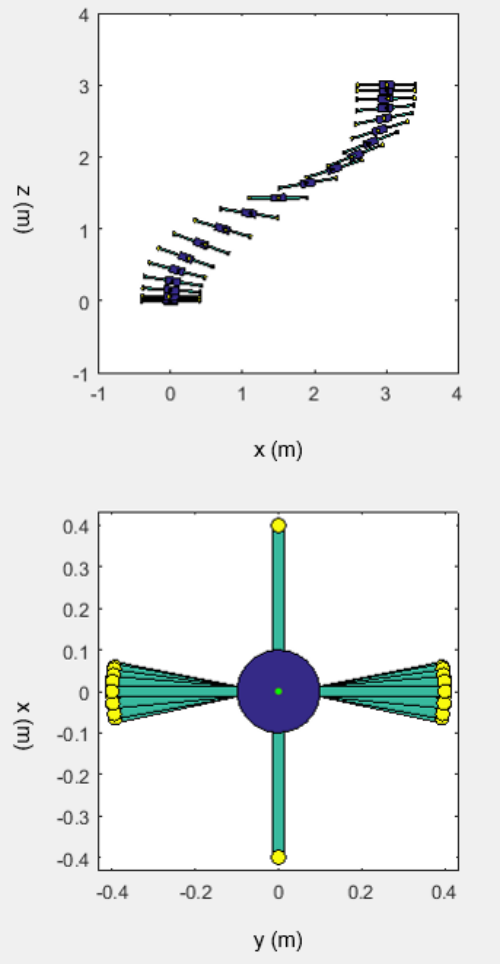

Figure 5.10: Overlaid animation frames for 2D trajectory animation with three second final time.

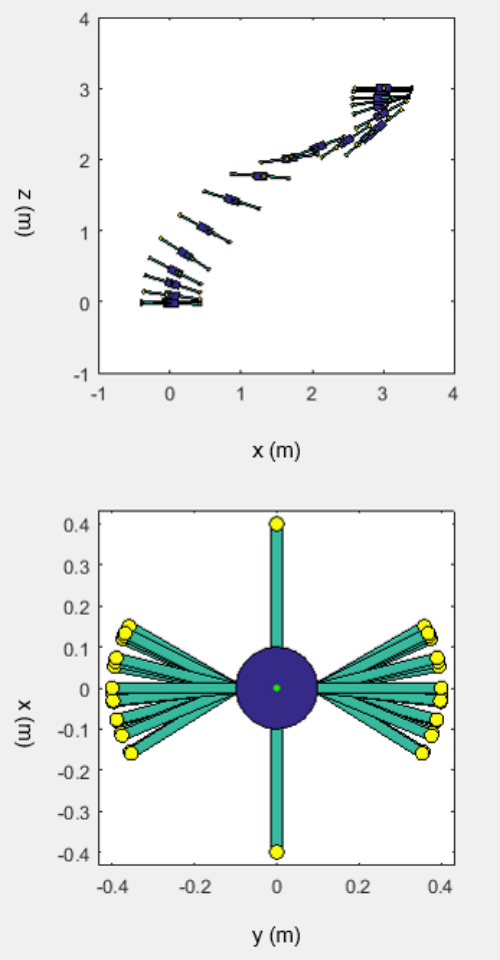

Figure 5.11: Overlaid animation frames for 2D trajectory animation with two second final time.

It is worth noting the speed of arm movement in Figure 5.11. The frames are approximately 0.1 seconds apart, and significant arm movement is observed between frames. This can be confirmed by noting the angular velocity in Figure 5.9 reaches magnitudes of approximately four radians per second. This angular velocity is likely not physically achievable with the oscillatory period required to actuate the vehicle. This will be worth studying before attempting to implement geometric control on a physical prototype to quantify limits arising from available hardware performance saturation.

5.4 3D Translation

The final tested version of the model adds three additional degrees of freedom: y, ϕ, and α_ϕ, as well as a single additional control channel, $\ddot{\alpha_\phi}$. The 3D model was initialized at the origin and commanded to move to $[3, 3, 3]$. The final time of two seconds was found to produce extremely unrealistic behavior, and thus the optimization was run only for final times of five, four, and three seconds. The results for five and four seconds were found to be very similar, and therefore the five second case results have been omitted here for brevity. The optimal controls for the four and three second cases can be found in Figures 5.12 and 5.13.

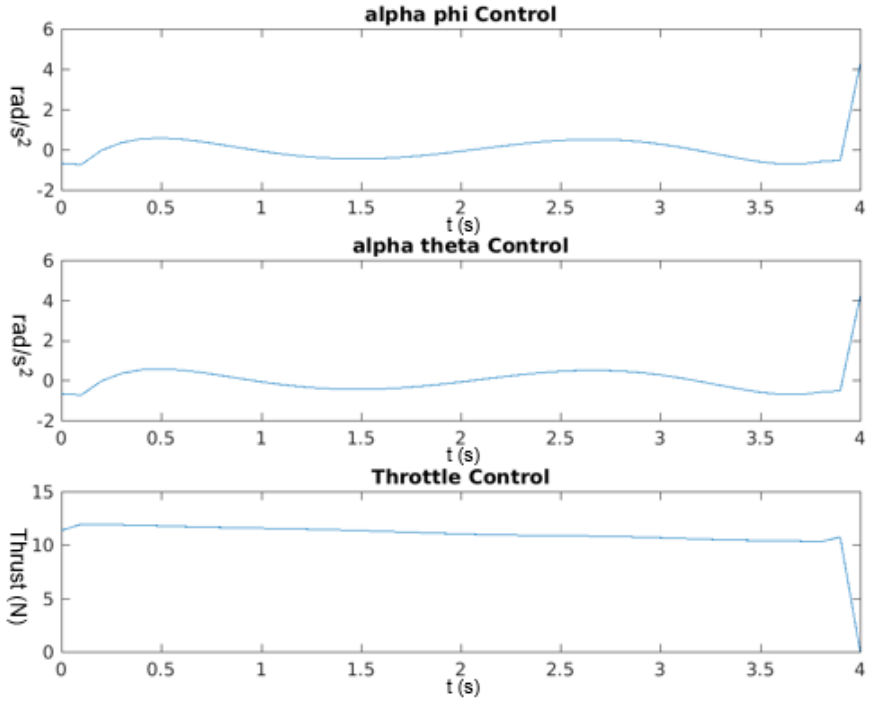

Figure 5.12: Optimal control inputs for arm angles and throttle for a four second move from the origin to $[3, 3, 3]$.

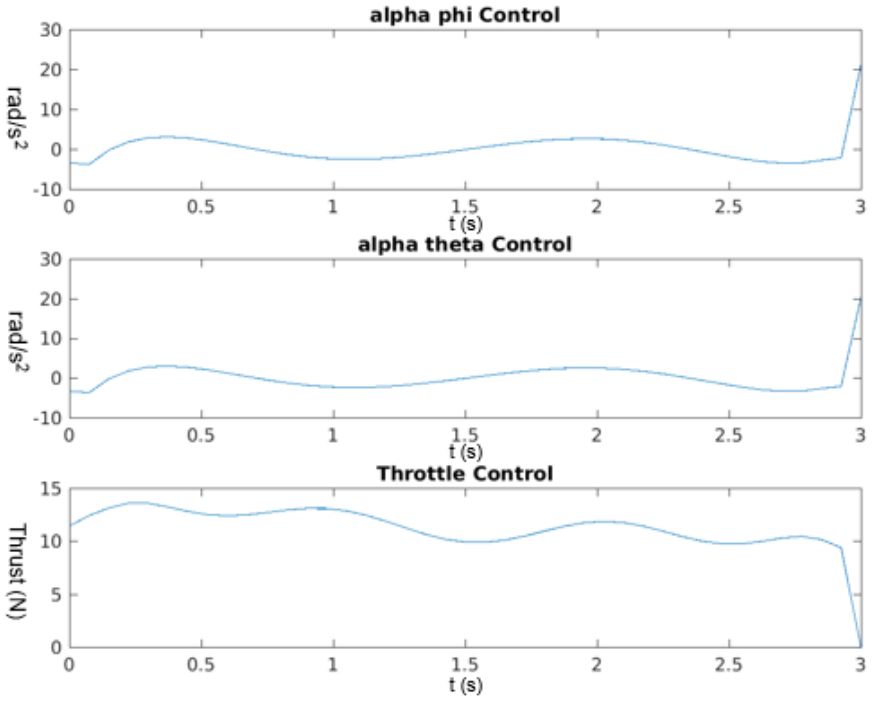

Figure 5.13: Optimal control inputs for arm angles and throttle for a three second move from the origin to $[3, 3, 3]$.

Behavior is again very similar to that observed in the 2D case. The arm angles are found to match perfectly, which matches intuition considering the vehicle is seeking equal displacement in both x and y, and thus will utilize equal rotation in ϕ and θ. Throttle modulation taking advantage of configuration begins to appear in the three second case as well. The state trajectories for both of these cases are exceedingly similar in form, as seen in Figures 5.14 and 5.15.

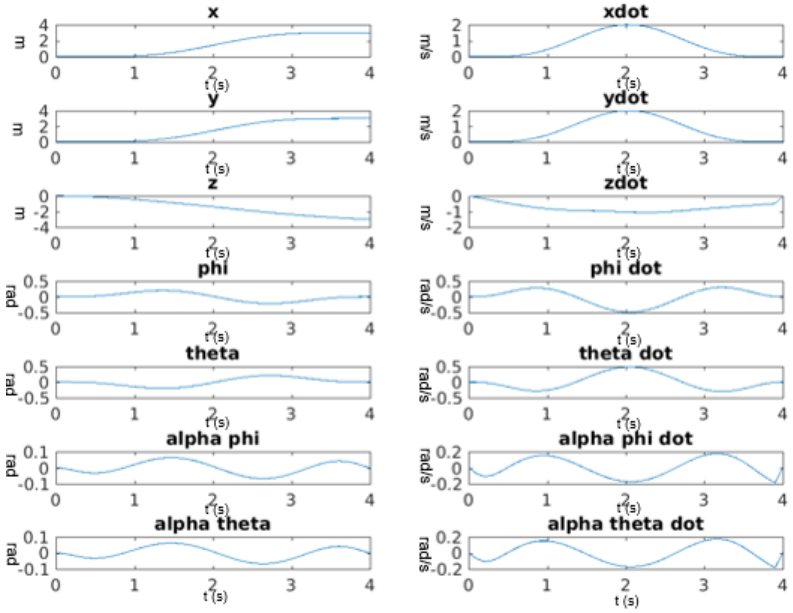

Figure 5.14: Optimal state trajectories from the origin to $[3, 3, 3]$ with a final time of four seconds.

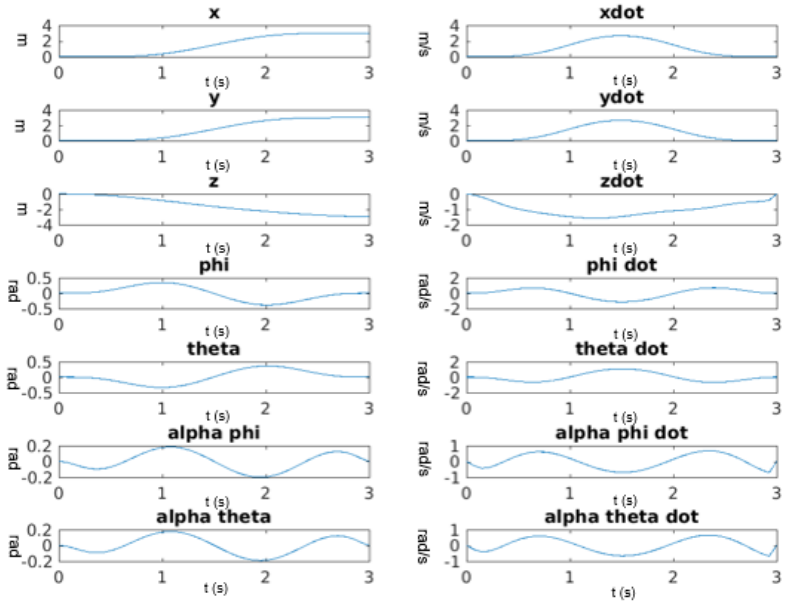

Figure 5.15: Optimal state trajectories from the origin to $[3, 3, 3]$ with a final time of three seconds.

The quadrotor's trajectory is visualized for the three second case only in Figure 5.16.

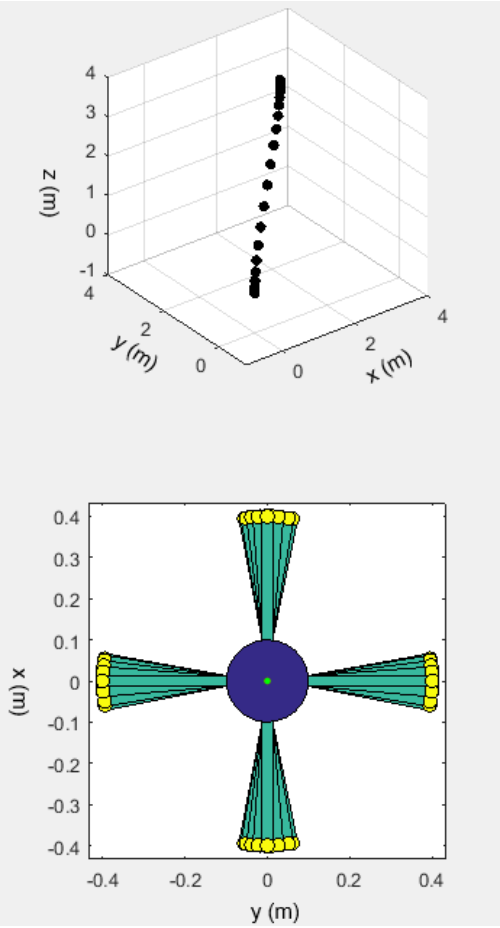

Figure 5.16: Overlaid animation frames for 3D trajectory animation with three second final time.

The quadrotor has thus been verified to be controllable in simulation in three dimensions through simultaneous actuation of pitch and roll via arm angle modulation. It is worth noting in this simple model, the vehicle is unforced in the ψ dimension and thus that degree of freedom can be excluded, however to allow a physical prototype to respond to ψ perturbations, an additional control input could be necessary, either in differential throttling between the motor pairs spinning each direction, or though the use of thrust vanes installed beneath the propellers. Additionally, this model excludes conservation of angular momentum quan-

tified in the $\dot{I}\omega$ term in the momentum form of Newton's Second Law, assuming a relatively constant momentum and/or low angular velocity in pitch and roll. Initial trials including this conservation were run, but found due to symbolic substitution at each dynamic step to slow the time per iteration to in excess of five minutes compared to the fractions of a second observed in these studies necessary to execute tens or even hundreds of thousands of iterations to reach convergence. This remains an area for future development in this topic.

Chapter 6

CONCLUSION

6.1 Conclusion

This research has been a broad initial examination of the dynamics and unique capabilities of the Robodub patented variable geometry morphing quadrotor. In Chapter 1, background material was provided pertaining to the development of the industry and utilization of drones, and in particular quadrotors. The chapter then examined proceeding work pertinent to quadrotor control development, and proposed the concept of the morphing quadrotor, along with its unique target capabilities.

In Chapter 2, mathematical and geometric definitions for the variable-geometry quadrotor were given. A full dynamic model was then derived assuming direct shape control. Quantification of reaction torques acting on the body was troublesome, and therefore a simplified symmetric model was constructed which continued to offer all unique target capabilities intended for investigation in this study. The dynamics of this symmetric model were found. Lastly, numerical values for a generic hobby-sized quadrotor were declared to allow for numerical calculations going forward into control development.

Chapter 3 investigated control of the complete system using LQR with a linearization about a hover at the origin with arms perpendicular and motors at the mid spans of the arms. The controller was found to be stabilizing, although it did not return to the origin in z translation. LQR controls were next calculated for the trirotor configuration to which the quadrotor would transform in the event of a motor loss. The linearized dynamics produced a controllability matrix which was full row rank, indicating the system should be controllable, however the nonlinear dynamics were found to be unstable in every dimension when applying the LQR gains. With the controllable matrix, LQR shows promise, however without a stable

controller at this point, this remains an area for future work.

Chapter 4 proposed the utilization of Set Point LQR Gain Scheduling to control the quadrotor during shape transitions by modeling it as a series of fixed-geometry quadrotors and passing through the various gain sets during a transformation. A simple transformation was modeled and an initial study using set points only at the beginning and end shapes showed great promise for rapid restabilization of the system. Increasing to three set points was found to dramatically decrease the pitch deviation experienced by the vehicle during the transition, however further increases in set point quantity yield negligible improvement. It was thus concluded three set points will be sufficient for simple shape transitions, although more complex transitions or different LQR cost-weighting matrices may alter this observation.

Chapter 5 considered the possibility of controlling the quadrotor using a single evenly-distributed thrust, and actuating vehicle roll and pitch using arm rotations in place of differential throttling. This was testing using discrete time nonlinear optimal controls calculated using the *fmincon* constrained numerical optimizer in MATLAB. The simulations verified the system to be controllable using arm angle pitch and roll actuation. The results showed strong control authority, with magnitudes of arm movements highly dependent on target flight duration. Short time periods produced optimal inputs beyond the reasonable capabilities of physical actuators however, so it will be important to consider actuator saturation for determining limits of operation in a physical prototype. Additionally, calculation times were long and therefore the control strategy is incapable of being applied in real time, however the nonlinear controls could be used to develop optimal target trajectories about which a real-time controller could be flown. The code is readily adaptable to various conditions and situations, and therefore shows potential for future studies.

6.2 Recommendations for Future Work

The dynamic model is mostly complete and allowed for considerable development and evaluation of unique vehicle capabilities. The next step for further developing the model will be to

quantify the internal torques resulting from asymmetric shape changes, thus allowing the full 14 DOF dimensionality of the quadrotor to be modeled. Once this is accomplished, the next major step to advance the dynamic model is to derive the model for the exact control channels to be used in the physical prototype, whether they be torques, velocities, voltage inputs, or any combination thereof. The fidelity of the model can further be improved by accounting for propeller dynamics including gyroscopic effects, lift interferences, and P-factor, as well as accounting for drag forces acting on the body and propellers. A potential reference for accounting these effects is [25], which develops a thorough dynamic model for a rigid-body quadrotor.

The LQR controller was found to stabilize the quadrotor, however the controller did not produce consistent returns to the origin. The first step necessary from this point is to identify the root cause of the nonconvergence to the origin and address it. Once that is complete, the LQR should be developed for additional flight maneuvers, beginning with simple trajectory tracking. The linearization of the system in the trirotor configuration after recovery from a motor loss should be scrutinized, as there is a suspected sign inversion resulting from an yet to be identified error in the code. Further troubleshooting of this code should result in controllability of the nonlinear trirotor model, as the controllability of the linearized model was confirmed using the controllability matrix.

LQR Set Point Control showed promise for controlling the vehicle during shape transformations prescribed to meet mission objectives, and therefore should be further developed as well. Similarly to the full model LQR, the controller was found to be stabilizing, but failed to produce a return to the origin. If the source of this error is identified for the full model, the correction will likely be similar in application to the set point model. Once the convergence issue has been addressed, a wide variety of transition shapes and durations should be tested to determine in which operations the three set-point result continues to be valid. Once a strong understanding of set point requirements has been gathered, a library of gain sets should be calculated for expected transitions between probable operating shapes, and the gain library should be tested on a flying prototype using shape state feedback to determine

which gain set is applicable.

The nonlinear control optimizer and simulator scripts are working and are written to be easily modifiable. They are ready for additional tests such as modeling sliding motor control, differential throttling, and any other desired combination of inputs, although increasing the number of input channels does lead to exponential growth in run time durations. The numerical accuracy of the simulations can be improved by converting the trajectory function to again use 4th order Runge-Kutta, possibly through MATLAB's *ode*45 function, as well as running the model at higher control resolutions than the 41 point models used in Chapter 5. Considering arm angle pitch and roll actuation of the vehicle, optimal trajectories can continue to be mapped using the numerical solver, however real-time control for physical prototyping could readily be achived through the implementation of LQR on the variable arm angle model.

BIBLIOGRAPHY

[1] D. Boddington, *Radio-controlled Model Aircraft*. Crowood Press, 2004.

[2] R. Whittle, *Predator: The Secret Origins of the Drone Revolution*. Macmillan, 2014.

[3] U.S. Air Force, "RQ-11B Raven." http://www.af.mil/AboutUs/FactSheets/Display/tabid/224/Article 11b-raven.aspx, October 2007.

[4] R. Varrier, "Drones are providing film and tv viewers a new perspective on the action." http://www.latimes.com/entertainment/envelope/cotown/la-et-ct-drones-hollywood-20151008-story.html, October 2015.

[5] Amazon, "Amazon prime air." http://www.amazon.com/b?node=8037720011, February 2016.

[6] DHL, "Dhl parcelcopter launches initial operations for research purposes." http://www.dhl.com/en/press/releases, September 2014.

[7] BBC, "Google plans drone delivery service for 2017." http://www.bbc.com/news/technology-34704868, November 2015.

[8] "Drone racing league." http://thedroneracingleague.com/, February 2016.

[9] S. Bouabdallah, A. Noth, and R. Siegwart, "Pid vs lq control techniques applied to an indoor micro quadrotor," in *Intelligent Robots and Systems, 2004. (IROS 2004). Proceedings. 2004 IEEE/RSJ International Conference on*, vol. 3, pp. 2451–2456 vol.3, Sept 2004.

[10] N. Michael, D. Mellinger, Q. Lindsey, and V. Kumar, "The grasp multiple micro-uav testbed," *IEEE Robotics Automation Magazine*, vol. 17, pp. 56–65, Sept 2010.

[11] D. Mellinger, N. Michael, M. Shomin, and V. Kumar, "Recent advances in quadrotor capabilities," in *Robotics and Automation (ICRA), 2011 IEEE International Conference on*, pp. 2964–2965, May 2011.

[12] D. Mellinger and V. Kumar, "Minimum snap trajectory generation and control for quadrotors," in *Robotics and Automation (ICRA), 2011 IEEE International Conference on*, pp. 2520–2525, May 2011.

[13] S. Sadr, S. A. A. Moosavian, and P. Zarafshan, "Dynamics modeling and control of a quadrotor with swing load," *Journal of Robotics*, vol. 2014, 2014.

[14] A. Faust, I. Palunko, P. Cruz, R. Fierro, and L. Tapia, "Learning swing-free trajectories for uavs with a suspended load," in *Robotics and Automation (ICRA), 2013 IEEE International Conference on*, pp. 4902–4909, May 2013.

[15] A. E. Jimenez-Cano, J. Martin, G. Heredia, A. Ollero, and R. Cano, "Control of an aerial robot with multi-link arm for assembly tasks," in *Robotics and Automation (ICRA), 2013 IEEE International Conference on*, pp. 4916–4921, May 2013.

[16] J. Villagomez, M. Vargas, and F. Rubio, "Backstepping and sliding-mode techniques applied to an underactuated camera onboard a rotorcraft mav," in *3rd Workshop on Visual Control of Mobile Robots, Vicomor*, pp. 1–7, 2014.

[17] J. P. Dyhr, N. J. Cowan, D. J. Colmenares, K. A. Morgansen, and T. L. Daniel, "Autostabilizing airframe articulation: Animal inspired air vehicle control," in *Decision and Control (CDC), 2012 IEEE 51st Annual Conference on*, pp. 3715–3720, IEEE, 2012.

[18] J. D. Becker, *Modeling and Control of a Quadrotor with Dynamic Inertia*. PhD thesis, 2013.

[19] F. Senkul and E. Altug, "Modeling and control of a novel tilt - roll rotor quadrotor uav," in *Unmanned Aircraft Systems (ICUAS), 2013 International Conference on*, pp. 1071–1076, May 2013.

[20] K. T. Oner, E. Cetinsoy, M. Unel, M. F. Aksit, I. Kandemir, and K. Gulez, "Dynamic model and control of a new quadrotor unmanned aerial vehicle with tilt-wing mechanism," *World Academy of Science, Engineering and Technology*, vol. 45, 2008.

[21] S. Datta, "Multicopters with variable flight characteristics," July 2015.

[22] L. M. Argentim, W. C. Rezende, P. E. Santos, and R. A. Aguiar, "Pid, lqr and lqr-pid on a quadcopter platform," in *Informatics, Electronics Vision (ICIEV), 2013 International Conference on*, pp. 1–6, May 2013.

[23] M. W. Mueller and R. D'Andrea, "Stability and control of a quadrocopter despite the complete loss of one, two, or three propellers," in *Robotics and Automation (ICRA), 2014 IEEE International Conference on*, pp. 45–52, IEEE, 2014.

[24] D. W. Yoo, H. D. Oh, D. Y. Won, and M. J. Tahk, "Dynamic modeling and control system design for tri-rotor uav," in *Systems and Control in Aeronautics and Astronautics (ISSCAA), 2010 3rd International Symposium on*, pp. 762–767, June 2010.

[25] A. Tayebi and S. McGilvray, "Attitude stabilization of a vtol quadrotor aircraft," *IEEE Transactions on control systems technology*, vol. 14, no. 3, pp. 562–571, 2006.

Appendix A

FULL FORM DYNAMIC EQUATIONS

This appendix shows the full-form symbolic dynamic equations for the simplified symmetric model, including both the CG-frame and body-frame translational dynamics. All equations were calculated in Mathematica using the process in Chapter 2.3 and 2.4.

A.1 $\ddot{x_{CG}}$

$(s_\theta(-u_A - u_B - u_C - u_D))/(m_{armA} + m_{armB} + m_{armC} + m_{armD} + m_{body} + m_{motA} + m_{motB} + m_{motC} + m_{motD})$

A.2 $\ddot{y_{CG}}$

$(c_\theta s_\phi(u_A + u_B + u_C + u_D))/(m_{armA} + m_{armB} + m_{armC} + m_{armD} + m_{body} + m_{motA} + m_{motB} + m_{motC} + m_{motD})$

A.3 $\ddot{z_{CG}}$

$g - (c_\theta c_\phi(u_A + u_B + u_C + u_D))/(m_{armA} + m_{armB} + m_{armC} + m_{armD} + m_{body} + m_{motA} + m_{motB} + m_{motC} + m_{motD})$

A.4 $\ddot{x}$

$(-c_\theta c_\psi(2m_{motA}\ddot{d_A}c_{\alpha_\phi} - 2m_{motC}\ddot{d_A}c_{\alpha_\phi} - 4m_{motA}\dot{d_A}\dot{\alpha_\phi}s_{\alpha_\phi} + 4m_{motC}\dot{d_A}\dot{\alpha_\phi}s_{\alpha_\phi} - 2m_{motA}d_A\ddot{\alpha_\phi}s_{\alpha_\phi} - 2m_{motA}d_A\dot{\alpha_\phi}^2c_{\alpha_\phi} + 2m_{motC}d_A\ddot{\alpha_\phi}s_{\alpha_\phi} + 2m_{motC}d_A\dot{\alpha_\phi}^2c_{\alpha_\phi} + 2m_{motB}\ddot{d_B}s_{\alpha_\theta} + 2m_{motD}\ddot{d_B}s_{\alpha_\theta} + 4(m_{motB} + m_{motD})\dot{d_B}\dot{\alpha_\theta}c_{\alpha_\theta} + \dot{\alpha_\theta}^2s_{\alpha_\theta}(-(2d_B(m_{motB} + m_{motD}) + l_Bm_{armB} + l_Dm_{armD})) + 2m_{motB}d_B\ddot{\alpha_\theta}c_{\alpha_\theta} + 2m_{motD}d_B\ddot{\alpha_\theta}c_{\alpha_\theta} - l_Am_{armA}\ddot{\alpha_\phi}s_{\alpha_\phi} - l_Am_{armA}\dot{\alpha_\phi}^2c_{\alpha_\phi} + l_Bm_{armB}\ddot{\alpha_\theta}c_{\alpha_\theta} + l_Cm_{armC}\ddot{\alpha_\phi}s_{\alpha_\phi} + l_Cm_{armC}\dot{\alpha_\phi}^2c_{\alpha_\phi} + l_Dm_{armD}\ddot{\alpha_\theta}c_{\alpha_\theta}) + (s_\theta c_\psi s_\phi + s_\psi c_\phi)(2m_{motA}\ddot{d_A}s_{\alpha_\phi} +$

$2m_{motC}\ddot{d_A}s_{\alpha_\phi} + 4m_{motA}\dot{d_A}\dot{\alpha_\phi}c_{\alpha_\phi} + 4m_{motC}\dot{d_A}\dot{\alpha_\phi}c_{\alpha_\phi} + 2m_{motA}d_A\ddot{\alpha_\phi}c_{\alpha_\phi} - 2m_{motA}d_A\dot{\alpha_\phi}^2 s_{\alpha_\phi} + 2m_{motC}d_A\ddot{\alpha_\phi}c_{\alpha_\phi} - 2m_{motC}d_A\dot{\alpha_\phi}^2 s_{\alpha_\phi} - 2m_{motB}\ddot{d_B}c_{\alpha_\theta} + 2m_{motD}\ddot{d_B}c_{\alpha_\theta} + 4(m_{motB} - m_{motD})\dot{d_B}\dot{\alpha_\theta}s_{\alpha_\theta} + \dot{\alpha_\theta}^2 c_{\alpha_\theta}(2d_B(m_{motB} - m_{motD}) + l_B m_{armB} - l_D m_{armD}) + 2m_{motB}d_B\ddot{\alpha_\theta}s_{\alpha_\theta} - 2m_{motD}d_B\ddot{\alpha_\theta}s_{\alpha_\theta} + l_A m_{armA}\ddot{\alpha_\phi}c_{\alpha_\phi} - l_A m_{armA}\dot{\alpha_\phi}^2 s_{\alpha_\phi} + l_B m_{armB}\ddot{\alpha_\theta}s_{\alpha_\theta} + l_C m_{armC}\ddot{\alpha_\phi}c_{\alpha_\phi} - l_C m_{armC}\dot{\alpha_\phi}^2 s_{\alpha_\phi} - l_D m_{armD}\ddot{\alpha_\theta}s_{\alpha_\theta}) - 2s_\theta(u_A + u_B + u_C + u_D))/(2(m_{armA} + m_{armB} + m_{armC} + m_{armD} + m_{body} + m_{motA} + m_{motB} + m_{motC} + m_{motD}))$

A.5 $\ddot{y}$

$(c_\theta s_\psi(2m_{motA}\ddot{d_A}c_{\alpha_\phi} - 2m_{motC}\ddot{d_A}c_{\alpha_\phi} - 4m_{motA}\dot{d_A}\dot{\alpha_\phi}s_{\alpha_\phi} + 4m_{motC}\dot{d_A}\dot{\alpha_\phi}s_{\alpha_\phi} - 2m_{motA}d_A\ddot{\alpha_\phi}s_{\alpha_\phi} - 2m_{motA}d_A\dot{\alpha_\phi}^2 c_{\alpha_\phi} + 2m_{motC}d_A\ddot{\alpha_\phi}s_{\alpha_\phi} + 2m_{motC}d_A\dot{\alpha_\phi}^2 c_{\alpha_\phi} + 2m_{motB}\ddot{d_B}s_{\alpha_\theta} + 2m_{motD}\ddot{d_B}s_{\alpha_\theta} + 4(m_{motB} + m_{motD})\dot{d_B}\dot{\alpha_\theta}c_{\alpha_\theta} + \dot{\alpha_\theta}^2 s_{\alpha_\theta}(-(2d_B(m_{motB} + m_{motD}) + l_B m_{armB} + l_D m_{armD})) + 2m_{motB}d_B\ddot{\alpha_\theta}c_{\alpha_\theta} + 2m_{motD}d_B\ddot{\alpha_\theta}c_{\alpha_\theta} - l_A m_{armA}\ddot{\alpha_\phi}s_{\alpha_\phi} - l_A m_{armA}\dot{\alpha_\phi}^2 c_{\alpha_\phi} + l_B m_{armB}\ddot{\alpha_\theta}c_{\alpha_\theta} + l_C m_{armC}\ddot{\alpha_\phi}s_{\alpha_\phi} + l_C m_{armC}\dot{\alpha_\phi}^2 c_{\alpha_\phi} + l_D m_{armD}\ddot{\alpha_\theta}c_{\alpha_\theta}) + (c_\psi c_\phi - s_\theta s_\psi s_\phi)(2m_{motA}\ddot{d_A}s_{\alpha_\phi} + 2m_{motC}\ddot{d_A}s_{\alpha_\phi} + 4m_{motA}\dot{d_A}\dot{\alpha_\phi}c_{\alpha_\phi} + 4m_{motC}\dot{d_A}\dot{\alpha_\phi}c_{\alpha_\phi} + 2m_{motA}d_A\ddot{\alpha_\phi}c_{\alpha_\phi} - 2m_{motA}d_A\dot{\alpha_\phi}^2 s_{\alpha_\phi} + 2m_{motC}d_A\ddot{\alpha_\phi}c_{\alpha_\phi} - 2m_{motC}d_A\dot{\alpha_\phi}^2 s_{\alpha_\phi} - 2m_{motB}\ddot{d_B}c_{\alpha_\theta} + 2m_{motD}\ddot{d_B}c_{\alpha_\theta} + 4(m_{motB} - m_{motD})\dot{d_B}\dot{\alpha_\theta}s_{\alpha_\theta} + \dot{\alpha_\theta}^2 c_{\alpha_\theta}(2d_B(m_{motB} - m_{motD}) + l_B m_{armB} - l_D m_{armD}) + 2m_{motB}d_B\ddot{\alpha_\theta}s_{\alpha_\theta} - 2m_{motD}d_B\ddot{\alpha_\theta}s_{\alpha_\theta} + l_A m_{armA}\ddot{\alpha_\phi}c_{\alpha_\phi} - l_A m_{armA}\dot{\alpha_\phi}^2 s_{\alpha_\phi} + l_B m_{armB}\ddot{\alpha_\theta}s_{\alpha_\theta} + l_C m_{armC}\ddot{\alpha_\phi}c_{\alpha_\phi} - l_C m_{armC}\dot{\alpha_\phi}^2 s_{\alpha_\phi} - l_D m_{armD}\ddot{\alpha_\theta}s_{\alpha_\theta}) + 2c_\theta s_\phi(u_A + u_B + u_C + u_D))/(2(m_{armA} + m_{armB} + m_{armC} + m_{armD} + m_{body} + m_{motA} + m_{motB} + m_{motC} + m_{motD}))$

A.6 $\ddot{z}$

$-(c_\theta s_\phi(2m_{motA}\ddot{d_A}s_{\alpha_\phi} + 2m_{motC}\ddot{d_A}s_{\alpha_\phi} + 4m_{motA}\dot{d_A}\dot{\alpha_\phi}c_{\alpha_\phi} + 4m_{motC}\dot{d_A}\dot{\alpha_\phi}c_{\alpha_\phi} + 2m_{motA}d_A\ddot{\alpha_\phi}c_{\alpha_\phi} - 2m_{motA}d_A\dot{\alpha_\phi}^2 s_{\alpha_\phi} + 2m_{motC}d_A\ddot{\alpha_\phi}c_{\alpha_\phi} - 2m_{motC}d_A\dot{\alpha_\phi}^2 s_{\alpha_\phi} - 2m_{motB}\ddot{d_B}c_{\alpha_\theta} + 2m_{motD}\ddot{d_B}c_{\alpha_\theta} + 4(m_{motB} - m_{motD})\dot{d_B}\dot{\alpha_\theta}s_{\alpha_\theta} + \dot{\alpha_\theta}^2 c_{\alpha_\theta}(2d_B(m_{motB} - m_{motD}) + l_B m_{armB} - l_D m_{armD}) + 2m_{motB}d_B\ddot{\alpha_\theta}s_{\alpha_\theta} - 2m_{motD}d_B\ddot{\alpha_\theta}s_{\alpha_\theta} + l_A m_{armA}\ddot{\alpha_\phi}c_{\alpha_\phi} - l_A m_{armA}\dot{\alpha_\phi}^2 s_{\alpha_\phi} + l_B m_{armB}\ddot{\alpha_\theta}s_{\alpha_\theta} + l_C m_{armC}\ddot{\alpha_\phi}c_{\alpha_\phi} - l_C m_{armC}\dot{\alpha_\phi}^2 s_{\alpha_\phi} - l_D m_{armD}\ddot{\alpha_\theta}s_{\alpha_\theta}))/(2(m_{armA} + m_{armB} + m_{armC} + m_{armD} + m_{body} + m_{motA} + m_{motB} + m_{motC} + m_{motD})) - (s_\theta(2m_{motA}\ddot{d_A}c_{\alpha_\phi} - 2m_{motC}\ddot{d_A}c_{\alpha_\phi} - 4m_{motA}\dot{d_A}\dot{\alpha_\phi}s_{\alpha_\phi} + 4m_{motC}\dot{d_A}\dot{\alpha_\phi}s_{\alpha_\phi} - 2m_{motA}d_A\ddot{\alpha_\phi}s_{\alpha_\phi} - 2m_{motA}d_A\dot{\alpha_\phi}^2 c_{\alpha_\phi} + 2m_{motC}d_A\ddot{\alpha_\phi}s_{\alpha_\phi} +$

$2m_{motC}d_A\dot{\alpha_\phi}^2c_{\alpha_\phi} + 2m_{motB}\ddot{d_B}s_{\alpha_\theta} + 2m_{motD}\ddot{d_B}s_{\alpha_\theta} + 4(m_{motB} + m_{motD})\dot{d_B}\dot{\alpha_\theta}c_{\alpha_\theta} + \dot{\alpha_\theta}^2s_{\alpha_\theta}(-(2d_B(m_{motB}+m_{motD})+l_Bm_{armB}+l_Dm_{armD})) + 2m_{motB}d_B\ddot{\alpha_\theta}c_{\alpha_\theta} + 2m_{motD}d_B\ddot{\alpha_\theta}c_{\alpha_\theta} - l_Am_{armA}\ddot{\alpha_\phi}s_{\alpha_\phi} - l_Am_{armA}\dot{\alpha_\phi}^2c_{\alpha_\phi} + l_Bm_{armB}\ddot{\alpha_\theta}c_{\alpha_\theta} + l_Cm_{armC}\ddot{\alpha_\phi}s_{\alpha_\phi} + l_Cm_{armC}\dot{\alpha_\phi}^2c_{\alpha_\phi} + l_Dm_{armD}\ddot{\alpha_\theta}c_{\alpha_\theta}))/(2(m_{armA} + m_{armB} + m_{armC} + m_{armD} + m_{body} + m_{motA} + m_{motB} + m_{motC} + m_{motD})) + g - (c_\theta c_\phi(u_A + u_B + u_C + u_D))/(m_{armA} + m_{armB} + m_{armC} + m_{armD} + m_{body} + m_{motA} + m_{motB} + m_{motC} + m_{motD})$

A.7 $\ddot{\phi}$

$(12((u_A + u_B + u_C + u_D)((-b_Bu_B + b_Du_D - (u_B - u_D)c_{\alpha_\theta}d_B + (u_A + u_C)d_As_{\alpha_\phi})/(u_A + u_B + u_C + u_D) - (-2b_Bm_{armB} - l_Bc_{\alpha_\theta}m_{armB} + 2b_Dm_{armD} - 2b_Bm_{motB} + 2b_Dm_{motD} + l_Dm_{armD}c_{\alpha_\theta} - 2(m_{motB} - m_{motD})c_{\alpha_\theta}d_B + l_Am_{armA}s_{\alpha_\phi} + l_Cm_{armC}s_{\alpha_\phi} + 2(m_{motA} + m_{motC})d_As_{\alpha_\phi})/(2(m_{armA} + m_{armB}+m_{armC}+m_{armD}+m_{body}+m_{motA}+m_{motB}+m_{motC}+m_{motD}))) - \frac{1}{12}((6m_{motB}(2b_Dm_{armA} - l_As_{\alpha_\phi}m_{armA} + 2b_Bm_{armB} + 2b_Dm_{armB} + 2b_Dm_{armC} + 2b_Dm_{body} + 2b_Dm_{motA} + 2b_Bm_{motB} + 2b_Dm_{motB} + 2b_Dm_{motC} + l_Bm_{armB}c_{\alpha_\theta} - l_Dm_{armD}c_{\alpha_\theta} + 2(m_{armA} + m_{armB} + m_{armC} + m_{armD} + m_{body}+m_{motA}+2m_{motB}+m_{motC})c_{\alpha_\theta}d_B - l_Cm_{armC}s_{\alpha_\phi} - 2(m_{motA}+m_{motC})d_As_{\alpha_\phi})(-2(m_{motA} + m_{motC})s_{\alpha_\phi}\dot{d_A} + 2(m_{armA} + m_{armB} + m_{armC} + m_{armD} + m_{body} + m_{motA} + 2m_{motB} + m_{motC})c_{\alpha_\theta}\dot{d_B} - l_Bm_{armB}s_{\alpha_\theta}\dot{\alpha_\theta} + l_Dm_{armD}s_{\alpha_\theta}\dot{\alpha_\theta} - 2(m_{armA} + m_{armB} + m_{armC} + m_{armD} + m_{body} + m_{motA} + 2m_{motB} + m_{motC})d_Bs_{\alpha_\theta}\dot{\alpha_\theta} - l_Am_{armA}c_{\alpha_\phi}\dot{\alpha_\phi} - l_Cm_{armC}c_{\alpha_\phi}\dot{\alpha_\phi} - 2(m_{motA} + m_{motC})c_{\alpha_\phi}d_A\dot{\alpha_\phi}))/((m_{armA} + m_{armB} + m_{armC} + m_{armD} + m_{body} + m_{motA} + m_{motB} + m_{motC} + m_{motD})^2) + (6m_{motD}(2b_Dm_{armA} - l_As_{\alpha_\phi}m_{armA} + 2b_Bm_{armB} + 2b_Dm_{armB} + 2b_Dm_{armC} + 2b_Dm_{body} + 2b_Dm_{motA} + 2b_Bm_{motB} + 2b_Dm_{motB} + 2b_Dm_{motC} + l_Bm_{armB}c_{\alpha_\theta} - l_Dm_{armD}c_{\alpha_\theta} + 2(m_{armA}+m_{armB}+m_{armC}+m_{armD}+m_{body}+m_{motA}+2m_{motB}+m_{motC})c_{\alpha_\theta}d_B - l_Cm_{armC}s_{\alpha_\phi} - 2(m_{motA}+m_{motC})d_As_{\alpha_\phi})(-2(m_{motA}+m_{motC})s_{\alpha_\phi}\dot{d_A} + 2(m_{armA}+m_{armB}+m_{armC}+m_{armD} + m_{body} + m_{motA} + 2m_{motB} + m_{motC})c_{\alpha_\theta}\dot{d_B} - l_Bm_{armB}s_{\alpha_\theta}\dot{\alpha_\theta} + l_Dm_{armD}s_{\alpha_\theta}\dot{\alpha_\theta} - 2(m_{armA} + m_{armB} + m_{armC} + m_{armD} + m_{body} + m_{motA} + 2m_{motB} + m_{motC})d_Bs_{\alpha_\theta}\dot{\alpha_\theta} - l_Am_{armA}c_{\alpha_\phi}\dot{\alpha_\phi} - l_Cm_{armC}c_{\alpha_\phi}\dot{\alpha_\phi} - 2(m_{motA}+m_{motC})c_{\alpha_\phi}d_A\dot{\alpha_\phi}))/((m_{armA}+m_{armB}+m_{armC}+m_{armD}+m_{body} + m_{motA} + m_{motB} + m_{motC} + m_{motD})^2) + (6m_{body}(-2b_Bm_{armB} - l_Bc_{\alpha_\theta}m_{armB} + 2b_Dm_{armD} - 2b_Bm_{motB} + 2b_Dm_{motD} + l_Dm_{armD}c_{\alpha_\theta} - 2(m_{motB} - m_{motD})c_{\alpha_\theta}d_B + l_Am_{armA}s_{\alpha_\phi} + l_Cm_{armC}s_{\alpha_\phi} +$

$$2(m_{motA}+m_{motC})d_A s_{\alpha_\phi})(2(m_{motA}+m_{motC})s_{\alpha_\phi}\dot{d_A}-2(m_{motB}-m_{motD})c_{\alpha_\theta}\dot{d_B}+l_B m_{armB}s_{\alpha_\theta}\dot{\alpha_\theta}-$$
$$l_D m_{armD}s_{\alpha_\theta}\dot{\alpha_\theta}+2(m_{motB}-m_{motD})d_B s_{\alpha_\theta}\dot{\alpha_\theta}+l_A m_{armA}c_{\alpha_\phi}\dot{\alpha_\phi}+l_C m_{armC}c_{\alpha_\phi}\dot{\alpha_\phi}+2(m_{motA}+$$
$$m_{motC})c_{\alpha_\phi}d_A\dot{\alpha_\phi}))/((m_{armA}+m_{armB}+m_{armC}+m_{armD}+m_{body}+m_{motA}+m_{motB}+m_{motC}+$$
$$m_{motD})^2)+(6m_{motA}(-2b_B m_{armB}-l_B c_{\alpha_\theta}m_{armB}+2b_D m_{armD}-2b_B m_{motB}+2b_D m_{motD}+$$
$$l_D m_{armD}c_{\alpha_\theta}-2(m_{motB}-m_{motD})c_{\alpha_\theta}d_B+l_A m_{armA}s_{\alpha_\phi}+l_C m_{armC}s_{\alpha_\phi}-2(m_{armA}+m_{armB}+$$
$$m_{armC}+m_{armD}+m_{body}+m_{motB}+m_{motD})d_A s_{\alpha_\phi})(-2(m_{armA}+m_{armB}+m_{armC}+m_{armD}+$$
$$m_{body}+m_{motB}+m_{motD})s_{\alpha_\phi}\dot{d_A}-2(m_{motB}-m_{motD})c_{\alpha_\theta}\dot{d_B}+l_B m_{armB}s_{\alpha_\theta}\dot{\alpha_\theta}-l_D m_{armD}s_{\alpha_\theta}\dot{\alpha_\theta}+$$
$$2(m_{motB}-m_{motD})d_B s_{\alpha_\theta}\dot{\alpha_\theta}+l_A m_{armA}c_{\alpha_\phi}\dot{\alpha_\phi}+l_C m_{armC}c_{\alpha_\phi}\dot{\alpha_\phi}-2(m_{armA}+m_{armB}+m_{armC}+$$
$$m_{armD}+m_{body}+m_{motB}+m_{motD})c_{\alpha_\phi}d_A\dot{\alpha_\phi}))/((m_{armA}+m_{armB}+m_{armC}+m_{armD}+m_{body}+$$
$$m_{motA}+m_{motB}+m_{motC}+m_{motD})^2)+(6m_{motC}(-2b_B m_{armB}-l_B c_{\alpha_\theta}m_{armB}+2b_D m_{armD}-$$
$$2b_B m_{motB}+2b_D m_{motD}+l_D m_{armD}c_{\alpha_\theta}-2(m_{motB}-m_{motD})c_{\alpha_\theta}d_B+l_A m_{armA}s_{\alpha_\phi}+l_C m_{armC}s_{\alpha_\phi}-$$
$$2(m_{armA}+m_{armB}+m_{armC}+m_{armD}+m_{body}+m_{motB}+m_{motD})d_A s_{\alpha_\phi})(-2(m_{armA}+m_{armB}+$$
$$m_{armC}+m_{armD}+m_{body}+m_{motB}+m_{motD})s_{\alpha_\phi}\dot{d_A}-2(m_{motB}-m_{motD})c_{\alpha_\theta}\dot{d_B}+l_B m_{armB}s_{\alpha_\theta}\dot{\alpha_\theta}-$$
$$l_D m_{armD}s_{\alpha_\theta}\dot{\alpha_\theta}+2(m_{motB}-m_{motD})d_B s_{\alpha_\theta}\dot{\alpha_\theta}+l_A m_{armA}c_{\alpha_\phi}\dot{\alpha_\phi}+l_C m_{armC}c_{\alpha_\phi}\dot{\alpha_\phi}-2(m_{armA}+$$
$$m_{armB}+m_{armC}+m_{armD}+m_{body}+m_{motB}+m_{motD})c_{\alpha_\phi}d_A\dot{\alpha_\phi}))/((m_{armA}+m_{armB}+m_{armC}+$$
$$m_{armD}+m_{body}+m_{motA}+m_{motB}+m_{motC}+m_{motD})^2)+m_{armD}(6(2b_D+l_D c_{\alpha_\theta}-(-2b_B m_{armB}-$$
$$l_B c_{\alpha_\theta}m_{armB}+2b_D m_{armD}-2b_B m_{motB}+2b_D m_{motD}+l_D m_{armD}c_{\alpha_\theta}-2(m_{motB}-m_{motD})c_{\alpha_\theta}d_B+$$
$$l_A m_{armA}s_{\alpha_\phi}+l_C m_{armC}s_{\alpha_\phi}+2(m_{motA}+m_{motC})d_A s_{\alpha_\phi})/(m_{armA}+m_{armB}+m_{armC}+m_{armD}+$$
$$m_{body}+m_{motA}+m_{motB}+m_{motC}+m_{motD}))(-l_D s_{\alpha_\theta}\dot{\alpha_\theta}-(2(m_{motA}+m_{motC})s_{\alpha_\phi}\dot{d_A}-2(m_{motB}-$$
$$m_{motD})c_{\alpha_\theta}\dot{d_B}+l_B m_{armB}s_{\alpha_\theta}\dot{\alpha_\theta}-l_D m_{armD}s_{\alpha_\theta}\dot{\alpha_\theta}+2(m_{motB}-m_{motD})d_B s_{\alpha_\theta}\dot{\alpha_\theta}+l_A m_{armA}c_{\alpha_\phi}\dot{\alpha_\phi}+$$
$$l_C m_{armC}c_{\alpha_\phi}\dot{\alpha_\phi}+2(m_{motA}+m_{motC})c_{\alpha_\phi}d_A\dot{\alpha_\phi})/(m_{armA}+m_{armB}+m_{armC}+m_{armD}+m_{body}+$$
$$m_{motA}+m_{motB}+m_{motC}+m_{motD}))-{l_D}^2 s_{2\alpha_\theta}\dot{\alpha_\theta})+m_{armA}(s_{2\alpha_\phi}\dot{\alpha_\phi}{l_A}^2+6(l_A s_{\alpha_\phi}-(-2b_B m_{armB}-$$
$$l_B c_{\alpha_\theta}m_{armB}+2b_D m_{armD}-2b_B m_{motB}+2b_D m_{motD}+l_D m_{armD}c_{\alpha_\theta}-2(m_{motB}-m_{motD})c_{\alpha_\theta}d_B+$$
$$l_A m_{armA}s_{\alpha_\phi}+l_C m_{armC}s_{\alpha_\phi}+2(m_{motA}+m_{motC})d_A s_{\alpha_\phi})/(m_{armA}+m_{armB}+m_{armC}+m_{armD}+$$
$$m_{body}+m_{motA}+m_{motB}+m_{motC}+m_{motD}))(l_A c_{\alpha_\phi}\dot{\alpha_\phi}-(2(m_{motA}+m_{motC})s_{\alpha_\phi}\dot{d_A}-2(m_{motB}-$$
$$m_{motD})c_{\alpha_\theta}\dot{d_B}+l_B m_{armB}s_{\alpha_\theta}\dot{\alpha_\theta}-l_D m_{armD}s_{\alpha_\theta}\dot{\alpha_\theta}+2(m_{motB}-m_{motD})d_B s_{\alpha_\theta}\dot{\alpha_\theta}+l_A m_{armA}c_{\alpha_\phi}\dot{\alpha_\phi}+$$
$$l_C m_{armC}c_{\alpha_\phi}\dot{\alpha_\phi}+2(m_{motA}+m_{motC})c_{\alpha_\phi}d_A\dot{\alpha_\phi})/(m_{armA}+m_{armB}+m_{armC}+m_{armD}+m_{body}+$$
$$m_{motA}+m_{motB}+m_{motC}+m_{motD})))+m_{armC}(s_{2\alpha_\phi}\dot{\alpha_\phi}{l_C}^2+6(l_C s_{\alpha_\phi}-(-2b_B m_{armB}-l_B c_{\alpha_\theta}m_{armB}+$$

$$2b_D m_{armD} - 2b_B m_{motB} + 2b_D m_{motD} + l_D m_{armD} c_{\alpha_\theta} - 2(m_{motB} - m_{motD}) c_{\alpha_\theta} d_B + l_A m_{armA} s_{\alpha_\phi} + l_C m_{armC} s_{\alpha_\phi} + 2(m_{motA} + m_{motC}) d_A s_{\alpha_\phi}) / (m_{armA} + m_{armB} + m_{armC} + m_{armD} + m_{body} + m_{motA} + m_{motB} + m_{motC} + m_{motD}))(l_C c_{\alpha_\phi} \dot{\alpha_\phi} - (2(m_{motA} + m_{motC}) s_{\alpha_\phi} \dot{d_A} - 2(m_{motB} - m_{motD}) c_{\alpha_\theta} \dot{d_B} + l_B m_{armB} s_{\alpha_\theta} \dot{\alpha_\theta} - l_D m_{armD} s_{\alpha_\theta} \dot{\alpha_\theta} + 2(m_{motB} - m_{motD}) d_B s_{\alpha_\theta} \dot{\alpha_\theta} + l_A m_{armA} c_{\alpha_\phi} \dot{\alpha_\phi} + l_C m_{armC} c_{\alpha_\phi} \dot{\alpha_\phi} + 2(m_{motA} + m_{motC}) c_{\alpha_\phi} d_A \dot{\alpha_\phi}) / (m_{armA} + m_{armB} + m_{armC} + m_{armD} + m_{body} + m_{motA} + m_{motB} + m_{motC} + m_{motD}))) + 12 m_{armB}((b_B + \tfrac{1}{2} l_B c_{\alpha_\theta} + (-2b_B m_{armB} - l_B c_{\alpha_\theta} m_{armB} + 2b_D m_{armD} - 2b_B m_{motB} + 2b_D m_{motD} + l_D m_{armD} c_{\alpha_\theta} - 2(m_{motB} - m_{motD}) c_{\alpha_\theta} d_B + l_A m_{armA} s_{\alpha_\phi} + l_C m_{armC} s_{\alpha_\phi} + 2(m_{motA} + m_{motC}) d_A s_{\alpha_\phi}) / (2(m_{armA} + m_{armB} + m_{armC} + m_{armD} + m_{body} + m_{motA} + m_{motB} + m_{motC} + m_{motD})))((2(m_{motA} + m_{motC}) s_{\alpha_\phi} \dot{d_A} - 2(m_{motB} - m_{motD}) c_{\alpha_\theta} \dot{d_B} + l_B m_{armB} s_{\alpha_\theta} \dot{\alpha_\theta} - l_D m_{armD} s_{\alpha_\theta} \dot{\alpha_\theta} + 2(m_{motB} - m_{motD}) d_B s_{\alpha_\theta} \dot{\alpha_\theta} + l_A m_{armA} c_{\alpha_\phi} \dot{\alpha_\phi} + l_C m_{armC} c_{\alpha_\phi} \dot{\alpha_\phi} + 2(m_{motA} + m_{motC}) c_{\alpha_\phi} d_A \dot{\alpha_\phi}) / (m_{armA} + m_{armB} + m_{armC} + m_{armD} + m_{body} + m_{motA} + m_{motB} + m_{motC} + m_{motD}) - l_B s_{\alpha_\theta} \dot{\alpha_\theta}) - \tfrac{1}{6} {l_B}^2 c_{\alpha_\theta} s_{\alpha_\theta} \dot{\alpha_\theta})) \dot{\phi}))) / ((3 m_{motB}(2b_D m_{armA} - l_A s_{\alpha_\phi} m_{armA} + 2b_B m_{armB} + 2b_D m_{armB} + 2b_D m_{armC} + 2b_D m_{body} + 2b_D m_{motA} + 2b_B m_{motB} + 2b_D m_{motB} + 2b_D m_{motC} + l_B m_{armB} c_{\alpha_\theta} - l_D m_{armD} c_{\alpha_\theta} + 2(m_{armA} + m_{armB} + m_{armC} + m_{armD} + m_{body} + m_{motA} + 2m_{motB} + m_{motC}) c_{\alpha_\theta} d_B - l_C m_{armC} s_{\alpha_\phi} - 2(m_{motA} + m_{motC}) d_A s_{\alpha_\phi})^2) / ((m_{armA} + m_{armB} + m_{armC} + m_{armD} + m_{body} + m_{motA} + m_{motB} + m_{motC} + m_{motD})^2) + (3 m_{motD}(2b_D m_{armA} - l_A s_{\alpha_\phi} m_{armA} + 2b_B m_{armB} + 2b_D m_{armB} + 2b_D m_{armC} + 2b_D m_{body} + 2b_D m_{motA} + 2b_B m_{motB} + 2b_D m_{motB} + 2b_D m_{motC} + l_B m_{armB} c_{\alpha_\theta} - l_D m_{armD} c_{\alpha_\theta} + 2(m_{armA} + m_{armB} + m_{armC} + m_{armD} + m_{body} + m_{motA} + 2m_{motB} + m_{motC}) c_{\alpha_\theta} d_B - l_C m_{armC} s_{\alpha_\phi} - 2(m_{motA} + m_{motC}) d_A s_{\alpha_\phi})^2) / ((m_{armA} + m_{armB} + m_{armC} + m_{armD} + m_{body} + m_{motA} + m_{motB} + m_{motC} + m_{motD})^2) + (3 m_{motA}(-2b_B m_{armB} - l_B c_{\alpha_\theta} m_{armB} + 2b_D m_{armD} - 2b_B m_{motB} + 2b_D m_{motD} + l_D m_{armD} c_{\alpha_\theta} - 2(m_{motB} - m_{motD}) c_{\alpha_\theta} d_B + l_A m_{armA} s_{\alpha_\phi} + l_C m_{armC} s_{\alpha_\phi} - 2(m_{armA} + m_{armB} + m_{armC} + m_{armD} + m_{body} + m_{motB} + m_{motD}) d_A s_{\alpha_\phi})^2) / ((m_{armA} + m_{armB} + m_{armC} + m_{armD} + m_{body} + m_{motA} + m_{motB} + m_{motC} + m_{motD})^2) + (3 m_{motC}(-2b_B m_{armB} - l_B c_{\alpha_\theta} m_{armB} + 2b_D m_{armD} - 2b_B m_{motB} + 2b_D m_{motD} + l_D m_{armD} c_{\alpha_\theta} - 2(m_{motB} - m_{motD}) c_{\alpha_\theta} d_B + l_A m_{armA} s_{\alpha_\phi} + l_C m_{armC} s_{\alpha_\phi} - 2(m_{armA} + m_{armB} + m_{armC} + m_{armD} + m_{body} + m_{motB} + m_{motD}) d_A s_{\alpha_\phi})^2) / ((m_{armA} + m_{armB} + m_{armC} + m_{armD} + m_{body} + m_{motA} + m_{motB} + m_{motC} + m_{motD})^2) + m_{body}({h_{body}}^2 + 3{\rho_{body}}^2 + (3(-2b_B m_{armB} - l_B c_{\alpha_\theta} m_{armB} + 2b_D m_{armD} - 2b_B m_{motB} + 2b_D m_{motD} + l_D m_{armD} c_{\alpha_\theta} - 2(m_{motB} - m_{motD}) c_{\alpha_\theta} d_B + l_A m_{armA} s_{\alpha_\phi} + l_C m_{armC} s_{\alpha_\phi} + 2(m_{motA} +$$

$m_{motC})d_A s_{\alpha_\phi})^2)/((m_{armA}+m_{armB}+m_{armC}+m_{armD}+m_{body}+m_{motA}+m_{motB}+m_{motC}+m_{motD})^2)) + m_{armD}(l_D{}^2 c_{\alpha_\theta}^2 + 3(2b_D + l_D c_{\alpha_\theta} - (-2b_B m_{armB} - l_B c_{\alpha_\theta} m_{armB} + 2b_D m_{armD} - 2b_B m_{motB} + 2b_D m_{motD} + l_D m_{armD} c_{\alpha_\theta} - 2(m_{motB} - m_{motD}) c_{\alpha_\theta} d_B + l_A m_{armA} s_{\alpha_\phi} + l_C m_{armC} s_{\alpha_\phi} + 2(m_{motA} + m_{motC}) d_A s_{\alpha_\phi})/(m_{armA} + m_{armB} + m_{armC} + m_{armD} + m_{body} + m_{motA} + m_{motB} + m_{motC} + m_{motD}))^2) + m_{armA}(l_A{}^2 s_{\alpha_\phi}^2 + 3(l_A s_{\alpha_\phi} - (-2b_B m_{armB} - l_B c_{\alpha_\theta} m_{armB} + 2b_D m_{armD} - 2b_B m_{motB} + 2b_D m_{motD} + l_D m_{armD} c_{\alpha_\theta} - 2(m_{motB} - m_{motD}) c_{\alpha_\theta} d_B + l_A m_{armA} s_{\alpha_\phi} + l_C m_{armC} s_{\alpha_\phi} + 2(m_{motA} + m_{motC}) d_A s_{\alpha_\phi})/(m_{armA} + m_{armB} + m_{armC} + m_{armD} + m_{body} + m_{motA} + m_{motB} + m_{motC} + m_{motD}))^2) + m_{armC}(l_C{}^2 s_{\alpha_\phi}^2 + 3(l_C s_{\alpha_\phi} - (-2b_B m_{armB} - l_B c_{\alpha_\theta} m_{armB} + 2b_D m_{armD} - 2b_B m_{motB} + 2b_D m_{motD} + l_D m_{armD} c_{\alpha_\theta} - 2(m_{motB} - m_{motD}) c_{\alpha_\theta} d_B + l_A m_{armA} s_{\alpha_\phi} + l_C m_{armC} s_{\alpha_\phi} + 2(m_{motA} + m_{motC}) d_A s_{\alpha_\phi})/(m_{armA} + m_{armB} + m_{armC} + m_{armD} + m_{body} + m_{motA} + m_{motB} + m_{motC} + m_{motD}))^2) + 12 m_{armB}(\frac{1}{12} l_B{}^2 c_{\alpha_\theta}^2 + (b_B + \frac{1}{2} l_B c_{\alpha_\theta} + (-2b_B m_{armB} - l_B c_{\alpha_\theta} m_{armB} + 2b_D m_{armD} - 2b_B m_{motB} + 2b_D m_{motD} + l_D m_{armD} c_{\alpha_\theta} - 2(m_{motB} - m_{motD}) c_{\alpha_\theta} d_B + l_A m_{armA} s_{\alpha_\phi} + l_C m_{armC} s_{\alpha_\phi} + 2(m_{motA} + m_{motC}) d_A s_{\alpha_\phi})/(2(m_{armA} + m_{armB} + m_{armC} + m_{armD} + m_{body} + m_{motA} + m_{motB} + m_{motC} + m_{motD})))^2))$

A.8 $\ddot{\theta}$

$(12((u_A+u_B+u_C+u_D)((b_A u_A - b_C u_C + (u_A - u_C) c_{\alpha_\phi} d_A + (u_B + u_D) d_B s_{\alpha_\theta})/(u_A+u_B+u_C+u_D) - (2b_A m_{armA} + l_A c_{\alpha_\phi} m_{armA} - 2b_C m_{armC} + 2b_A m_{motA} - 2b_C m_{motC} - l_C m_{armC} c_{\alpha_\phi} + 2(m_{motA} - m_{motC}) c_{\alpha_\phi} d_A + l_B m_{armB} s_{\alpha_\theta} + l_D m_{armD} s_{\alpha_\theta} + 2(m_{motB} + m_{motD}) d_B s_{\alpha_\theta})/(2(m_{armA} + m_{armB} + m_{armC} + m_{armD} + m_{body} + m_{motA} + m_{motB} + m_{motC} + m_{motD}))) - \frac{1}{12}((6m_{motB}(2b_A m_{armA} + l_A c_{\alpha_\phi} m_{armA} - 2b_C m_{armC} + 2b_A m_{motA} - 2b_C m_{motC} - l_C m_{armC} c_{\alpha_\phi} + 2(m_{motA} - m_{motC}) c_{\alpha_\phi} d_A + l_B m_{armB} s_{\alpha_\theta} + l_D m_{armD} s_{\alpha_\theta} - 2(m_{armA} + m_{armB} + m_{armC} + m_{armD} + m_{body} + m_{motA} + m_{motC}) d_B s_{\alpha_\theta})(2(m_{motA} - m_{motC}) c_{\alpha_\phi} \dot{d}_A - 2(m_{armA} + m_{armB} + m_{armC} + m_{armD} + m_{body} + m_{motA} + m_{motC}) s_{\alpha_\theta} \dot{d}_B + l_B m_{armB} c_{\alpha_\theta} \dot{\alpha}_\theta + l_D m_{armD} c_{\alpha_\theta} \dot{\alpha}_\theta - 2(m_{armA} + m_{armB} + m_{armC} + m_{armD} + m_{body} + m_{motA} + m_{motC}) c_{\alpha_\theta} d_B \dot{\alpha}_\theta - l_A m_{armA} s_{\alpha_\phi} \dot{\alpha}_\phi + l_C m_{armC} s_{\alpha_\phi} \dot{\alpha}_\phi - 2(m_{motA} - m_{motC}) d_A s_{\alpha_\phi} \dot{\alpha}_\phi))/((m_{armA} + m_{armB} + m_{armC} + m_{armD} + m_{body} + m_{motA} + m_{motB} + m_{motC} + m_{motD})^2) + (6m_{motD}(2b_A m_{armA} + l_A c_{\alpha_\phi} m_{armA} - 2b_C m_{armC} + 2b_A m_{motA} - 2b_C m_{motC} - l_C m_{armC} c_{\alpha_\phi} + 2(m_{motA} - m_{motC}) c_{\alpha_\phi} d_A + l_B m_{armB} s_{\alpha_\theta} + l_D m_{armD} s_{\alpha_\theta} - 2(m_{armA} + m_{armB} +$

$$m_{armC} + m_{armD} + m_{body} + m_{motA} + m_{motC})d_B s_{\alpha_\theta})(2(m_{motA} - m_{motC})c_{\alpha_\phi}\dot{d}_A - 2(m_{armA} + m_{armB} + m_{armC} + m_{armD} + m_{body} + m_{motA} + m_{motC})s_{\alpha_\theta}\dot{d}_B + l_B m_{armB} c_{\alpha_\theta}\dot{\alpha}_\theta + l_D m_{armD} c_{\alpha_\theta}\dot{\alpha}_\theta - 2(m_{armA} + m_{armB} + m_{armC} + m_{armD} + m_{body} + m_{motA} + m_{motC})c_{\alpha_\theta} d_B \dot{\alpha}_\theta - l_A m_{armA} s_{\alpha_\phi}\dot{\alpha}_\phi + l_C m_{armC} s_{\alpha_\phi}\dot{\alpha}_\phi - 2(m_{motA} - m_{motC})d_A s_{\alpha_\phi}\dot{\alpha}_\phi))/((m_{armA} + m_{armB} + m_{armC} + m_{armD} + m_{body} + m_{motA} + m_{motB} + m_{motC} + m_{motD})^2) + (6m_{body}(2b_A m_{armA} + l_A c_{\alpha_\phi} m_{armA} - 2b_C m_{armC} + 2b_A m_{motA} - 2b_C m_{motC} - l_C m_{armC} c_{\alpha_\phi} + 2(m_{motA} - m_{motC})c_{\alpha_\phi} d_A + l_B m_{armB} s_{\alpha_\theta} + l_D m_{armD} s_{\alpha_\theta} + 2(m_{motB} + m_{motD})d_B s_{\alpha_\theta})(2(m_{motA} - m_{motC})c_{\alpha_\phi}\dot{d}_A + 2(m_{motB} + m_{motD})s_{\alpha_\theta}\dot{d}_B + l_B m_{armB} c_{\alpha_\theta}\dot{\alpha}_\theta + l_D m_{armD} c_{\alpha_\theta}\dot{\alpha}_\theta + 2(m_{motB} + m_{motD})c_{\alpha_\theta} d_B \dot{\alpha}_\theta - l_A m_{armA} s_{\alpha_\phi}\dot{\alpha}_\phi + l_C m_{armC} s_{\alpha_\phi}\dot{\alpha}_\phi - 2(m_{motA} - m_{motC})d_A s_{\alpha_\phi}\dot{\alpha}_\phi))/((m_{armA} + m_{armB} + m_{armC} + m_{armD} + m_{body} + m_{motA} + m_{motB} + m_{motC} + m_{motD})^2) + (6m_{motC}(2b_A m_{armA} + 2b_C m_{armA} + l_A c_{\alpha_\phi} m_{armA} + 2b_C m_{armB} + 2b_C m_{armD} + 2b_C m_{body} + 2b_A m_{motA} + 2b_C m_{motA} + 2b_C m_{motB} + 2b_C m_{motD} - l_C m_{armC} c_{\alpha_\phi} + 2(m_{armA} + m_{armB} + m_{armC} + m_{armD} + m_{body} + 2m_{motA} + m_{motB} + m_{motD})c_{\alpha_\phi} d_A + l_B m_{armB} s_{\alpha_\theta} + l_D m_{armD} s_{\alpha_\theta} + 2(m_{motB} + m_{motD})d_B s_{\alpha_\theta})(2(m_{armA} + m_{armB} + m_{armC} + m_{armD} + m_{body} + 2m_{motA} + m_{motB} + m_{motD})c_{\alpha_\phi}\dot{d}_A + 2(m_{motB} + m_{motD})s_{\alpha_\theta}\dot{d}_B + l_B m_{armB} c_{\alpha_\theta}\dot{\alpha}_\theta + l_D m_{armD} c_{\alpha_\theta}\dot{\alpha}_\theta + 2(m_{motB} + m_{motD})c_{\alpha_\theta} d_B \dot{\alpha}_\theta - l_A m_{armA} s_{\alpha_\phi}\dot{\alpha}_\phi + l_C m_{armC} s_{\alpha_\phi}\dot{\alpha}_\phi - 2(m_{armA} + m_{armB} + m_{armC} + m_{armD} + m_{body} + 2m_{motA} + m_{motB} + m_{motD})d_A s_{\alpha_\phi}\dot{\alpha}_\phi))/((m_{armA} + m_{armB} + m_{armC} + m_{armD} + m_{body} + m_{motA} + m_{motB} + m_{motC} + m_{motD})^2) + 24m_{motA}(b_A + c_{\alpha_\phi} d_A - (2b_A m_{armA} + l_A c_{\alpha_\phi} m_{armA} - 2b_C m_{armC} + 2b_A m_{motA} - 2b_C m_{motC} - l_C m_{armC} c_{\alpha_\phi} + 2(m_{motA} - m_{motC})c_{\alpha_\phi} d_A + l_B m_{armB} s_{\alpha_\theta} + l_D m_{armD} s_{\alpha_\theta} + 2(m_{motB} + m_{motD})d_B s_{\alpha_\theta})/(2(m_{armA} + m_{armB} + m_{armC} + m_{armD} + m_{body} + m_{motA} + m_{motB} + m_{motC} + m_{motD})))(c_{\alpha_\phi}\dot{d}_A - d_A s_{\alpha_\phi}\dot{\alpha}_\phi - (2(m_{motA} - m_{motC})c_{\alpha_\phi}\dot{d}_A + 2(m_{motB} + m_{motD})s_{\alpha_\theta}\dot{d}_B + l_B m_{armB} c_{\alpha_\theta}\dot{\alpha}_\theta + l_D m_{armD} c_{\alpha_\theta}\dot{\alpha}_\theta + 2(m_{motB} + m_{motD})c_{\alpha_\theta} d_B \dot{\alpha}_\theta - l_A m_{armA} s_{\alpha_\phi}\dot{\alpha}_\phi + l_C m_{armC} s_{\alpha_\phi}\dot{\alpha}_\phi - 2(m_{motA} - m_{motC})d_A s_{\alpha_\phi}\dot{\alpha}_\phi)/(2(m_{armA} + m_{armB} + m_{armC} + m_{armD} + m_{body} + m_{motA} + m_{motB} + m_{motC} + m_{motD}))) + m_{armB}(s_{2\alpha_\theta}\dot{\alpha}_\theta {l_B}^2 + 6(l_B s_{\alpha_\theta} - (2b_A m_{armA} + l_A c_{\alpha_\phi} m_{armA} - 2b_C m_{armC} + 2b_A m_{motA} - 2b_C m_{motC} - l_C m_{armC} c_{\alpha_\phi} + 2(m_{motA} - m_{motC})c_{\alpha_\phi} d_A + l_B m_{armB} s_{\alpha_\theta} + l_D m_{armD} s_{\alpha_\theta} + 2(m_{motB} + m_{motD})d_B s_{\alpha_\theta})/(m_{armA} + m_{armB} + m_{armC} + m_{armD} + m_{body} + m_{motA} + m_{motB} + m_{motC} + m_{motD}))(l_B c_{\alpha_\theta}\dot{\alpha}_\theta - (2(m_{motA} - m_{motC})c_{\alpha_\phi}\dot{d}_A + 2(m_{motB} + m_{motD})s_{\alpha_\theta}\dot{d}_B + l_B m_{armB} c_{\alpha_\theta}\dot{\alpha}_\theta + l_D m_{armD} c_{\alpha_\theta}\dot{\alpha}_\theta + 2(m_{motB} + m_{motD})c_{\alpha_\theta} d_B \dot{\alpha}_\theta - l_A m_{armA} s_{\alpha_\phi}\dot{\alpha}_\phi + l_C m_{armC} s_{\alpha_\phi}\dot{\alpha}_\phi - 2(m_{motA} - m_{motC})d_A s_{\alpha_\phi}\dot{\alpha}_\phi)/(m_{armA} + m_{armB} + m_{armC} + m_{armD} + m_{body} + m_{motA} + m_{motB} +$$

$$m_{motC} + m_{motD}))) + m_{armD}(s_{2\alpha_\theta}\dot{\alpha_\theta}{l_D}^2 + 6(l_D s_{\alpha_\theta} - (2b_A m_{armA} + l_A c_{\alpha_\phi} m_{armA} - 2b_C m_{armC} + 2b_A m_{motA} - 2b_C m_{motC} - l_C m_{armC} c_{\alpha_\phi} + 2(m_{motA} - m_{motC}) c_{\alpha_\phi} d_A + l_B m_{armB} s_{\alpha_\theta} + l_D m_{armD} s_{\alpha_\theta} + 2(m_{motB} + m_{motD}) d_B s_{\alpha_\theta})/(m_{armA} + m_{armB} + m_{armC} + m_{armD} + m_{body} + m_{motA} + m_{motB} + m_{motC} + m_{motD}))(l_D c_{\alpha_\theta}\dot{\alpha_\theta} - (2(m_{motA} - m_{motC}) c_{\alpha_\phi}\dot{d_A} + 2(m_{motB} + m_{motD}) s_{\alpha_\theta}\dot{d_B} + l_B m_{armB} c_{\alpha_\theta}\dot{\alpha_\theta} + l_D m_{armD} c_{\alpha_\theta}\dot{\alpha_\theta} + 2(m_{motB} + m_{motD}) c_{\alpha_\theta} d_B\dot{\alpha_\theta} - l_A m_{armA} s_{\alpha_\phi}\dot{\alpha_\phi} + l_C m_{armC} s_{\alpha_\phi}\dot{\alpha_\phi} - 2(m_{motA} - m_{motC}) d_A s_{\alpha_\phi}\dot{\alpha_\phi})/(m_{armA} + m_{armB} + m_{armC} + m_{armD} + m_{body} + m_{motA} + m_{motB} + m_{motC} + m_{motD}))) + 12 m_{armA}(2(b_A + \tfrac{1}{2} l_A c_{\alpha_\phi} - (2b_A m_{armA} + l_A c_{\alpha_\phi} m_{armA} - 2b_C m_{armC} + 2b_A m_{motA} - 2b_C m_{motC} - l_C m_{armC} c_{\alpha_\phi} + 2(m_{motA} - m_{motC}) c_{\alpha_\phi} d_A + l_B m_{armB} s_{\alpha_\theta} + l_D m_{armD} s_{\alpha_\theta} + 2(m_{motB} + m_{motD}) d_B s_{\alpha_\theta})/(2(m_{armA} + m_{armB} + m_{armC} + m_{armD} + m_{body} + m_{motA} + m_{motB} + m_{motC} + m_{motD})))(-\tfrac{1}{2} l_A s_{\alpha_\phi}\dot{\alpha_\phi} - (2(m_{motA} - m_{motC}) c_{\alpha_\phi}\dot{d_A} + 2(m_{motB} + m_{motD}) s_{\alpha_\theta}\dot{d_B} + l_B m_{armB} c_{\alpha_\theta}\dot{\alpha_\theta} + l_D m_{armD} c_{\alpha_\theta}\dot{\alpha_\theta} + 2(m_{motB} + m_{motD}) c_{\alpha_\theta} d_B\dot{\alpha_\theta} - l_A m_{armA} s_{\alpha_\phi}\dot{\alpha_\phi} + l_C m_{armC} s_{\alpha_\phi}\dot{\alpha_\phi} - 2(m_{motA} - m_{motC}) d_A s_{\alpha_\phi}\dot{\alpha_\phi})/(2(m_{armA} + m_{armB} + m_{armC} + m_{armD} + m_{body} + m_{motA} + m_{motB} + m_{motC} + m_{motD}))) - \tfrac{1}{6}{l_A}^2 c_{\alpha_\phi} s_{\alpha_\phi}\dot{\alpha_\phi}) + 12 m_{armC}((b_C + \tfrac{1}{2} l_C c_{\alpha_\phi} + (2b_A m_{armA} + l_A c_{\alpha_\phi} m_{armA} - 2b_C m_{armC} + 2b_A m_{motA} - 2b_C m_{motC} - l_C m_{armC} c_{\alpha_\phi} + 2(m_{motA} - m_{motC}) c_{\alpha_\phi} d_A + l_B m_{armB} s_{\alpha_\theta} + l_D m_{armD} s_{\alpha_\theta} + 2(m_{motB} + m_{motD}) d_B s_{\alpha_\theta})/(2(m_{armA} + m_{armB} + m_{armC} + m_{armD} + m_{body} + m_{motA} + m_{motB} + m_{motC} + m_{motD})))((2(m_{motA} - m_{motC}) c_{\alpha_\phi}\dot{d_A} + 2(m_{motB} + m_{motD}) s_{\alpha_\theta}\dot{d_B} + l_B m_{armB} c_{\alpha_\theta}\dot{\alpha_\theta} + l_D m_{armD} c_{\alpha_\theta}\dot{\alpha_\theta} + 2(m_{motB} + m_{motD}) c_{\alpha_\theta} d_B\dot{\alpha_\theta} - l_A m_{armA} s_{\alpha_\phi}\dot{\alpha_\phi} + l_C m_{armC} s_{\alpha_\phi}\dot{\alpha_\phi} - 2(m_{motA} - m_{motC}) d_A s_{\alpha_\phi}\dot{\alpha_\phi})/(m_{armA} + m_{armB} + m_{armC} + m_{armD} + m_{body} + m_{motA} + m_{motB} + m_{motC} + m_{motD}) - l_C s_{\alpha_\phi}\dot{\alpha_\phi}) - \tfrac{1}{6}{l_C}^2 c_{\alpha_\phi} s_{\alpha_\phi}\dot{\alpha_\phi}))\dot{\theta}))/((3m_{motB}(2b_A m_{armA} + l_A c_{\alpha_\phi} m_{armA} - 2b_C m_{armC} + 2b_A m_{motA} - 2b_C m_{motC} - l_C m_{armC} c_{\alpha_\phi} + 2(m_{motA} - m_{motC}) c_{\alpha_\phi} d_A + l_B m_{armB} s_{\alpha_\theta} + l_D m_{armD} s_{\alpha_\theta} - 2(m_{armA} + m_{armB} + m_{armC} + m_{armD} + m_{body} + m_{motA} + m_{motC}) d_B s_{\alpha_\theta})^2)/((m_{armA} + m_{armB} + m_{armC} + m_{armD} + m_{body} + m_{motA} + m_{motB} + m_{motC} + m_{motD})^2) + (3m_{motD}(2b_A m_{armA} + l_A c_{\alpha_\phi} m_{armA} - 2b_C m_{armC} + 2b_A m_{motA} - 2b_C m_{motC} - l_C m_{armC} c_{\alpha_\phi} + 2(m_{motA} - m_{motC}) c_{\alpha_\phi} d_A + l_B m_{armB} s_{\alpha_\theta} + l_D m_{armD} s_{\alpha_\theta} - 2(m_{armA} + m_{armB} + m_{armC} + m_{armD} + m_{body} + m_{motA} + m_{motC}) d_B s_{\alpha_\theta})^2)/((m_{armA} + m_{armB} + m_{armC} + m_{armD} + m_{body} + m_{motA} + m_{motB} + m_{motC} + m_{motD})^2) + (3m_{motC}(2b_A m_{armA} + 2b_C m_{armA} + l_A c_{\alpha_\phi} m_{armA} + 2b_C m_{armB} + 2b_C m_{armD} + 2b_C m_{body} + 2b_A m_{motA} + 2b_C m_{motA} + 2b_C m_{motB} + 2b_C m_{motD} - l_C m_{armC} c_{\alpha_\phi} + 2(m_{armA} + m_{armB} + m_{armC} + m_{armD} + m_{body} + 2m_{motA} + m_{motB} + m_{motD}) c_{\alpha_\phi} d_A + l_B m_{armB} s_{\alpha_\theta} + l_D m_{armD} s_{\alpha_\theta} + 2(m_{motB} +$$

$m_{motD})d_B s_{\alpha_\theta})^2)/((m_{armA} + m_{armB} + m_{armC} + m_{armD} + m_{body} + m_{motA} + m_{motB} + m_{motC} + m_{motD})^2) + 12m_{motA}(b_A + c_{\alpha_\phi} d_A - (2b_A m_{armA} + l_A c_{\alpha_\phi} m_{armA} - 2b_C m_{armC} + 2b_A m_{motA} - 2b_C m_{motC} - l_C m_{armC} c_{\alpha_\phi} + 2(m_{motA} - m_{motC}) c_{\alpha_\phi} d_A + l_B m_{armB} s_{\alpha_\theta} + l_D m_{armD} s_{\alpha_\theta} + 2(m_{motB} + m_{motD}) d_B s_{\alpha_\theta})/(2(m_{armA} + m_{armB} + m_{armC} + m_{armD} + m_{body} + m_{motA} + m_{motB} + m_{motC} + m_{motD})))^2 + m_{body}({h_{body}}^2 + 3{\rho_{body}}^2 + (3(2b_A m_{armA} + l_A c_{\alpha_\phi} m_{armA} - 2b_C m_{armC} + 2b_A m_{motA} - 2b_C m_{motC} - l_C m_{armC} c_{\alpha_\phi} + 2(m_{motA} - m_{motC}) c_{\alpha_\phi} d_A + l_B m_{armB} s_{\alpha_\theta} + l_D m_{armD} s_{\alpha_\theta} + 2(m_{motB} + m_{motD}) d_B s_{\alpha_\theta})^2)/((m_{armA} + m_{armB} + m_{armC} + m_{armD} + m_{body} + m_{motA} + m_{motB} + m_{motC} + m_{motD})^2)) + m_{armB}({l_B}^2 s_{\alpha_\theta}^2 + 3(l_B s_{\alpha_\theta} - (2b_A m_{armA} + l_A c_{\alpha_\phi} m_{armA} - 2b_C m_{armC} + 2b_A m_{motA} - 2b_C m_{motC} - l_C m_{armC} c_{\alpha_\phi} + 2(m_{motA} - m_{motC}) c_{\alpha_\phi} d_A + l_B m_{armB} s_{\alpha_\theta} + l_D m_{armD} s_{\alpha_\theta} + 2(m_{motB} + m_{motD}) d_B s_{\alpha_\theta})/(m_{armA} + m_{armB} + m_{armC} + m_{armD} + m_{body} + m_{motA} + m_{motB} + m_{motC} + m_{motD}))^2) + m_{armD}({l_D}^2 s_{\alpha_\theta}^2 + 3(l_D s_{\alpha_\theta} - (2b_A m_{armA} + l_A c_{\alpha_\phi} m_{armA} - 2b_C m_{armC} + 2b_A m_{motA} - 2b_C m_{motC} - l_C m_{armC} c_{\alpha_\phi} + 2(m_{motA} - m_{motC}) c_{\alpha_\phi} d_A + l_B m_{armB} s_{\alpha_\theta} + l_D m_{armD} s_{\alpha_\theta} + 2(m_{motB} + m_{motD}) d_B s_{\alpha_\theta})/(m_{armA} + m_{armB} + m_{armC} + m_{armD} + m_{body} + m_{motA} + m_{motB} + m_{motC} + m_{motD}))^2) + 12m_{armA}(\frac{1}{12}{l_A}^2 c_{\alpha_\phi}^2 + (b_A + \frac{1}{2} l_A c_{\alpha_\phi} - (2b_A m_{armA} + l_A c_{\alpha_\phi} m_{armA} - 2b_C m_{armC} + 2b_A m_{motA} - 2b_C m_{motC} - l_C m_{armC} c_{\alpha_\phi} + 2(m_{motA} - m_{motC}) c_{\alpha_\phi} d_A + l_B m_{armB} s_{\alpha_\theta} + l_D m_{armD} s_{\alpha_\theta} + 2(m_{motB} + m_{motD}) d_B s_{\alpha_\theta})/(2(m_{armA} + m_{armB} + m_{armC} + m_{armD} + m_{body} + m_{motA} + m_{motB} + m_{motC} + m_{motD})))^2) + 12m_{armC}(\frac{1}{12}{l_C}^2 c_{\alpha_\phi}^2 + (b_C + \frac{1}{2} l_C c_{\alpha_\phi} + (2b_A m_{armA} + l_A c_{\alpha_\phi} m_{armA} - 2b_C m_{armC} + 2b_A m_{motA} - 2b_C m_{motC} - l_C m_{armC} c_{\alpha_\phi} + 2(m_{motA} - m_{motC}) c_{\alpha_\phi} d_A + l_B m_{armB} s_{\alpha_\theta} + l_D m_{armD} s_{\alpha_\theta} + 2(m_{motB} + m_{motD}) d_B s_{\alpha_\theta})/(2(m_{armA} + m_{armB} + m_{armC} + m_{armD} + m_{body} + m_{motA} + m_{motB} + m_{motC} + m_{motD})))^2))$

A.9 $\ddot{\psi}$

$(12(m_{armA} + m_{armB} + m_{armC} + m_{armD} + m_{body} + m_{motA} + m_{motB} + m_{motC} + m_{motD})(0.5(u_A - u_B - u_D) + ((8m_{motA} m_{motC} s_{2\alpha_\phi} \dot{\alpha_\phi} d_A^2 - 4(m_{armB} m_{motA} + m_{armC} m_{motA} + m_{armD} m_{motA} + m_{body} m_{motA} + m_{motB} m_{motA} + 2m_{motC} m_{motA} + m_{motD} m_{motA} + 2m_{motC} c_{2\alpha_\phi} m_{motA} + m_{armB} m_{motC} + m_{armC} m_{motC} + m_{armD} m_{motC} + m_{body} m_{motC} + m_{motB} m_{motC} + m_{armA}(m_{motA} + m_{motC}) + m_{motC} m_{motD}) \dot{d_A} d_A + 2(2(m_{motB} + m_{motD})(m_{motA} s_{\alpha_\theta + \alpha_\phi} - m_{motC} s_{\alpha_\theta - \alpha_\phi}) \dot{d_B} + l_B m_{armB} m_{motA} c_{\alpha_\theta - \alpha_\phi} (\dot{\alpha_\theta} - \dot{\alpha_\phi}) - l_D m_{armD} m_{motC} c_{\alpha_\theta - \alpha_\phi} (\dot{\alpha_\theta} -$

$$\dot{\alpha_\phi}) - 2b_B m_{armB} m_{motA} c_{\alpha_\phi} \dot{\alpha_\phi} + 2b_D m_{armD} m_{motA} c_{\alpha_\phi} \dot{\alpha_\phi} + 2b_D m_{motA} m_{motB} c_{\alpha_\phi} \dot{\alpha_\phi} - 2b_B m_{armB} m_{motC} c_{\alpha_\phi} \dot{\alpha_\phi} + 2b_D m_{armD} m_{motC} c_{\alpha_\phi} \dot{\alpha_\phi} + 2b_D m_{motB} m_{motC} c_{\alpha_\phi} \dot{\alpha_\phi} + 2b_D m_{motA} m_{motD} c_{\alpha_\phi} \dot{\alpha_\phi} + 2b_D m_{motC} m_{motD} c_{\alpha_\phi} \dot{\alpha_\phi} + 2(b_A(m_{armB} m_{motA} + m_{armC} m_{motA} + m_{armD} m_{motA} + m_{body} m_{motA} + m_{motB} m_{motA} + 2m_{motC} m_{motA} + m_{motD} m_{motA} + m_{armA} m_{motC}) + b_C(m_{armC} m_{motA} + m_{motC}(m_{armA} + m_{armB} + m_{armD} + m_{body} + 2m_{motA} + m_{motB} + m_{motD})))s_{\alpha_\phi} \dot{\alpha_\phi} + 2l_C m_{armC} m_{motA} s_{2\alpha_\phi} \dot{\alpha_\phi} + 2l_A m_{armA} m_{motC} s_{2\alpha_\phi} \dot{\alpha_\phi} + l_D m_{armD} m_{motA} c_{\alpha_\theta + \alpha_\phi}(\dot{\alpha_\theta} + \dot{\alpha_\phi}) - l_B m_{armB} m_{motC} c_{\alpha_\theta + \alpha_\phi}(\dot{\alpha_\theta} + \dot{\alpha_\phi}) + 2(m_{motB} + m_{motD}) d_B (m_{motA} c_{\alpha_\theta + \alpha_\phi}(\dot{\alpha_\theta} + \dot{\alpha_\phi}) - m_{motC} c_{\alpha_\theta - \alpha_\phi}(\dot{\alpha_\theta} - \dot{\alpha_\phi})))d_A + 2(l_A m_{armA} m_{motA} - l_C m_{armC} c_{2\alpha_\phi} m_{motA} + l_B m_{armB} s_{\alpha_\theta - \alpha_\phi} m_{motA} - 2b_B m_{armB} s_{\alpha_\phi} m_{motA} + 2b_D m_{armD} s_{\alpha_\phi} m_{motA} + 2b_D m_{motB} s_{\alpha_\phi} m_{motA} + 2b_D m_{motD} s_{\alpha_\phi} m_{motA} + l_D m_{armD} s_{\alpha_\theta + \alpha_\phi} m_{motA} + l_C m_{armC} m_{motC} - 2(b_A(m_{armB} m_{motA} + m_{armC} m_{motA} + m_{armD} m_{motA} + m_{body} m_{motA} + m_{motB} m_{motA} + 2m_{motC} m_{motA} + m_{motD} m_{motA} + m_{armA} m_{motC}) + b_C(m_{armC} m_{motA} + m_{motC}(m_{armA} + m_{armB} + m_{armD} + m_{body} + 2m_{motA} + m_{motB} + m_{motD})))c_{\alpha_\phi} - l_A m_{armA} m_{motC} c_{2\alpha_\phi} - l_D m_{armD} m_{motC} s_{\alpha_\theta - \alpha_\phi} - 2b_B m_{armB} m_{motC} s_{\alpha_\phi} + 2b_D m_{armD} m_{motC} s_{\alpha_\phi} + 2b_D m_{motB} m_{motC} s_{\alpha_\phi} + 2b_D m_{motC} m_{motD} s_{\alpha_\phi} - l_B m_{armB} m_{motC} s_{\alpha_\theta + \alpha_\phi} + 2(m_{motB} + m_{motD}) d_B (m_{motA} s_{\alpha_\theta + \alpha_\phi} - m_{motC} s_{\alpha_\theta - \alpha_\phi}))\dot{d_A} - 4(2c_{2\alpha_\theta} {m_{motB}}^2 + 2{m_{motB}}^2 + m_{armB} m_{motB} + m_{armC} m_{motB} + m_{armD} m_{motB} + m_{body} m_{motB} + m_{motA} m_{motB} + m_{motC} m_{motB} + m_{armB} m_{motD} + m_{armC} m_{motD} + m_{armD} m_{motD} + m_{body} m_{motD} + m_{motA} m_{motD} + m_{motC} m_{motD} + m_{armA}(m_{motB} + m_{motD}))d_B \dot{d_B} + 2((m_{motB} + m_{motD})(l_D m_{armD} - l_B m_{armB} c_{2\alpha_\theta} + 2(b_A(m_{armA} + m_{motA}) - b_C(m_{armC} + m_{motC}))s_{\alpha_\theta} - l_C m_{armC} s_{\alpha_\theta - \alpha_\phi} + l_A m_{armA} s_{\alpha_\theta + \alpha_\phi}) - 2(b_B(2{m_{motB}}^2 + m_{armB}(m_{motB} + m_{motD})) + b_D(2{m_{motB}}^2 + m_{armC} m_{motB} + m_{body} m_{motB} + m_{motA} m_{motB} + m_{motC} m_{motB} + m_{armC} m_{motD} + m_{body} m_{motD} + m_{motA} m_{motD} + m_{motC} m_{motD} + m_{armA}(m_{motB} + m_{motD}) + m_{armB}(m_{motB} + m_{motD})))c_{\alpha_\theta})\dot{d_B} + 2b_A l_B m_{armA} m_{armB} c_{\alpha_\theta} \dot{\alpha_\theta} - 2b_C l_B m_{armB} m_{armC} c_{\alpha_\theta} \dot{\alpha_\theta} + 2b_A l_D m_{armA} m_{armD} c_{\alpha_\theta} \dot{\alpha_\theta} - 2b_C l_D m_{armC} m_{armD} c_{\alpha_\theta} \dot{\alpha_\theta} + 2b_A l_B m_{armB} m_{motA} c_{\alpha_\theta} \dot{\alpha_\theta} + 2b_A l_D m_{armD} m_{motA} c_{\alpha_\theta} \dot{\alpha_\theta} - 2b_C l_B m_{armB} m_{motC} c_{\alpha_\theta} \dot{\alpha_\theta} - 2b_C l_D m_{armD} m_{motC} c_{\alpha_\theta} \dot{\alpha_\theta} + 2b_B l_B m_{armA} m_{armB} s_{\alpha_\theta} \dot{\alpha_\theta} + 2b_B l_B m_{armB} m_{armC} s_{\alpha_\theta} \dot{\alpha_\theta} + 2b_D l_D m_{armA} m_{armD} s_{\alpha_\theta} \dot{\alpha_\theta} + 2b_B l_B m_{armB} m_{armD} s_{\alpha_\theta} \dot{\alpha_\theta} + 2b_D l_B m_{armB} m_{armD} s_{\alpha_\theta} \dot{\alpha_\theta} + 2b_B l_D m_{armB} m_{armD} s_{\alpha_\theta} \dot{\alpha_\theta} + 2b_D l_D m_{armB} m_{armD} s_{\alpha_\theta} \dot{\alpha_\theta} + 2b_D l_D m_{armC} m_{armD} s_{\alpha_\theta} \dot{\alpha_\theta} + 2b_B l_B m_{armB} m_{body} s_{\alpha_\theta} \dot{\alpha_\theta} + 2b_D l_D m_{armD} m_{body} s_{\alpha_\theta} \dot{\alpha_\theta} + 2b_B l_B m_{armB} m_{motA} s_{\alpha_\theta} \dot{\alpha_\theta} + 2b_D l_D m_{armD} m_{motA} s_{\alpha_\theta} \dot{\alpha_\theta} +$$

$$2b_B l_B m_{armB} m_{motB} s_{\alpha_\theta} \dot{\alpha_\theta} + 2b_D l_B m_{armB} m_{motB} s_{\alpha_\theta} \dot{\alpha_\theta} + 2b_B l_B m_{armB} m_{motC} s_{\alpha_\theta} \dot{\alpha_\theta} +$$
$$2b_D l_D m_{armD} m_{motC} s_{\alpha_\theta} \dot{\alpha_\theta} + 2b_B l_B m_{armB} m_{motD} s_{\alpha_\theta} \dot{\alpha_\theta} + 2b_D l_B m_{armB} m_{motD} s_{\alpha_\theta} \dot{\alpha_\theta} +$$
$$8{m_{motB}}^2 d_B^2 s_{2\alpha_\theta} \dot{\alpha_\theta} + 2l_B l_D m_{armB} m_{armD} s_{2\alpha_\theta} \dot{\alpha_\theta} + l_A l_B m_{armA} m_{armB} c_{\alpha_\theta - \alpha_\phi} (\dot{\alpha_\theta} - \dot{\alpha_\phi}) -$$
$$l_C l_D m_{armC} m_{armD} c_{\alpha_\theta - \alpha_\phi} (\dot{\alpha_\theta} - \dot{\alpha_\phi}) - 2b_B l_A m_{armA} m_{armB} c_{\alpha_\phi} \dot{\alpha_\phi} - 2b_B l_C m_{armB} m_{armC} c_{\alpha_\phi} \dot{\alpha_\phi} +$$
$$2b_D l_A m_{armA} m_{armD} c_{\alpha_\phi} \dot{\alpha_\phi} + 2b_D l_C m_{armC} m_{armD} c_{\alpha_\phi} \dot{\alpha_\phi} + 2b_D l_A m_{armA} m_{motB} c_{\alpha_\phi} \dot{\alpha_\phi} +$$
$$2b_D l_C m_{armC} m_{motB} c_{\alpha_\phi} \dot{\alpha_\phi} + 2b_D l_A m_{armA} m_{motD} c_{\alpha_\phi} \dot{\alpha_\phi} + 2b_D l_C m_{armC} m_{motD} c_{\alpha_\phi} \dot{\alpha_\phi} +$$
$$2b_A l_A m_{armA} m_{armB} s_{\alpha_\phi} \dot{\alpha_\phi} + 2b_A l_A m_{armA} m_{armC} s_{\alpha_\phi} \dot{\alpha_\phi} + 2b_C l_A m_{armA} m_{armC} s_{\alpha_\phi} \dot{\alpha_\phi} +$$
$$2b_A l_C m_{armA} m_{armC} s_{\alpha_\phi} \dot{\alpha_\phi} + 2b_C l_C m_{armA} m_{armC} s_{\alpha_\phi} \dot{\alpha_\phi} + 2b_C l_C m_{armB} m_{armC} s_{\alpha_\phi} \dot{\alpha_\phi} +$$
$$2b_A l_A m_{armA} m_{armD} s_{\alpha_\phi} \dot{\alpha_\phi} + 2b_C l_C m_{armC} m_{armD} s_{\alpha_\phi} \dot{\alpha_\phi} + 2b_A l_A m_{armA} m_{body} s_{\alpha_\phi} \dot{\alpha_\phi} +$$
$$2b_C l_C m_{armC} m_{body} s_{\alpha_\phi} \dot{\alpha_\phi} + 2b_A l_C m_{armC} m_{motA} s_{\alpha_\phi} \dot{\alpha_\phi} + 2b_C l_C m_{armC} m_{motA} s_{\alpha_\phi} \dot{\alpha_\phi} +$$
$$2b_A l_A m_{armA} m_{motB} s_{\alpha_\phi} \dot{\alpha_\phi} + 2b_C l_C m_{armC} m_{motB} s_{\alpha_\phi} \dot{\alpha_\phi} + 2b_A l_A m_{armA} m_{motC} s_{\alpha_\phi} \dot{\alpha_\phi} +$$
$$2b_C l_A m_{armA} m_{motC} s_{\alpha_\phi} \dot{\alpha_\phi} + 2b_A l_A m_{armA} m_{motD} s_{\alpha_\phi} \dot{\alpha_\phi} + 2b_C l_C m_{armC} m_{motD} s_{\alpha_\phi} \dot{\alpha_\phi} +$$
$$2l_A l_C m_{armA} m_{armC} s_{2\alpha_\phi} \dot{\alpha_\phi} - l_B l_C m_{armB} m_{armC} c_{\alpha_\theta + \alpha_\phi} (\dot{\alpha_\theta} + \dot{\alpha_\phi}) + l_A l_D m_{armA} m_{armD} c_{\alpha_\theta + \alpha_\phi} (\dot{\alpha_\theta} +$$
$$\dot{\alpha_\phi}) + 2d_B (2(b_B(2{m_{motB}}^2 + m_{armB}(m_{motB} + m_{motD})) + b_D(2{m_{motB}}^2 + m_{armC} m_{motB} +$$
$$m_{body} m_{motB} + m_{motA} m_{motB} + m_{motC} m_{motB} + m_{armC} m_{motD} + m_{body} m_{motD} + m_{motA} m_{motD} +$$
$$m_{motC} m_{motD} + m_{armA}(m_{motB} + m_{motD}) + m_{armB}(m_{motB} + m_{motD}))) s_{\alpha_\theta} \dot{\alpha_\theta} + (m_{motB} +$$
$$m_{motD})(2(b_A(m_{armA} + m_{motA}) - b_C(m_{armC} + m_{motC})) c_{\alpha_\theta} \dot{\alpha_\theta} + 2l_B m_{armB} s_{2\alpha_\theta} \dot{\alpha_\theta} -$$
$$l_C m_{armC} c_{\alpha_\theta - \alpha_\phi} (\dot{\alpha_\theta} - \dot{\alpha_\phi}) + l_A m_{armA} c_{\alpha_\theta + \alpha_\phi} (\dot{\alpha_\theta} + \dot{\alpha_\phi})))) \dot{\psi}) / (2(m_{armA} + m_{armB} + m_{armC} + m_{armD} +$$
$$m_{body} + m_{motA} + m_{motB} + m_{motC} + m_{motD})))) / (12 m_{armA} m_{armB} {b_A}^2 + 12 m_{armA} m_{armC} {b_A}^2 +$$
$$12 m_{armA} m_{armD} {b_A}^2 + 12 m_{armA} m_{body} {b_A}^2 + 12 m_{armB} m_{motA} {b_A}^2 + 12 m_{armC} m_{motA} {b_A}^2 +$$
$$12 m_{armD} m_{motA} {b_A}^2 + 12 m_{body} m_{motA} {b_A}^2 + 12 m_{armA} m_{motB} {b_A}^2 + 12 m_{motA} m_{motB} {b_A}^2 +$$
$$12 m_{armA} m_{motC} {b_A}^2 + 12 m_{motA} m_{motC} {b_A}^2 + 12 m_{armA} m_{motD} {b_A}^2 + 12 m_{motA} m_{motD} {b_A}^2 +$$
$$24 b_C m_{armA} m_{armC} b_A + 24 b_C m_{armC} m_{motA} b_A + 24 b_C m_{armA} m_{motC} b_A + 24 b_C m_{motA} m_{motC} b_A +$$
$$12 l_A m_{armA} m_{armB} c_{\alpha_\phi} b_A + 12 l_A m_{armA} m_{armC} c_{\alpha_\phi} b_A + 12 l_C m_{armA} m_{armC} c_{\alpha_\phi} b_A +$$
$$12 l_A m_{armA} m_{armD} c_{\alpha_\phi} b_A + 12 l_A m_{armA} m_{body} c_{\alpha_\phi} b_A + 12 l_C m_{armC} m_{motA} c_{\alpha_\phi} b_A +$$
$$12 l_A m_{armA} m_{motB} c_{\alpha_\phi} b_A + 12 l_A m_{armA} m_{motC} c_{\alpha_\phi} b_A + 12 l_A m_{armA} m_{motD} c_{\alpha_\phi} b_A -$$
$$12 l_B m_{armA} m_{armB} s_{\alpha_\theta} b_A - 12 l_D m_{armA} m_{armD} s_{\alpha_\theta} b_A - 12 l_B m_{armB} m_{motA} s_{\alpha_\theta} b_A -$$
$$12 l_D m_{armD} m_{motA} s_{\alpha_\theta} b_A + {l_A}^2 {m_{armA}}^2 + {l_B}^2 {m_{armB}}^2 + {l_C}^2 {m_{armC}}^2 + {l_D}^2 {m_{armD}}^2 + 12 {b_B}^2 {m_{motB}}^2 +$$

$$12{b_D}^2{m_{motB}}^2 + 24b_Bb_Dm_{motB}{}^2 + 6{m_{body}}^2{\rho_{body}}^2 + 6m_{armA}m_{body}{\rho_{body}}^2 + 6m_{armB}m_{body}{\rho_{body}}^2 + 6m_{armC}m_{body}{\rho_{body}}^2 + 6m_{armD}m_{body}{\rho_{body}}^2 + 6m_{body}m_{motA}{\rho_{body}}^2 + 6m_{body}m_{motB}{\rho_{body}}^2 + 6m_{body}m_{motC}{\rho_{body}}^2 + 6m_{body}m_{motD}{\rho_{body}}^2 + 12(m_{armB}m_{motA} + m_{armC}m_{motA} + m_{armD}m_{motA} + m_{body}m_{motA} + m_{motB}m_{motA} + 2m_{motC}m_{motA} + m_{motD}m_{motA} + 2m_{motC}c_{2\alpha_\phi}m_{motA} + m_{armB}m_{motC} + m_{armC}m_{motC} + m_{armD}m_{motC} + m_{body}m_{motC} + m_{motB}m_{motC} + m_{armA}(m_{motA} + m_{motC}) + m_{motC}m_{motD})d_A^2 + 12(2c_{2\alpha_\theta}m_{motB}{}^2 + 2m_{motB}{}^2 + m_{armB}m_{motB} + m_{armC}m_{motB} + m_{armD}m_{motB} + m_{body}m_{motB} + m_{motA}m_{motB} + m_{motC}m_{motB} + m_{armB}m_{motD} + m_{armC}m_{motD} + m_{armD}m_{motD} + m_{body}m_{motD} + m_{motA}m_{motD} + m_{motC}m_{motD} + m_{armA}(m_{motB} + m_{motD}))d_B^2 + 12{b_B}^2m_{armA}m_{armB} + 4{l_A}^2m_{armA}m_{armB} + 4{l_B}^2m_{armA}m_{armB} + 12{b_C}^2m_{armA}m_{armC} + 4{l_A}^2m_{armA}m_{armC} + 4{l_C}^2m_{armA}m_{armC} + 12{b_B}^2m_{armB}m_{armC} + 12{b_C}^2m_{armB}m_{armC} + 4{l_B}^2m_{armB}m_{armC} + 4{l_C}^2m_{armB}m_{armC} + 12{b_D}^2m_{armA}m_{armD} + 4{l_A}^2m_{armA}m_{armD} + 4{l_D}^2m_{armA}m_{armD} + 12{b_B}^2m_{armB}m_{armD} + 12{b_D}^2m_{armB}m_{armD} + 4{l_B}^2m_{armB}m_{armD} + 4{l_D}^2m_{armB}m_{armD} + 24b_Bb_Dm_{armB}m_{armD} + 12{b_C}^2m_{armC}m_{armD} + 12{b_D}^2m_{armC}m_{armD} + 4{l_C}^2m_{armC}m_{armD} + 4{l_D}^2m_{armC}m_{armD} + 4{l_A}^2m_{armA}m_{body} + 12{b_B}^2m_{armB}m_{body} + 4{l_B}^2m_{armB}m_{body} + 12{b_C}^2m_{armC}m_{body} + 4{l_C}^2m_{armC}m_{body} + 12{b_D}^2m_{armD}m_{body} + 4{l_D}^2m_{armD}m_{body} + 4{l_A}^2m_{armA}m_{motA} + 12{b_B}^2m_{armB}m_{motA} + 4{l_B}^2m_{armB}m_{motA} + 12{b_C}^2m_{armC}m_{motA} + 4{l_C}^2m_{armC}m_{motA} + 12{b_D}^2m_{armD}m_{motA} + 4{l_D}^2m_{armD}m_{motA} + 12{b_D}^2m_{armA}m_{motB} + 4{l_A}^2m_{armA}m_{motB} + 12{b_B}^2m_{armB}m_{motB} + 12{b_D}^2m_{armB}m_{motB} + 4{l_B}^2m_{armB}m_{motB} + 24b_Bb_Dm_{armB}m_{motB} + 12{b_C}^2m_{armC}m_{motB} + 12{b_D}^2m_{armC}m_{motB} + 4{l_C}^2m_{armC}m_{motB} + 4{l_D}^2m_{armD}m_{motB} + 12{b_D}^2m_{body}m_{motB} + 12{b_D}^2m_{motA}m_{motB} + 12{b_C}^2m_{armA}m_{motC} + 4{l_A}^2m_{armA}m_{motC} + 12{b_B}^2m_{armB}m_{motC} + 12{b_C}^2m_{armB}m_{motC} + 4{l_B}^2m_{armB}m_{motC} + 4{l_C}^2m_{armC}m_{motC} + 12{b_C}^2m_{armD}m_{motC} + 12{b_D}^2m_{armD}m_{motC} + 4{l_D}^2m_{armD}m_{motC} + 12{b_C}^2m_{body}m_{motC} + 12{b_C}^2m_{motA}m_{motC} + 12{b_C}^2m_{motB}m_{motC} + 12{b_D}^2m_{motB}m_{motC} + 12{b_D}^2m_{armA}m_{motD} + 4{l_A}^2m_{armA}m_{motD} + 12{b_B}^2m_{armB}m_{motD} + 12{b_D}^2m_{armB}m_{motD} + 4{l_B}^2m_{armB}m_{motD} + 24b_Bb_Dm_{armB}m_{motD} + 12{b_C}^2m_{armC}m_{motD} + 12{b_D}^2m_{armC}m_{motD} + 4{l_C}^2m_{armC}m_{motD} + 4{l_D}^2m_{armD}m_{motD} + 12{b_D}^2m_{body}m_{motD} + 12{b_D}^2m_{motA}m_{motD} + 12{b_C}^2m_{motC}m_{motD} + 12{b_D}^2m_{motC}m_{motD} + 12b_Bl_Bm_{armA}m_{armB}c_{\alpha_\theta} + 12b_Bl_Bm_{armB}m_{armC}c_{\alpha_\theta} + 12b_Dl_Dm_{armA}m_{armD}c_{\alpha_\theta} + 12b_Bl_Bm_{armB}m_{armD}c_{\alpha_\theta} + 12b_Dl_Bm_{armB}m_{armD}c_{\alpha_\theta} +$$

$$12b_B l_D m_{armB} m_{armD} c_{\alpha_\theta} + 12b_D l_D m_{armB} m_{armD} c_{\alpha_\theta} + 12b_D l_D m_{armC} m_{armD} c_{\alpha_\theta} +$$
$$12b_B l_B m_{armB} m_{body} c_{\alpha_\theta} + 12b_D l_D m_{armD} m_{body} c_{\alpha_\theta} + 12b_B l_B m_{armB} m_{motA} c_{\alpha_\theta} +$$
$$12b_D l_D m_{armD} m_{motA} c_{\alpha_\theta} + 12b_B l_B m_{armB} m_{motB} c_{\alpha_\theta} + 12b_D l_B m_{armB} m_{motB} c_{\alpha_\theta} +$$
$$12b_B l_B m_{armB} m_{motC} c_{\alpha_\theta} + 12b_D l_D m_{armD} m_{motC} c_{\alpha_\theta} + 12b_B l_B m_{armB} m_{motD} c_{\alpha_\theta} +$$
$$12b_D l_B m_{armB} m_{motD} c_{\alpha_\theta} + 6l_B l_D m_{armB} m_{armD} c_{2\alpha_\theta} + 12b_C l_A m_{armA} m_{armC} c_{\alpha_\phi} +$$
$$12b_C l_C m_{armA} m_{armC} c_{\alpha_\phi} + 12b_C l_C m_{armB} m_{armC} c_{\alpha_\phi} + 12b_C l_C m_{armC} m_{armD} c_{\alpha_\phi} +$$
$$12b_C l_C m_{armC} m_{body} c_{\alpha_\phi} + 12b_C l_C m_{armC} m_{motA} c_{\alpha_\phi} + 12b_C l_C m_{armC} m_{motB} c_{\alpha_\phi} +$$
$$12b_C l_A m_{armA} m_{motC} c_{\alpha_\phi} + 12b_C l_C m_{armC} m_{motD} c_{\alpha_\phi} + 6l_A l_C m_{armA} m_{armC} c_{2\alpha_\phi} +$$
$$12b_C l_B m_{armB} m_{armC} s_{\alpha_\theta} + 12b_C l_D m_{armC} m_{armD} s_{\alpha_\theta} + 12b_C l_B m_{armB} m_{motC} s_{\alpha_\theta} +$$
$$12b_C l_D m_{armD} m_{motC} s_{\alpha_\theta} - 6l_A l_B m_{armA} m_{armB} s_{\alpha_\theta - \alpha_\phi} + 6l_C l_D m_{armC} m_{armD} s_{\alpha_\theta - \alpha_\phi} +$$
$$12b_B l_A m_{armA} m_{armB} s_{\alpha_\phi} + 12b_B l_C m_{armB} m_{armC} s_{\alpha_\phi} - 12b_D l_A m_{armA} m_{armD} s_{\alpha_\phi} -$$
$$12b_D l_C m_{armC} m_{armD} s_{\alpha_\phi} - 12b_D l_A m_{armA} m_{motB} s_{\alpha_\phi} - 12b_D l_C m_{armC} m_{motB} s_{\alpha_\phi} -$$
$$12b_D l_A m_{armA} m_{motD} s_{\alpha_\phi} - 12b_D l_C m_{armC} m_{motD} s_{\alpha_\phi} + 6l_B l_C m_{armB} m_{armC} s_{\alpha_\theta + \alpha_\phi} -$$
$$6l_A l_D m_{armA} m_{armD} s_{\alpha_\theta + \alpha_\phi} - 12d_B((m_{motB} + m_{motD})(l_D m_{armD} - l_B m_{armB} c_{2\alpha_\theta} + 2(b_A(m_{armA} +$$
$$m_{motA}) - b_C(m_{armC} + m_{motC}))s_{\alpha_\theta} - l_C m_{armC} s_{\alpha_\theta - \alpha_\phi} + l_A m_{armA} s_{\alpha_\theta + \alpha_\phi}) - 2(b_B(2{m_{motB}}^2 +$$
$$m_{armB}(m_{motB} + m_{motD})) + b_D(2{m_{motB}}^2 + m_{armC} m_{motB} + m_{body} m_{motB} + m_{motA} m_{motB} +$$
$$m_{motC} m_{motB} + m_{armC} m_{motD} + m_{body} m_{motD} + m_{motA} m_{motD} + m_{motC} m_{motD} + m_{armA}(m_{motB} +$$
$$m_{motD}) + m_{armB}(m_{motB} + m_{motD})))c_{\alpha_\theta}) - 12d_A(l_A m_{armA} m_{motA} - l_C m_{armC} c_{2\alpha_\phi} m_{motA} +$$
$$l_B m_{armB} s_{\alpha_\theta - \alpha_\phi} m_{motA} - 2b_B m_{armB} s_{\alpha_\phi} m_{motA} + 2b_D m_{armD} s_{\alpha_\phi} m_{motA} + 2b_D m_{motB} s_{\alpha_\phi} m_{motA} +$$
$$2b_D m_{motD} s_{\alpha_\phi} m_{motA} + l_D m_{armD} s_{\alpha_\theta + \alpha_\phi} m_{motA} + l_C m_{armC} m_{motC} - 2(b_A(m_{armB} m_{motA} +$$
$$m_{armC} m_{motA} + m_{armD} m_{motA} + m_{body} m_{motA} + m_{motB} m_{motA} + 2m_{motC} m_{motA} + m_{motD} m_{motA} +$$
$$m_{armA} m_{motC}) + b_C(m_{armC} m_{motA} + m_{motC}(m_{armA} + m_{armB} + m_{armD} + m_{body} + 2m_{motA} +$$
$$m_{motB} + m_{motD})))c_{\alpha_\phi} - l_A m_{armA} m_{motC} c_{2\alpha_\phi} - l_D m_{armD} m_{motC} s_{\alpha_\theta - \alpha_\phi} - 2b_B m_{armB} m_{motC} s_{\alpha_\phi} +$$
$$2b_D m_{armD} m_{motC} s_{\alpha_\phi} + 2b_D m_{motB} m_{motC} s_{\alpha_\phi} + 2b_D m_{motC} m_{motD} s_{\alpha_\phi} - l_B m_{armB} m_{motC} s_{\alpha_\theta + \alpha_\phi} +$$
$$2(m_{motB} + m_{motD}) d_B(m_{motA} s_{\alpha_\theta + \alpha_\phi} - m_{motC} s_{\alpha_\theta - \alpha_\phi})))$$